VUV generation using 4-wave mixing and frequency tripling

Diploma work performed by
Erland Johnson

LRAP 64 (1986)

VUV GENERATION USING 4-WAVE MIXING AND FREQUENCY TRIPLING

And the Lord said, Behold, the people is one, and they have all one language; and this they begin to do: and now nothing will be restrained from them, which they have imagined to do.

LUND 86-07-31

PREFACE

This work is a diploma work, completing my education in physical engineering.

A major part of the work has been of experimental nature. These experiments have been a part of one branch of the basic research program at the department of physics. I have however tried to understand some of the theoretical background from which I have put together an overview.

In the introduction I start to define the intentions of the work and how it possibly could be useful to other people. Following these intentions is a historical review. Here I hope it will be clarified what has been done in the field at the same time as some theoretical and experimental information will be given, waiting for a more rigorous explanation in the coming chapters.

In the second chapter and its references, a theoretical foundation is given briefly in a mathematical description. The interaction between light and a medium,(a rare gas),is described with the help of the laws of classical electrodynamics combined with some results from quantum mechanics. Light, in the special form of laser beams, is given a mathematical description, which is then used in the earlier calculated results. This results in some requirements on the beam parameters for the conversion process to be useful. Finally I look at a set of more general modes of laser beams, not restricted to the earlier described beam with a Gaussian intensity distribution. These beams, which are more useful for a relevant desrciption of reality, often have a bit lower generation efficiencies and also a bit different conditions for optimal conversion. These conditions are given at the end of the theoretical section.

In the third chapter I tell about my work performed in the lab. I give the experimental results and comment their relationship to the theoretical predictions done in the preceeding chapter. Since I did experiments both in the summer 1985 and in the spring 1986 there is an artificial distinction of this chapter, not motivated with respect to

its contents. The contents of these two parts are partially overlapping. First I deal with the 1985-experiment performed in Xenon, generating radiation at 200nm. An ordinary monochromator (filled with air) was used in this experiment. The influence of different polarization directions and different laser modes of the incoming laser beams were examined. Also the influence of other parameters, as for example the Xenon pressure and different geometrical factors were investigated. Then I tell about my experiments in the vacuum ultra-violet region (VUV). After the solution of leak problems and the performance of a wavelength calibration, I reproduce one similar experiment as above, performed in Krypton. Finally I tell about the generation of 120nm-light in Krypton. Besides the dependence of the parameters discussed above for the earlier experiments, I investigate the possibility of absorption in the cell and the monochromator. The intensity distribution of a cross section of the generated radiation is also measured.At the end I have a section about different phenomena which could be responsible for the saturation character of the output power, and also one experiment concerning the tunability of the generated light, when scanning the dye wavelength.

At the end of the report I give the references, that I have used. Litterature giving an introduction to the field is given in the general references part, while those referred to in the text are given in the reference part. In the appendix, I have gathered data on the major part of the equipment.

Finally I want to thank Hans Lundberg for guidance and help in the lab and for answering a lot of questions, Stefan Kröll for interesting discussions, Hans Hallstadius for the companionship, the practical help and the contribution of ideas that you gave me when working together with me in the lab in March and April 1986, Lars Gramstad for helping me with word processing problems on Lucas, Åke Bergqvist for electrical equipment and John Bergin, Rolf Olofsson and Göran Werner for doing a lot of mechanical equipment to the monochromator. I also want to thank Rainer Hilbig at the University in Bielefeld for an interesting lecture and demonstration of his lab equipment for nonlinear optical phenomena in July 1985.

CONTENTS

I. INTRODUCTION

1. INTENTIONS

The purpose of this work is to generate coherent monochromatic electromagnetic waves in the VUV- and XUV-region, wavelengths shorter than those, which are possible to receive from ordinary lasers. I am only using the method of third-harmonic generation in rare gases. There are other possibilities to do this, which are not treated here. The generated VUV-light have, among other things, many applications in spectroscopy and photoionization studies. It could also be used for determination of absolute values of for instance the nonlinear susceptibility.

I have arranged the experimental setup, done some introductory experiments (in the regions around 1200Å and 2000Å) and have by that been forced to solve some fundamental problems. The performed experiments, the collection of references and the work done on putting together the theory, I hope will be a positive contribution to those who want to start working in the field. I also hope that it could serve as an experimental and theoretical overview if you want a general knowledge about progresses and possibilities in the field.

2. HISTORICAL REVIEW

The invention of the laser in the 60s made it possible to study different nonlinear optical phenomena. In that decade mostly second harmonic generation (SHG), frequency doubling or the generation of the sum frequency of two frequencies was studied. The theory of SHG had been examined by Kleinmann in the early 60s. Within the late 60s the theory of third harmonic generation (THG) also had been investigated

by, among others: Maker, Terhune, Bloembergen, Puell and Vidal. This theoretical foundation together with the more and more powerful laser sources developed, made it possible for the experimentalists to do THG-experiments. During the 70s many experiments were concentrated on generation of light in the Lyman-alpha region. At the same time theorists, i.e. Björklund, Yiu and McIlrath calculated the necessary conditions for high-efficiency THG for different nonlinear media, different spectral regions and different focusing geometries. These calculations led to more systematical experimental investigations in the late 70s and early 80s.

In 1973 and 1974 A. H. Kung generated third harmonics in rare gases [1], [2]. A pulse from a 1.064-μ Nd:YAG laser was frequency doubled in an ADP crystal to 5320Å, which was mixed with remaining 1.064-μ radiation to yield 3547Å. From this beam he obtained 1182Å through THG in a mixture of Xenon and Argon. The rare gas mixture had to be phase matched by a variation of the ratio of negatively dispersive Xenon and positively dispersive Argon. As we will see [II.3.3] it's necessary to have a negatively dispersive medium if tripling is performed in a tight focusing arrangement. Theoretically computed values of the dispersion, or the refractive index as a function of wavelength, were not available at that time [II.3.4]. By a combination of third-order sum generation and third-order difference generation, he was able to obtain tunable radiation spanning the region from 1180Å to 1946Å.

THG could be used for absolute measurements. In 1974 Levenson used the interference between resonant and nonresonant four-wave mixing to determine values of the nonlinear susceptibility in a number of materials [3].

Mahon, McIlrath and Koopmann used tripling in Krypton for generation of tunable coherent radiation at 1215Å [4]. They made a great effort to construct a tunable laser with a high-quality beam profile. The conversion efficiency depends namely very much on the modes of the fundamental beams [II.4].They analyzed the Kr pressure dependence of the tripling efficiency, which provided a measure of the dispersion of Krypton at those frequencies studied. Again the lacking of exact knowledge of refractive index data posed some problems: The refractive

index of Krypton at 1216Å is the result of a near cancellation of a positive contribution from the shorter wavelength transitions, particularly at 1165Å, and a negative contribution at longer wavelengths, notably at 1236Å.

In the late 70s Cotter [5], [6] and Langer, Puell and Röhr [7] produced tunable radiation at around 1200Å. They were able to verify, to a very high degree, the rare gas optimal pressures, calculated by Björklund [8]. Deviations from this theory could be partly interpreted as the presence of higher-order modes [II.4] or different saturation phenomena, which also set an upper limit of the conversion efficiency. It's shown that you can force up this limit a bit by using a mixture of different rare gases [II.3.5].

Mahon and Yiu investigated different rare gases and compared their saturation limits [9]. They were able to improve the estimates of the conversion efficiencies because of better known values of saturation limits. Zapka and Cotter did some tripling in Xenon around 1060Å, just above the transmission limit of LiF, commonly used as exit window from the gas cell [10]. Egger, Hawkins, Bokor, Pummer, Rotschild and Rhodes explored the spectral region below this limit [11]. At these wavelengths there exist no transmitting windows. The gas cell must therefore be in direct contact with the monochromator through a differentially pumped chamber.

Miller, Compton, Payne and Garrett observed the competition between ionization and third-harmonic generation [12], [13]. They were able to explain this competition by a theoretical model of collective emission. The higher the power and the more spectral regions covered by the VUV-sources the more useful they became for different spectroscopic applications. Vidal showed one application of this in 1980 [14]. Under certain conditions higher order conversions (fifth, seventh and so on) become important, explored by Reintjes in 1980 [15], [II.3.6].

During the early 80s Yiu, Bonin and McIlrath generated coherent radiation at various VUV wavelengths, through four-wave mixing processes enhanced by two-photon resonances in Xenon. Resonant upconversion had before only been done in metal vapours, where

intermediate resonances are easier to reach.

Kung used a pulsed supersonic jet of Xenon, crossing the generating laser beams [16]. He showed that this method could be as efficient as the gas cell and sometimes even better. For ordinary sum frequency generation in the negatively dispersive regions, the conversion efficiency was a little bit less than for the gas cell, however, for the positively dispersive regions the conversion efficiency was much bigger when using the jet. This is due to the requirement of negative dispersion for sum-frequency generation in the tight-focusing case [II.3.3]. Continuous coverage over a broader spectral region, spanning regions of both positive and negative dispersion is thereby possible using only sum frequency generation. The well-confined beam geometry substantially reduced the reabsorption of the generated radiation by the medium outside the generating region. The modest pumping requirement is also advantageous for generation of radiation in the windowless region below 1050Å. (The LiF transmission limit.) Of course on the other hand the practical arrangements are easier with the ordinary gas cell.

During the 80s Wallenstein and Hilbig (Bielefeld) started a systematic research on different kinds of conversion processes, covering a broad part of the VUV and XUV spectral regions. They varied a lot of parameters and made careful comparisons with the developed theory, which led to a rather complete investigation of the possibilities of VUV generation in gas cells. After some VUV generations around the Lyman-alpha wavelength, they investigated a lot of different difference frequency generation schemes: $\omega(vuv)=2\omega(uv)-\omega(1)$, $2\omega'(uv)-\omega(1)$, $2\omega(uv)-\omega(ir)$, $2\omega'(uv)-\omega(1)$ and $2\omega'(uv)-\omega(ir)$ where $\omega'(uv)=\omega(uv)+\omega(ir)$ and $\omega(1)$= the dye frequency, $\omega(uv)=2\omega(1)$= the double of the dye frequency and $\omega(ir)$ is the fundamental YAG frequency. These processes together covered the spectral region $\lambda(vuv)$ = 1200Å - 2100Å. Later on they performed tripling in Xenon and Krypton and also in Neon and Argon, which is possible only in the windowless region a bit below 1000Å, where Argon and Neon are negatively dispersive. They also performed third-harmonic generation in Mercury vapour. The conversion efficiency is a bit

higher there but instead there are additional problems in handling the Mercury [17], [18], [19], [20], [21], [22], [23], [24], [25] and [26].

II. THEORY

1.FUNDAMENTAL RELATIONS

In this chapter I will briefly deal with the fundamental equations describing what is happening to a medium which is exposed to incoming radiation. The incoming E-field will create a polarization, P, in the medium, related to the E-field through the susceptibility tensor X. To receive all important information about X, it's necessary to make a quantum mechanical approach. This treatment is complicated and will not be treated here [27], [28]. I will however outline the general ideas and give the basic results.

1.1 General ideas

Consider the E-field component of incoming, monochromatic radiation into an isotropic medium $E=E\sin(\omega t-kx)$. Since a constant E-field will displace the electrons of the atoms a distance d from the center of the nucleus, it is reasonable to assume that the periodic field will create a periodically varying displacement. Because of the inertia of the electrons, there will be a phase shift ϕ between the field and the displacement, according to $d=\delta\sin(\omega t-\phi)$. The displacements of each change in a medium manifest themselves as a macroscopic polarization, P. Also the polarization is linearly related to the E-field (for weak intensities) according to the relation $P = \varepsilon X E\sin(\omega t-\phi)$, where X is called the susceptibility of the matter in question.

The oscillating electrons, which are the microscopic cause of the periodically varying polarization, give rise to an electric field with the same frequency. This field, delayed from the incoming field by the phase ϕ, will be superimposed on it, and a resulting field will remain.

According to this simple model the electrons are elastically bound to the nuclei and consequently a resonance frequency will exist. When the frequency of the incoming light is near or equal to this resonance frequency, the oscillations of the electrons will be very big. At the same frequency, however, the absorption increases and the light grow weaker. These observations imply a frequency dependence on all these defined optical quantities. Near the resonance frequency we have the following appearance for the absorption α and the refractive index n.

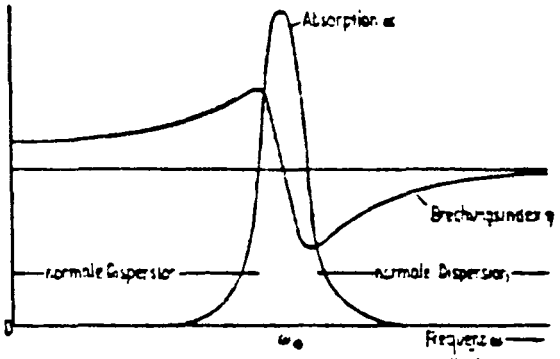

Fig. 1. The variation of the absorption and the index of refraction along the frequency scale near a resonance frequency.

The index of refraction, n is related to the susceptibility, X, according to the relation n=sqrt(1+X). It is easy to realise that there should be a relation between these two. Since X relates the incoming E-field to the polarization, which later produces a new E-field, X must in some sense be related to the delay of the light, n. On the other hand n gives the value of the speed of light in the medium, in comparison to that in vacuum.

When the amplitude of the light is getting bigger the displacement and hence the polarization will not be able to follow the E-field with such a sinusoidal variation. We will still have a periodically varying polarization, but the shape is distorted. Such a function could be expanded into a Fourier series, where we now have a sum of an infinite number of sinus-functions with increasing frequencies, integer

multiples of the incoming frequencies. If you think of these as a number of dipoles, oscillating with different frequencies, it's reasonable that there will come out light waves at all these frequencies.

This introduction could now be finished with an important remark. If the medium is isotropic, which means that no direction is distinguishable from any other, the polarization will change sign when the E-field is inverted, while the amplitude remains fixed. This means that P will be an antisymmetric function of E, which could be expanded in powers of E where only the odd powers of E will be present. Hence the third term will be the lowest order non-linear contribution.

1.2 How the susceptibility tensor show up

From the density matrix theory it's possible to calculate the polarization density from the relation $P=N\langle\upsilon\rangle=NTr(\upsilon\rho)$ [28], where N= number of atoms, υ= dipole moment operator and ρ= the density matrix. This theory justifies that the polarization density can be expanded as a power series in the incident amplitudes, if we only consider steady state:

$$P_A = \Sigma(\chi^1_{AB} E_B) + \Sigma(\chi^2_{ABC} E_B E_C) + \Sigma(\chi^3_{ABCD} E_B E_C E_D) + \ldots \qquad (1)$$

where the subscript refer to different cartesian components of the fields. The contribution from the nth term is big in comparison to that of the (n+1)th term. In this expression the susceptibility of different orders is present. For instance, the susceptibility of the first order have 2 subindex. It could be represented as a 3x3 matrix, where one index refer to the input cartesian direction and the other one to the observed cartesian direction. When we look at susceptibilities of order higher than 2, it's very difficult to visualize them. One would need a 3x3x3x3 (four-dimensional!) matrix to do this, in the case of the susceptibility of the third order. One could however represent each element with the help of four arrows,

representing the output polarization direction looked at and the polarizations of the three incoming E-fields looked at, in an ordinary three-dimensional Cartesian system. Each element of the susceptibility tensor could then be represented by such a three-dimensional picture together with a value of that X-element, the value representing the strength of the polarization component that the E-fields in given directions give rise to.

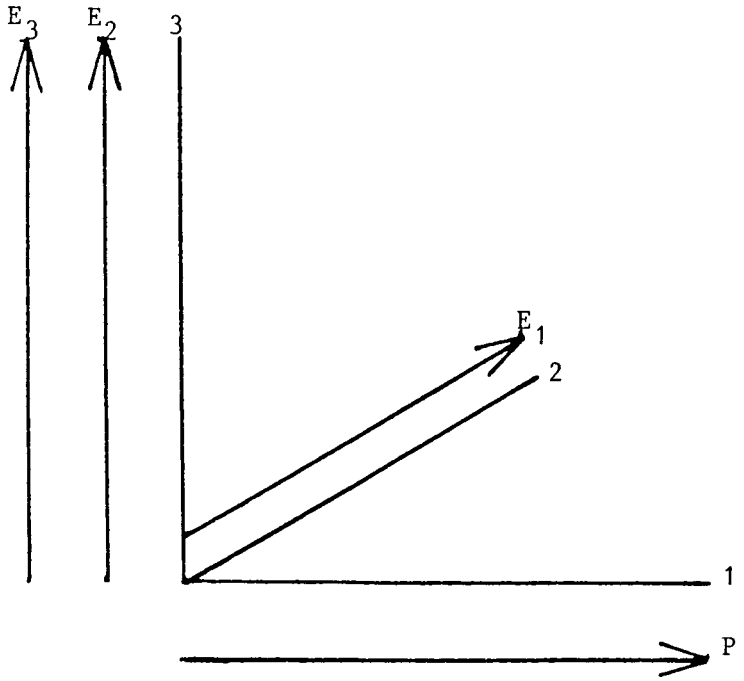

Fig.2 Visualization of the susceptibility tensor element X_{1233}, representing the coupling between the E-fields with the polarizations shown in the figure and the Cartesian component of the polarization of the medium also shown in the figure

Eq. (1) can be motivated theoretically according to the following arguments [26].

If the polarization is independent of the time of interaction, it's time dependence can be written:

$$P_{\mu}^{(n)}(t) = \int_{-\infty}^{\infty} d\tau_1 \ldots \int_{-\infty}^{\infty} d\tau_n \cdot \sum_{\alpha:s} R_{\mu\alpha_1\ldots\alpha_n}^{(n)}(\tau_1\ldots\tau_n) \cdot E_{\alpha_1}(t-\tau_1)\ldots E_{\alpha_n}(t-\tau_n) \qquad (2)$$

R is a tensor which must be a real function of $(t-\tau_1)$, $(t-\tau_2)$, ... If some of the τ:s, are negative then R must be negative because of casuality. R must also be invariant under the n! permutations of the α:s. However, as will be seen later, it's better to express the fields in frequencies than in time. This is done with the Fourier transform and the inversion formula.

$$E(t)=\int d\omega E(\omega)\exp(-i\omega t), \qquad E(w)=(1/2\Pi)\int d\tau E(\tau)\exp(i\omega t) \tag{3}$$

and we receive the result

$$P^{(n)}(t) = \int_{-\infty}^{\infty} d\omega_1 \ldots \int_{-\infty}^{\infty} d\omega_n \, \chi^{(n)}(-\omega_s, \omega_1, \ldots \omega_n) \, E(\omega_1)\ldots E(\omega_n) e^{-i\omega_s t} \tag{4}$$

where

$$\omega_s = \sum_1^n \omega_j \tag{5}$$

and

$$\chi^{(n)}(-\omega_s, \omega_1, \ldots, \omega_n) = \int_{-\infty}^{\infty} d\tau_1 \ldots \int_{-\infty}^{\infty} d\tau_n R^{(n)}(\tau_1 \ldots \tau_n) e^{i\sum_1^n \omega_j \tau_j} \tag{6}$$

If the electromagnetic field is a superposition of a finite number of monochromatic waves, the integrals in eq (2) could be replaced with sums and P(t) could also be expressed as a sum of polarization contributions at different frequencies:

$$P(t) = \frac{1}{2}\sum_1^n (P(\omega_j)e^{-i\omega_j t} + P^*(-\omega_j)e^{i\omega_j t}) \tag{7}$$

All these polarization coefficients expressed in frequencies will now satisfy the relation:

$$P_{\mu}^{(n)}(\omega_s) =$$

$$D(-\omega_s, \omega_1, \ldots, \omega_n) \sum_{\alpha_i} (\chi_{\mu\alpha_1\ldots\alpha_n}^{(n)}(-\omega_s, \omega_1, \ldots, \omega_n) E_{\alpha_1}(\omega_1) \ldots E_{\alpha_n}(\omega_n) \qquad (8)$$

The factor D is the number of indistinguishable permutations of the ω:s [29]. The expression in eq (8) corresponds to the nth term in eq (1). The susceptibility must satisfy the relations:

$$\{\chi^{(n)}(-\omega_s, \omega_1, \ldots, \omega_n)\}^* = \chi^{(n)}(+\omega_s^*, -\omega_1^*, -\omega_2^*, \ldots, -\omega_n^*) \qquad (9)$$

where the frequencies ω_1, ω_2, ... could be complex numbers. It must also be invariant under the n! permutations of the pairs (α_1,ω_1), (α_2,ω_2), ... For example, in the case n=3, we have:

$$\chi_{ijkl}^{(3)}(-\omega_3, \omega_2, \omega_1, \omega_0) = \chi_{kijl}^{(3)}(\omega_1, -\omega_3, \omega_0, \omega_2) \qquad (10)$$

1.3 The susceptibility - a formula

With the help of the density matrix theory it's possible to calculate a complete expression for the susceptibility of the third order, the order which will be interesting here. This expression accounts correctly for all of the nonlinear resonances that can occur involving four different waves

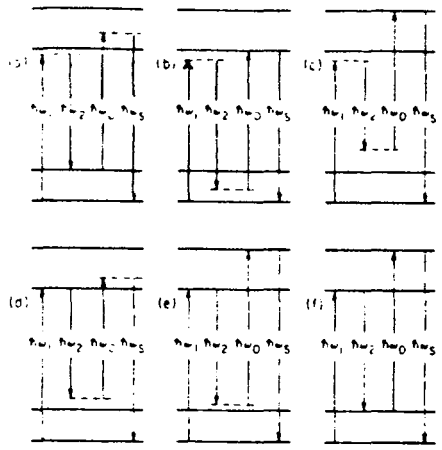

Fig. 3. Different conversion processes, resonant and non-resonant.

The different resonance situations [30] corresponds to different terms being important in the expression for the susceptibility tensor, X^3:

$$< v \mid \chi^{(3)}_{\alpha\beta\gamma\delta}(-\omega_p, \omega_0, \omega_1, -\omega_2) \mid u > \qquad (1)$$

This matrix element corresponds to the nonlinear susceptibility provided solely by transitions between state v and state u. The total third order nonlinear susceptibility tensor can then be written as

$$\chi^{(3)}_{\alpha\beta\gamma\delta}(-\omega_s,\omega_0,\omega_1,-\omega_2) = N \sum_{u,v} \left\langle v|\tilde{\chi}^{(3)}_{\alpha\beta\gamma\delta}(-\omega_s,\omega_0,\omega_1,-\omega_2)|u\right\rangle \rho^{e}_{uu} \qquad (2)$$

where ρ(uu)e is an equilibrium value of the density matrix, that is with the incident lasers turned off. The tensor matrix elements can be written as

$$\left\langle v|\tilde{\chi}^{(3)}_{\alpha\beta\gamma\delta}(-\omega_s,\omega_0,\omega_1,-\omega_2)|u\right\rangle = \frac{1}{48\hbar^3}(\tilde{\mu}_{um}\tilde{\mu}_{nv}\tilde{\mu}_{vm}\tilde{\mu}_{mu})$$

$$\times\left\{\frac{1}{[\tilde{\omega}_{vu}-(\omega_1-\omega_2)](\tilde{\omega}_{nu}+\omega_2)}\left(\frac{\delta_{\gamma\beta\alpha}}{\tilde{\omega}_{mu}-\omega_s}+\frac{\delta_{\gamma\alpha\beta}[1+\kappa_1(\Omega_3,\Omega_2)]}{\tilde{\Omega}^{*}_{mu}+\omega_0}\right)\right.$$

$$+\frac{1}{[\hat{\Omega}_{vu}-(\omega_1-\omega_2)](\hat{\Omega}_{nu}-\omega_1)}\left(\frac{\gamma\delta\beta\alpha}{\hat{\Omega}_{mu}-\omega_s}+\frac{\gamma\delta\alpha\beta[1+\kappa_1(\Omega_3,\Omega_1)]}{\hat{\Omega}^*_{mu}+\omega_0}\right)$$

$$+\frac{1}{[\hat{\Omega}_{vu}-(\omega_0-\omega_2)](\hat{\Omega}_{nu}+\omega_2)}\left(\frac{\delta\beta\gamma\alpha}{\hat{\Omega}_{mu}-\omega_s}+\frac{\delta\beta\alpha\gamma[1+\kappa_1(\Omega_1,\Omega_3)]}{\hat{\Omega}^*_{mu}+\omega_1}\right)$$

$$+\frac{1}{[\hat{\Omega}_{vu}-(\omega_0-\omega_2)](\hat{\Omega}_{nu}-\omega_0)}\left(\frac{\beta\delta\gamma\alpha}{\hat{\Omega}_{mu}-\omega_s}+\frac{\beta\delta\alpha\gamma[1+\kappa_1(\Omega_2,\Omega_1)]}{\hat{\Omega}^*_{mu}+\omega_1}\right)$$

$$+\frac{1}{[\hat{\Omega}_{vu}-(\omega_0+\omega_1)](\hat{\Omega}_{nu}-\omega_1)}\left(\frac{\gamma\beta\delta\alpha}{\hat{\Omega}_{mu}-\omega_s}+\frac{\gamma\beta\alpha\delta[1+\kappa_1(\Omega_1,\Omega_3)]}{\hat{\Omega}^*_{mu}-\omega_2}\right)$$

$$+\frac{1}{[\hat{\Omega}_{vu}-(\omega_0+\omega_1)](\hat{\Omega}_{nu}-\omega_0)}\left(\frac{\beta\gamma\delta\alpha}{\hat{\Omega}_{mu}-\omega_s}+\frac{\beta\gamma\alpha\delta[1+\kappa_1(\Omega_1,\Omega_2)]}{\hat{\Omega}^*_{mu}-\omega_2}\right)$$

$$+\frac{1}{(\hat{\Omega}^*_{vu}+\omega_1-\omega_2)(\hat{\Omega}^*_{mu}-\omega_2)}\left(\frac{\alpha\beta\gamma\delta}{\hat{\Omega}^*_{nu}+\omega_s}+\frac{\beta\alpha\gamma\delta[1+\kappa_2(\Omega_3,\Omega_2)]}{\hat{\Omega}_{nu}-\omega_0}\right)$$

$$+\frac{1}{(\hat{\Omega}^*_{vu}+\omega_1-\omega_2)(\hat{\Omega}^*_{mu}+\omega_1)}\left(\frac{\alpha\beta\delta\gamma}{\hat{\Omega}^*_{nu}+\omega_s}+\frac{\beta\alpha\delta\gamma[1+\kappa_2(\Omega_3,\Omega_1)]}{\hat{\Omega}_{nu}-\omega_0}\right)$$

$$+\frac{1}{(\hat{\Omega}^*_{vu}+\omega_0-\omega_2)(\hat{\Omega}_{mu}-\omega_2)}\left(\frac{\alpha\gamma\beta\delta}{\hat{\Omega}^*_{nu}+\omega_s}+\frac{\gamma\alpha\beta\delta[1+\kappa_2(\Omega_2,\Omega_3)]}{\hat{\Omega}_{nu}-\omega_1}\right)$$

$$+\frac{1}{(\hat{\Omega}^*_{vu}+\omega_0-\omega_2)(\hat{\Omega}_{mu}+\omega_1)}\left(\frac{\alpha\gamma\delta\beta}{\hat{\Omega}^*_{nu}+\omega_s}+\frac{\gamma\alpha\delta\beta[1+\kappa_2(\Omega_2,\Omega_1)]}{\hat{\Omega}_{nu}-\omega_1}\right)$$

$$+\frac{1}{(\hat{\Omega}^*_{vu}+\omega_0+\omega_1)(\hat{\Omega}^*_{mu}+\omega_1)}\left(\frac{\alpha\delta\beta\gamma}{\hat{\Omega}^*_{nu}+\omega_s}+\frac{\delta\alpha\beta\gamma[1+\kappa_2(\Omega_1,\Omega_3)]}{\hat{\Omega}_{nu}+\omega_2}\right)$$

$$+\frac{1}{(\hat{\Omega}^*_{vu}+\omega_0+\omega_1)(\hat{\Omega}^*_{mu}+\omega_0)}\left(\frac{\alpha\delta\gamma\beta}{\hat{\Omega}^*_{nu}+\omega_s}+\frac{\delta\alpha\gamma\beta[1+\kappa_2(\Omega_1,\Omega_2)]}{\hat{\Omega}_{nu}+\omega_2}\right)\Bigg| \qquad (3)$$

where the resonance frequencies could be complex, and the symbol $\alpha\beta\gamma\delta$ denotes the order of the cartesian components of the dipole matrix elements. Two correction factors appear in this expression

$$\kappa_1(\Omega_j,\Omega_k)=\frac{i(\Gamma_{vn}-\Gamma_{vu}-\Gamma_{un})+i(\Gamma_{mn}-\Gamma_{mu}-\Gamma_{un})(\hat{\Omega}_{vu}-\Omega_j)/(\hat{\Omega}_{mn}-\Omega_k)}{\hat{\Omega}_{vn}-\omega_s}$$

$$\kappa_2(\Omega_j,\Omega_k)=\frac{i(\Gamma_{vn}-\Gamma_{vu}-\Gamma_{un})+i(\Gamma_{mn}-\Gamma_{mu}-\Gamma_{un})(\hat{\Omega}^*_{vu}+\Omega_j)/(\hat{\Omega}_{mn}-\Omega_k)}{\hat{\Omega}^*_{vn}+\omega_s} \qquad (4)$$

with arguments $\Omega_1=\omega_0+\omega_1$, $\Omega_2=\omega_0+\omega_2$ and $\Omega_3=\omega_0+\omega_3$.

From eq (2), (3) it is evident that matrix elements from one state to itself contribute a new resonance peaked near $\omega_1-\omega_2=0$ or $\omega_0-\omega_2=0$. Generally two different kinds of resonances could be distinguished. The one-photon-type resonance occurs when a fundamental frequency or the output frequency is equal to the frequency of an one-photon transition of the material system. Two-photon-type resonances occur when the sum of two frequencies is equal to the frequency of an allowed two-photon transition of the system. One-photon resonances are not interesting because although the susceptibility is increased, the absorption will increase so much that the power of the generated light will decrease. On the other hand, for two-photon resonances the absorption will be small and it's therefore possible to increase the efficiency of the generated light.

1.3.1 Symmetries of the susceptibility tensor.

X^3 is a fourth rank tensor with 81 elements. Symmetries of the nonlinear medium could however reduce the number of independent nonvanishing elements. Since only rare gases are treated in this study, and since they are isotropic, which means that no direction is distinguishable from any other direction, only the isotropic case is considered.

Of the four vectors one can obviously fix one from the beginning, for instance the output polarization direction, since because of isotropy no direction is specific. 27 specific elements will then be left. Again because of isotropy you can't make any difference between left and right and hence elements as X_{1233} and X_{1322} must be the same. If you take into account the isotropy when doing quantum mechanical calculations of the susceptibility tensor you are left with only 21 nonzero elements of which only 4 have different values, namely X_{1111}, X_{1122}, X_{1212}, and X_{1221}. There are only three independent elements since these four elements fulfil the relationship

$$X_{1111} = X_{1122} + X_{1212} + X_{1221} \qquad (1)$$

This relation could be interpreted as a superposition of each of the directions, illustrated in the following figure.

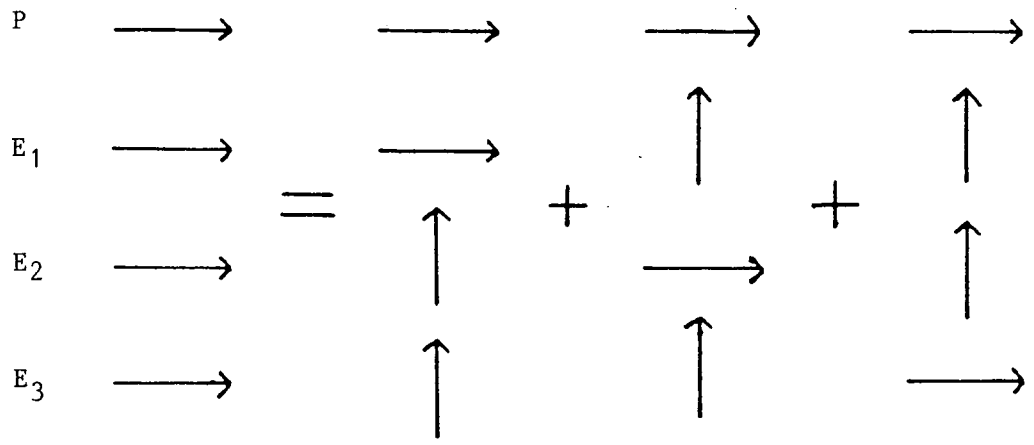

Fig.4 Illustration of the relationship (1), which is true in isotropic media. One arbitrary component of the polarization of the medium will be the same if you put on three E-fields in this direction at the same time, as if you take the sum of the contributions when one of them each time is parallel to the polarization direction while the other ones are orthogonal to it.

When the optical frequencies are much less than the frequencies of electronic transitions, the frequency arguments of the background (non-Raman-resonant) nonlinear susceptibility may be permuted separately from the polarization subscripts. This condition, termed Kleinmann symmetry implies furthermore that

$$X_{1122}=X_{1212}=X_{1221}=X_{1111}/3 \qquad (2)$$

From eq (8) [1.2] it's seen that the factor D, the number of indistinguishable permutations of the ω:s, together with X determinate the generated polarization. We will have different cases depending on the polarization of the incoming E-fields, which the following table shows:

E_0	E_1	E_2	$DX(eff)(-\omega_0 - \omega_1 + \omega_2, \omega_0, \omega_1 - \omega_2)$
↑	↑	↑	$6X_{1111}$
→	→	↑	$6X_{1221}$
↑	→	→	$6X_{1122}$
→	↑	→	$6X_{1212}$
↺	↻	→	$3i[X_{1122} - X_{1212}]$
→	↻	↻	$3i[X_{1212} - X_{1221}]$
↖	↗	→	$3[X_{1212}\sin\theta\cos\phi - X_{1122}\cos\theta\sin\phi]$

1.4 Generation of a new wave

The generated polarization created by the incident fields according to eq (7) [1.2] will give rise to a new electromagnetic wave at that frequency. This follows from the insertion of the polarization into the electromagnetic wave equation. Hence, the E-field of the created wave could be related to the incoming E-fields. In this section it is done for planar waves while more special cases are treated further on. The wave propagation equation is given by

$$\nabla \times \nabla \times E + \mu_0 \varepsilon_0 \frac{\partial^2 E}{\partial t^2} + \mu_0 \frac{\partial^2 P}{\partial t^2} = 0 \qquad (1)$$

where P is given by

$$P = \varepsilon X E + \text{nonlinear contributions in E} \qquad (2)$$

according to equations (7) and (8) [1.2].

If the nonlinear terms are small, it's convenient to move them to the right side of the equation (1). They can be regarded as new distributed source terms, contributing additional waves which, to a very good approximation, are superimposed on those of the homogeneous solution (appendix, [31]). The homogeneous solution consists of a linear combination of all the plane waves that can propagate in the lilinear medium at a certain frequency. If we apply the slowly varying envelope approximation, which means that the signal varies little within a distance equal to the wavelength of the light, and if we also treat the incident beams as uniform plane waves with amplitudes much bigger than the output amplitude, it's possible to derive the output signal amplitude ([27] p61)

$$E_s = \frac{-4\pi i}{n(\omega_p)} \frac{\omega}{c} p\, l\, P_0^{(n)}(\omega_p)\, \mathrm{sinc}((k_s - k_p)\tfrac{l}{2})\, e^{-i(k_s - k_p)l/2} \qquad (3)$$

The dipole moments at various positions within the sample add coherently to produce an appreciable output wave only when the wave-vector matching condition $|k_s - k_p| \ll \pi/l$ is fulfilled.

It is possible to relate the output power as a function of the input powers. For the special case of tripling we have:

$$P_3(L) \alpha N^2 |X^3(-3\omega,\omega,\omega,\omega)|^2 P^3 L^2 \mathrm{sinc}(\Delta kL/2) \qquad (4)$$

This equation, describing planar waves, where no absorption or scattering is present and when $P_3(0) = 0$, relates the output power P_3 at the frequency 3ω and at the position L in the interaction cell to the susceptibility X, the gas density N, the input power P and the wave-vector difference Δk. Δk is defined as $\Delta k = k(3\omega)-3k(\omega) = 3(\omega/c)(n_3-n_1)$, where n_1 and n_3 are the refractive indices at the frequency ω and 3ω respectively.

From the relation (4) we can see that the output power will have a maximum when $\Delta k=0$ which means that the induced polarization, propagating with the speed $c/n(\omega)$ and the generated VUV-wave, propagating with the speed $c/n(3\omega)$, have the same phase velocity. There will also be local maxima for $|\Delta kL| = 3\Pi + n$, $n=0,1,2,...$

For gases both N and X^3 are small (in contrast to solids) and it's necessary to have a high power laser input to get something measurable out. To describe the frequency conversion of the light from a high power laser it's impossible to use the planar wave description from above. Instead the spatial distribution of the intensity could, as a first approximation, be better described by a Gaussian distribution.

2. WAVE ANALYSIS OF BEAMS

In this section Gaussian waves will be discussed.

2.1 The wave equation

In laser beams the intensity is concentrated near the axis of propagation and the phase front is slightly curved.
Consider a field component u of the coherent light. It must satisfy the scalar wave equation

$$\Delta u + k^2 u = 0 \qquad (1)$$

where $k=2\Pi/\lambda$, the propagation constant in the medium. Light travelling in the z direction can be written

$$u = \Psi(x,y,z)\ \exp(-ikz) \qquad (2)$$

where Ψ is a slowly varying complex function, which represents the differences between the beam and a plane wave. Insertion of (2) in (1) assuming $\partial^2\Psi/\partial z^2 \approx 0$ gives the equation

$$\partial^2\Psi/\partial x^2 + \partial^2\Psi/\partial y^2 - 2ik\partial\Psi/\partial z = 0 \qquad (3)$$

It's easy to check that

$$\Psi = \exp\{-i(P+kr^2/2q)\} \tag{4}$$

is one solution, where $r = x^2 + y^2$. The parameter P(z) represents a complex phase shift which is associated with the propagation of the light beam and q(z) is a complex beam parameter. These two functions could be solved for if the solution (4) is put into eq (3), which gives

$$dq/dz = 1 \tag{5}$$

$$dP/dz = -i/q \tag{6}$$

Integration of eq (5) implies

$$q = q_0 + z \tag{7}$$

2.2 Propagation laws for the fundamental modes

The solution which was found above, is not the only solution to the wave quation, but an important one . It has a Gaussian intensity profile and it's often called the fundamental mode.

Two real beam parameters, R and ω, are introduced according to

$$1/q = 1/R - i\lambda/\pi\omega^2 \tag{8}$$

q is called the complex beam parameter.

Insertion of eq.(8) into eq.(4) makes it clear that R(z) is the radius of curvature of the wavefront that intersects the axis at z, and $\omega(z)$, often called the beam radius or the spot size, is the distance along a radius in the xy-plane, at which the amplitude decreases to 1/e times that on the axes, at the coordinate position z along the beam.

The gaussian beam contracts to a minimum diameter $2\omega_0$, at the beam

waist, where we set z=0. At this position q is pure imaginary since R=∞. Eq (7) together with

$$q_0 = i\pi\omega_0^2/\lambda \tag{9}$$

gives us

$$q = i\pi\omega_0^2/\lambda + z \tag{10}$$

If this equation is compared to eq (8) we get

$$\omega^2(z) = \omega_0^2\left[1+(\lambda z/\pi\omega_0^2)^2\right] \tag{11}$$

and

$$R(z) = z\left[1+(\pi\omega_0^2/\lambda z)^2\right] \tag{12}$$

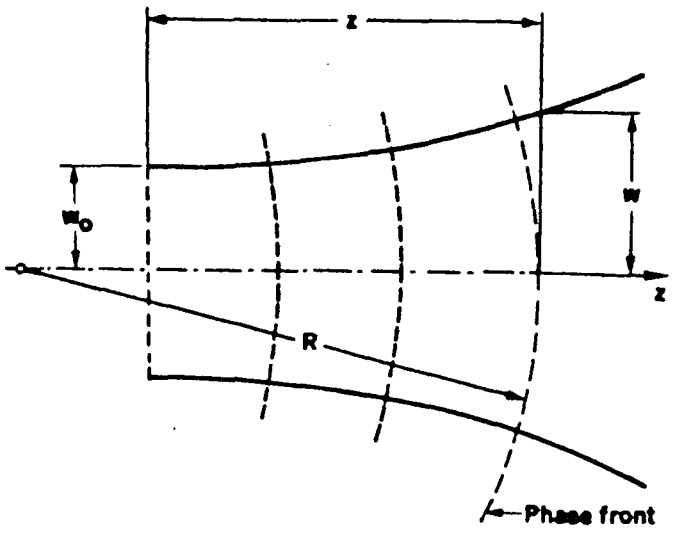

Fig.5 Propagation of a Gaussian beam. The beam radius and the phase front curvature radius are shown.

The beam contour ω(z) is a hyperbola with asymptotes inclined to the axis at an angle

$$\theta = \lambda/\pi\omega_0 \tag{13}$$

This is the far-field diffraction angle of the fundamental mode. Insertion of eq (10) into eq (6) makes it possible to evaluate the complex phase shift at a distance z away from the waist

$$dP/dz = -i/q = -i/\{z + i(\pi\omega_0^2/\lambda)\} \tag{14}$$

and if this relation is integrated, one yields the result

$$iP(z) = \ln[1-i(\lambda z/\pi\omega_0^2)] = (1/2)\ln\{1+(\lambda z/\pi\omega_0^2)^2\}-i\arctan(\lambda z/\pi\omega_0^2) \tag{15}$$

The real part of P represents a phase shift difference ϕ between the Gaussian beam and an ideal plane wave, while the imaginary part produces an amplitude factor ω_0/ω which gives the expected intensity decrease on the axis due to the expansion of the beam. The fundamental Gaussian beam can now be written in the form

$$u(r,z) = (\omega_0/\omega)\exp\{-i(kz - \phi) - r^2(1/\omega^2 + ik/2R)\} \tag{16}$$

where

$$\Phi = \arctan(\lambda z/\pi\omega_0^2) \tag{17}$$

3. EFFECTS OF FOCUSING ON THIRD-ORDER NONLINEAR PROCESSES IN ISOTROPIC MEDIA

3.1 Formulas for the generated E-field in three important cases

Consider three fundamental beams at ω_1, ω_2 and ω_3 which are assumed to be lowest order Gaussian modes, propagating concentrically along the z-axis with identical waist locations and identical confocal

parameters defined in below. The wave vectors of these beams in the nonlinear medium are taken as k_1, k_2 and k_3. The total E-field of these beams could be written

$$E(r,t) = Re\left[E_1(r)\exp(-i\omega_1 t) + E_2(r)\exp(-i\omega_2 t) + E_3(r)\exp(-i\omega_3 t)\right] \quad (1)$$

with

$$E_A(r) = E_{A_0}\exp(ik_A z)(1+i\varepsilon)^{-1}\exp\left[-k_A(x^2+y^2)/(b(1+i\varepsilon))\right] \quad (2)$$

if b, the confocal parameter, is defined by

$$b = 2\pi\omega_0^2/\lambda = 2\pi w_0^2 n/\lambda_0 = 2\lambda_0/n\theta^2 = k\omega_0^2 \quad (3)$$

where ω_0 is the beam-waist radius, n is the index of refraction, and λ_0 is the vacuum wavelength. Let E be a normalized coordinate along the z axis defined as

$$E = 2(z-f)/b \quad (4)$$

where f is the position of the focus, the beam waist, along the z-axis. Then E(r,t) in eq (1) has the same real part as u(r,z) in eq (16) [2.2]. In fact u(r,z) is the complex conjugate of E(r,z).
We will consider three interesting conversion processes:

I) $\omega_1 + \omega_2 + \omega_3 = \omega_4$
II) $\omega_1 + \omega_2 - \omega_3 = \omega_4$
III) $\omega_1 - \omega_2 - \omega_3 = \omega_4$

Suppose that the fundamental and generated beams are polarized in the same direction. This implies that the tensor nature of the susceptibility can be neglected. For these situations eq.(7) [1.2] gives us for the driving polarization at ω_4:

$$P_4(r,t) = Re\left[P_4(r)\exp(-i\omega_4 t)\right] \quad (5)$$

where for the three processes given above $P_4(r)$ =

$$\text{I)} \quad (3/2)NX(-\omega_4;\omega_1, \omega_2, \omega_3)E_1(r)E_2(r)E_3(r) \tag{6}$$

$$\text{II)} \quad (3/2)NX(-\omega_4;\omega_1, \omega_2,-\omega_3)E_1(r)E_2(r)E_3(r) \tag{7}$$

$$\text{III)} \quad (3/2)NX(-\omega_4;\omega_3,-\omega_2,-\omega_1)E_1(r)E_2(r)E_3(r) \tag{8}$$

When two or three of the input frequencies are degenerate, the factor of 3/2 in (6) - (8) must be changed to 3/4 or 1/4 respectively.

For each of the processes it's possible to insert the E-field expressions in eq (1), (2) into eq (6) - (8) and get an expression for the driving polarization at ω_4. The next step is to perform a spatial Fourier decomposition of $P_4(r)$ to determine the amplitudes of the plane-wave components of the driving polarization. From Maxwells equations, the generated radiation field arising from each plane-wave component can be obtained. The total generated E-field is then calculated through summing over all these contributions. The results are:

PROCESS I: $(\omega_1 + \omega_2 + \omega_3 = \omega_4)$

$$E_4(r) = i\frac{3N}{2k_4}\pi k_0^2 b\chi(-\omega_4, \omega_1, \omega_2, \omega_3)\, E_{10}\, E_{20}\, E_{30}\, e^{ik'z}\, (1 + i\varepsilon)^{-1} \cdot$$

$$\exp\frac{-k'(x^2 + y^2)}{b(1 + i\varepsilon)} \cdot \int_{-\zeta}^{\varepsilon} \frac{\exp\{(-ib/2)\Delta k(\varepsilon' - \varepsilon)\}}{(1 + i\varepsilon')^2} d\varepsilon' \tag{9}$$

$$\zeta = \frac{2f}{b}, \quad k' = k_1 + k_2 + k_3 \tag{10),(11}$$

PROCESS II: $(\omega_1 + \omega_2 + \omega_3 = \omega_4)$

$$E_4(r) = i\frac{3N}{2k_4} k_0^2 b\chi(-\omega_4, \omega_1, \omega_2,-\omega_3)\, E_{10}\, E_{20}\, E_{30}\, e^{ik'z} \cdot$$

$$\int_{-\zeta}^{\varepsilon} \frac{\exp -(ib/2)\Delta k(\varepsilon' - \varepsilon)}{(1 + i\varepsilon')(k'' - ik'\varepsilon')H} \exp\frac{-(x^2 + y^2)}{b \cdot H} d\varepsilon' \tag{12}$$

$$k'' = k_1 + k_2 + k_3 \tag{13}$$

$$k' = k_1 + k_2 - k_3 \tag{14}$$

$$\zeta = \frac{2f}{b} \tag{15}$$

PROCESS III: $(\omega_1 + \omega_2 + \omega_3 = \omega_4)$

$$E_4(r) = i\frac{3N}{2k_4}\, k\, b\, (-\omega_4, \omega_1, -\omega_2, -\omega_3)\, E_{10}\, E_{20}\, E_{30}\, e^{ik'z}$$
$$\int_{-\zeta}^{\varepsilon} \frac{\exp -(ib/2)\Delta k(\varepsilon' - \varepsilon)}{(1 + i\varepsilon')(k'' - ik'\varepsilon')H} \exp\{\frac{-(x^2 + y^2)}{b \cdot H}\} d\varepsilon' \tag{16}$$

$$k'' = k_1 + k_2 + k_3 \tag{17}$$

$$k' = k_1 - k_2 - k_3 \tag{18}$$

$$\zeta = \frac{2f}{b} \tag{19}$$

The function H is defined by

$$H = H(\varepsilon, \varepsilon') = \frac{(1 + \varepsilon'^2)}{k'' - ik'\varepsilon'} - i\,\frac{(\varepsilon' - \varepsilon)}{k'} \tag{20}$$

It can be seen from (9) that for the process $\omega_1 + \omega_2 + \omega_3 = \omega_4$, $E_4(r)$ is always a lowest order Gaussian mode with the same confocal parameter and waist location as the input beams. However (12), (16) show that for the other two processes $E_4(r)$ is not in general a single Gaussian mode except when $k'' = k'$. The multimode output of difference-mixing processes may be explained as resulting from the mismatch between the size of the driving polarization beam waist, and the size of the generated radiation beam waist. This mismatch may be represented by the ratio k''/k'. When $k''/k' = 1$, these beam waists are of the same size, and a lowest order Gaussian beam with the same confocal parameter and waist location as the input beams can be

produced. The sum-mixing process $\omega_1 + \omega_2 + \omega_3 = \omega_4$ always has $k''/k' = 1$ and thus always produces a lowest order Gaussian beam output.

3.2 A formula for the third harmonic Power in the Gaussian beam case

If the nonlinear medium is contained in a cell of length L with input window located at z=0 and with the location of the focus at z=f, then eq (9), (12) and (16) in [3.1] could be converted to expressions for the output power as a function of the input power by solving the integral $\int 2\pi r|E_4(r)|^2 dr$.

Define the dimensionless function F_A by

$$F_A(b\Delta k,\ b/L,\ f/L,\ k''/k') = \frac{8}{9}\frac{k_4^2 k'}{\pi^3 k_0^4}\frac{1}{b^3\chi^2|E_{10}E_{20}E_{30}|^2}\int_0^\infty 2\pi R|E_4(R)|^2 dR \quad (1)$$

where A = 1, 2 and 3 denotes the three considered processes. k' is defined as earlier specificly for each process. $\Delta k = k'' - k'$, the wave vector mismatch, with all wave vectors expressed in units of cm^{-1}, b in cm, N in atoms/cm^3, X in ESU/atom and with total power in Watts, the total power P_4 is given by

$$P_4 = (6.318\cdot 10^{-4})\, k_0^4 k_1 k_2 k/(k_4^2 k')N^2X^2P_1P_2P_3F_A(b\Delta k, b/L, f/L, k''/k') \quad (2)$$

where P_1, P_2 and P_3 are the total powers of each of the fundamental beams. When two or three of the input frequencies are degenerate, there will be an additional factor 1/4 or 1/36 respectively.

For each of the processes the integral expression for the corresponding F_A-function now will be given. In the tight focusing limit where b is short compared to the cell length L, it's possible to solve the integral in closed form. For the processes containing differences it's also assumed that k'' = k', and that the entire focal region is contained within the cell.

In the tight focusing limit where b<<L it's clear that ε(=E in

eq.(4)), $\zeta \to \infty$ according to eq (4) and eq (10) [3.1].

I. $\omega_1 + \omega_2 + \omega_3 \to \omega_4$

$$F_1(b\Delta k,\ b/L,\ f/L,\ k''/k') = \left| \int_{-\zeta}^{\varepsilon} d\varepsilon' \frac{\exp\{-(ib/2)\Delta k\varepsilon'\}}{(1 + i\varepsilon')^2} \right|^2 \tag{3}$$

$$F_1(b\Delta k,\ 0,\ 0.5,\ 1) = \begin{cases} \pi^2 (b\Delta k)^2 \exp(b\Delta k/2) & k<0 \\ 0 & k\geq 0 \end{cases} \tag{4}$$

II. $\omega_1 + \omega_2 - \omega_3 \to \omega_4$

$$F_2(b\Delta k,\ b/L,\ f/L,\ k''/k') = \frac{2k'}{\pi b} \int_0^{\infty} 2\pi R\, dR \left| \int_{-\zeta}^{\varepsilon} d\varepsilon' \frac{\exp\{(-ib/2)\Delta k\varepsilon'\}}{(1 + i\varepsilon')(k'' - ik'\varepsilon')H} \cdot \right.$$

$$\left. \exp\left\{\frac{-R^2}{b \cdot H}\right\} \right| \tag{5}$$

$$F_2(b\Delta k,\ 0,\ 0.5,\ 1) = \pi^2 \exp\{-b|\Delta k|\} \tag{6}$$

III. $\omega_1 - \omega_2 - \omega_3 \to \omega_4$

$$F_3(b\Delta k,\ b/L,\ f/L,\ k''/k') = \frac{2k'}{\pi b} \int_0^{\infty} 2\pi R\, dR \left| \int_{-\zeta}^{\varepsilon} d\varepsilon' \frac{\exp\{(-ib/2)\Delta k\varepsilon'\}}{(1 - i\varepsilon')(k'' - ik'\varepsilon')H} \right.$$

$$\left. \exp\left\{\frac{R^2}{bH}\right\} \right|^2 \tag{7}$$

For other values of the input parameters of F_A and for continuous variations of these, FFT calculations have been done to evaluate the F_A functions [8]. Some of these results will be shown in diagrammatic form in the next section.

3.2.1 Evaluation of the F_A-functions

The behaviour of the F_A near the tight focusing limit have been studied in detail. It was determined that when $b/L < 0.1$ and $b < L-b$, the F_A:s as functions of $b\Delta k$ may, to a good approximation, be represented by the curve for F_A versus $b\Delta k$ corresponding to the infinitely tight-focusing limit where $b/L = 0.0$, $f/L = 0.5$. For instance, the maximum deviation of the numerically computed $F_1(b\Delta k,0.1,0.5,1)$ from the analytically derived $F_1(b\Delta k,0,0.5,1)$ is less than 0.1 for all values of $b\Delta k$.

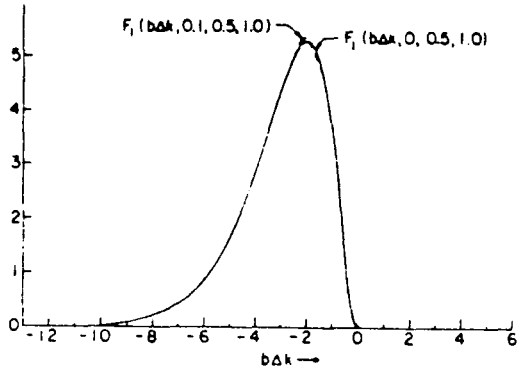

Fig. 6. F_1 versus $b\Delta k$ for $b/L < 0.1$ and $f/L = 0.5$.

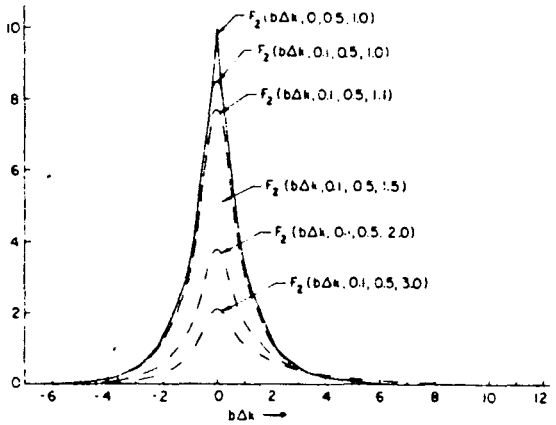

Fig. 7. F_2 versus $b\Delta k$ for $b/L < 0.1$; $f/L = 0.5$; and $k''/k' = 1.0$, 1.1, 1.5, 2.0, and 3.0.

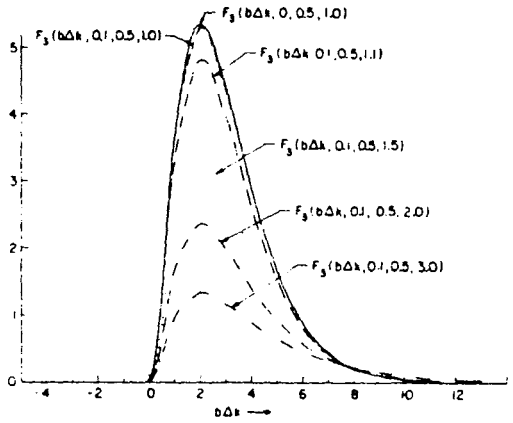

Fig. 8. F_3 versus $b\Delta k$ for $b/L < 0.1$, $f/L = 0.5$; and $k''/k' = 1.0$, 1.1, 1.5, 2.0, and 3.0.

We see that when b/L increases, some sidelobe structure appears far in the wings. However, as long as the fundamental beam-waist region is contained entirely in the cell, these sidelobes are always less than 0.1% of the magnitude of the peak value of F_A. In the case of very loose focusing, the F_A approaches the plane-wave limit:

$$F_A(b\Delta k, b/L, 0.5, k''/k') \rightarrow 4L^2/b^2 \cdot \mathrm{sinc}^2(\Delta kL/2) \text{ when } b/L \rightarrow \infty \qquad (1)$$

(compare eq (4) [I.1.4])

For the function F_1, the case of sum frequency generation, the complete evolution from the tight focusing limit to the plane-wave limit is demonstrated in the following two figures

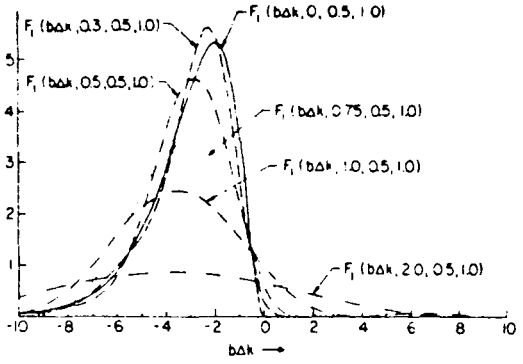

Fig. 9. F_1 versus $b\Delta k$ for f/L = 0.5 and b/L = 0, 0.3, 0.5, 0.75, 1.0, and 2.0.

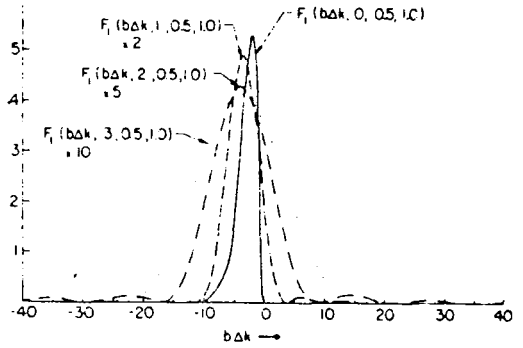

Fig. 10. F_1 versus $b\Delta k$ for f/L = 0.5 and b/L = 0, 1, 2, and 3.

We observe the decrease of the peak value for looser focusing. The peak is also shifted towards lower values of $b\Delta k$. For the cases b/L = 2 and 3 it's possible to observe the sidelobe structures.

We now observe the influence of the location of the focus, the variation of the value of f/L. Fig 6 shows that, for tight focusing, F_A versus $b\Delta k$ is relatively unchanged as long as the fundamental beam-waist region is entirely contained within the cell. Fig 10 illustrates that, for b much larger than L, F_A versus $b\Delta k$ is relatively unchanged as long as the cell is located close to the

beam-waist location. Figs 7-9 show the intermediate cases. In every case the location of the peak of the F_A lies very near to $b\Delta k = 0$ when the beam-waist location is far outside of the cell.

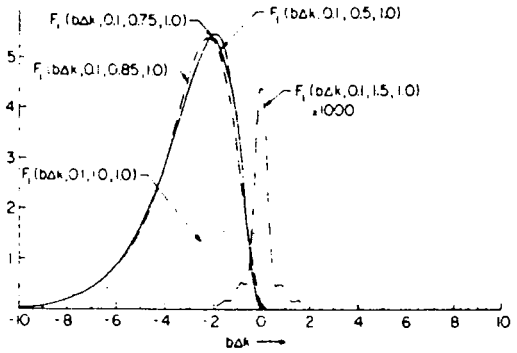

Fig. 11. F_1 versus $b\Delta k$ for b/L = 0.1 and f/L = 0.5, 0.75, 0.85, 1.0, and 1.5.

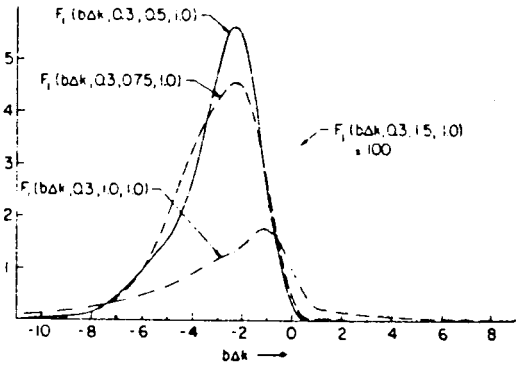

Fig. 12. F_1 versus $b\Delta k$ for b/L = 0.3 and f/L = 0.5, 0.75, 1.0, and 1.5.

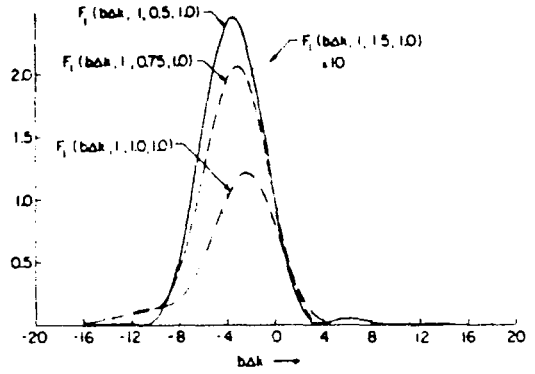

Fig. 13. F_1 versus $b\Delta k$ for b/L = 1 and f/L = 0.5, 0.75, 1.0, and 1.5.

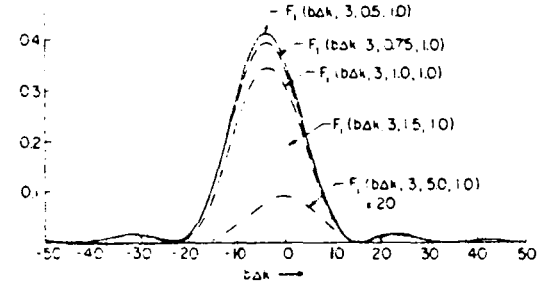

Fig. 14. F_1 versus $b\Delta k$ for b/L = 3 and f/L = 0.5, 0.75, 1.0, 1.5, and 5.0.

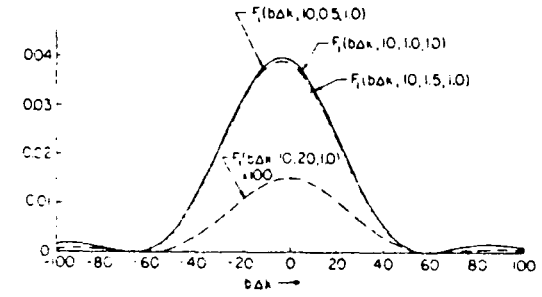

Fig. 15. F_1 versus $b\Delta k$ for b/L = 10 and f/L = 0.5, 1.0, 1.5, and 20.0.

For the processes $\omega_1 + \omega_2 - \omega_3 \rightarrow \omega_4$ and $\omega_1 - \omega_2 - \omega_3 \rightarrow \omega_4$, where k"/k' is not equal 1, there will be a multimode output although the input is a Gaussian [3.1]. The far-field intensity distribution will however be

Gaussian. This Gaussian shape evolves to a circularly symmetric ring pattern as $b\Delta k$ becomes large and positive.

3.3 Optimization in the tight focusing case

Consider the case of tight focusing ($b/L < 0.1$) with the fundamental beam-waist region entirely contained in the cell. Neglect limiting processes as pump depletion, absorption, breakdown, saturation, thermal defocusing and the quadratic Kerr effect. The total generated power is given by eq (2) [3.2]. The parameters P_1, P_2, P_3, X and k''/k' are considered to be constant and then the optimization procedure reduces to maximizing the quantity $N^2F_A(b\Delta k, b/L, f/L, k''/k')$ by varying the parameters N, $b\Delta k$, b/L and f/L. When N is a parameter which is independent of $b\Delta k$, b/L, and f/L the optimization procedure simplifies to increasing N to the highest possible value while independently maximizing F_A according to Fig 6,7 and 8 [3.2.1], $b\Delta k$(optimal)=

$$\begin{aligned} &-2 \text{ for } \omega_1 + \omega_2 + \omega_3 \rightarrow \omega_4 \\ &\ 0 \text{ for } \omega_1 + \omega_2 - \omega_3 \rightarrow \omega_4 \\ &\ 2 \text{ for } \omega_1 - \omega_2 - \omega_3 \rightarrow \omega_4 \end{aligned} \qquad (1)$$

The parameter $b\Delta k$ may be adjusted to its optimum value by means of altering b or Δk. The value of b may be altered by varying the focus, as long as $b/L < 0.1$, the tight-focusing approximation assumed in this section. In order to make Δk a parameter (which in this case is assumed to be independent of N) another medium with negligible nonlinearity but appreciable dispersion may be mixed with the nonlinear medium. The procedure of optimizing by adjusting b is valid only if the nonlinear medium can tolerate the high-power density introduced by very tight focusing. If this is not possible, the best compromise is to reduce b to the smallest permissible value and then to adjust Δk to reach $b\Delta k$(optimal). It's particularly important to note that the process $\omega_1 + \omega_2 + \omega_3 \rightarrow \omega_4$ requires that $b\Delta k$ is nonzero and positive while the process $\omega_1 - \omega_2 - \omega_3 \rightarrow \omega_4$ requires that $b\Delta k$ is

nonzero and negative.

Different optimization procedures are required when N is a parameter which is not independent of bΔk. One important case occurs when Δk is constrained to be proportional to N while b is constrained to be constant and N is a free parameter. In this case $\Delta k^2 F_A(b\Delta k, b/L, f/L, k''/k')$ must be maximized. This quantity however depends on the absolute value of b: It's therefore appropriate to define the dimensionless function

$$G_A(b\Delta k,\ b/L,\ f/L,\ k''/k') = (\Delta kb)^2 F_A(b\Delta k,\ b/L,\ f/L,\ k''/k') \qquad (2)$$

and then maximize $(1/b^2)G_A$.

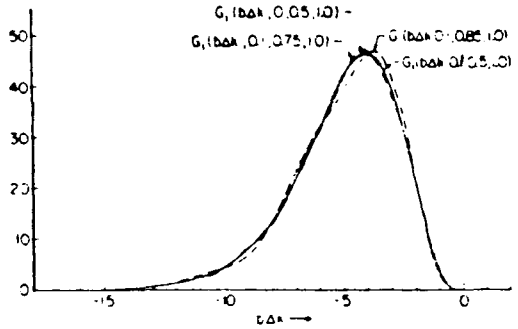

Fig. 16. G_1 versus bΔk for b/L < 0.1 and f/L = 0.5, 0.75, and 0.85.

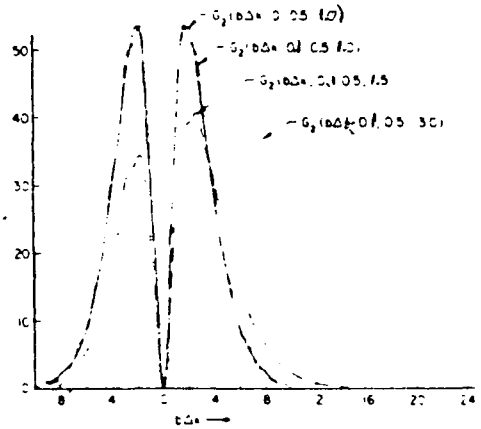

Fig. 17. G_2 versus bΔk for b/L < 0.1; f/L = 0.5; and k"/k' = 1.0, 1.5, and 3.0.

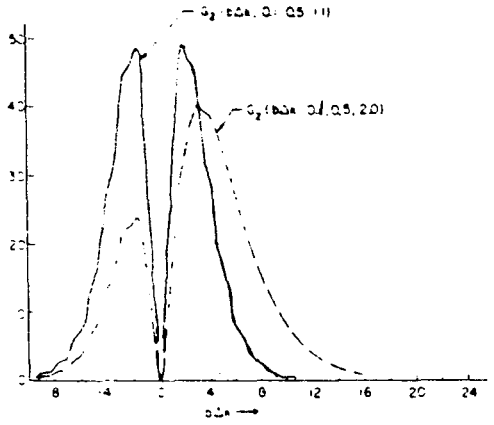

Fig. 18. G_2 versus $b\Delta k$ for $b/L < 0.1$; $f/L = 0.5$; and $k''/k' = 1.1$ and 2.0.

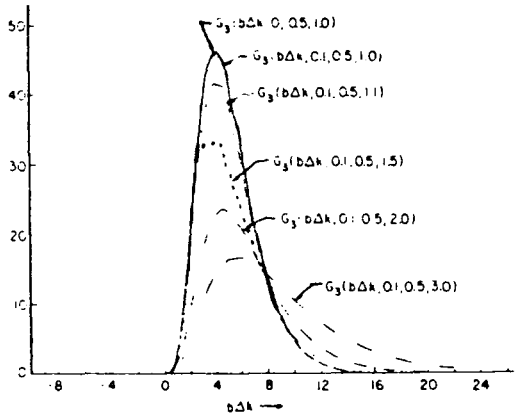

Fig. 19. G_3 versus $b\Delta k$ for $b/L < 0.1$; $f/L = 0.5$; and $k''/k' = 1.0$, 1.1, 1.5, 2.0, and 3.0.

Here it's apparent, as in the case of the F_A, that the value of b/L in the G_A may to a good approximation be replaced by 0 for $b/L < 0.1$. In addition, for tight focusing, the G_A:s are independent of the value of f/L as long as the entire input beam-waist region is contained within the cell.

Since N is the only free parameter, the optimization procedure is to adjust $b\Delta k$ to maximize G_A by adjusting N. Define α according to $\Delta k =$

αN. Then the optimization procedure reduces to adjusting N to the value N(opt)=(bΔk)(opt)/αb. Eq (2) [3.2] and eq (2) [3.3] now gives a formula for the total generated power in this optimized case.

$$P_4 = (6.318\cdot10^{-4})\cdot k_0^4 k_1 k_2 k_3/(k_4 k')\cdot X^2 P_1 P_2 P_3 G_A/(\alpha^2 b^2) \qquad (3)$$

where G_A has the peak values according to fig 16 - 19. In order to reach this optimized condition, α must be negative for the process I while α must be positive for the process III. For the process II, α may be either negative or positive.

In the VUV and soft X-ray spectral regions, index of refraction data (see the next section) are often completely lacking, and even the sign of the wave-vector mismatch produced by various media may be unknown. In this case, if Δk is of the wrong sign and/or if b is of the wrong value, the efficiencies of the processes I and III may be reduced by several orders of magnitude. Thus the process II with very tight focusing has the highest probability of successfully producing a sufficient output for detection. If, on the other hand, b>>L, the sum frequency beam could be represented by plane waves and there are no restrictions on the dispersion. Also in the case b=L it's possible to get a sum frequency wave in the positively dispersive regions of the spectrum although the value of F_1 is less than 20% of its peak value which occurs in the negatively dispersive regions.

3.4 Calculations of the refractive index n

We have seen earlier that in the case of sum frequency generation with a tightly focused beam,it's required that the nonlinear medium is negatively dispersive. Ergo there is a need of data of the refractive index as a function of wavelength. This is also needed for calculating the wave vector mismatch Δk.

Refractive indices are evaluated by summing the contributions, (n-1)(lines), due to the allowed transitions from the $p^6\ {}^1S_0$ ground state of the inert gases and (n-1)(cont) obtained by integration

through the continuum. The former requires knowledge of the absorption oscillator strengths and the latter requires detailed photoionization cross-sectional data. The standard Sellmeier formula [M. Born and E. Wolf, Principles of Optics. New York: Pergamon 1959, p.95] gives the refractive index at wavelength λ(cm) due to N atoms/cm^3.

$$(n-1)(\text{lines}) = (N\cdot r/2\pi)\Sigma(f_A/(\lambda_A^{-2} - \lambda^{-2})) \qquad (1)$$

where $r=2.818\cdot10^{-3}$ cm is the classical electron radius, f_A is the absorption oscillator strength of the Ath transition, and λ_A(cm) is the wavelength of the Ath transition. Likewise, the contribution to the refractive index due to the continuum is given by

$$(n-1)(\text{cont}) = (N/2\pi^2)\int(\sigma d\nu_A/(\nu_A^2 - \nu^2)) \qquad (2)$$

where σ(cm^2) is the photoionization cross section and ν(cm^{-1}) = λ^{-1}. For calculations, experimentally oscillator strengths and photoionization cross sections are used.

Calculations of refractive indices for Argon, Krypton and Xenon have been performed [32]. From these data the k vector mismatch per atom for frequency tripling, C, which is defined by $\Delta k = CN = 2\pi(n_1 - n_3)/\lambda$ where λ is the vacuum wavelength of the generated harmonic wave, have been computed. The results are shown in the following figures:

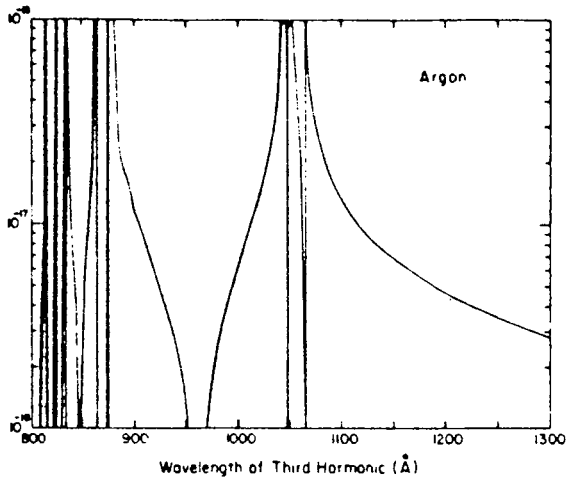

Fig. 20. Wave vector mismatch per atom for frequency tripling in Argon versus wavelength of the generated third harmonic.

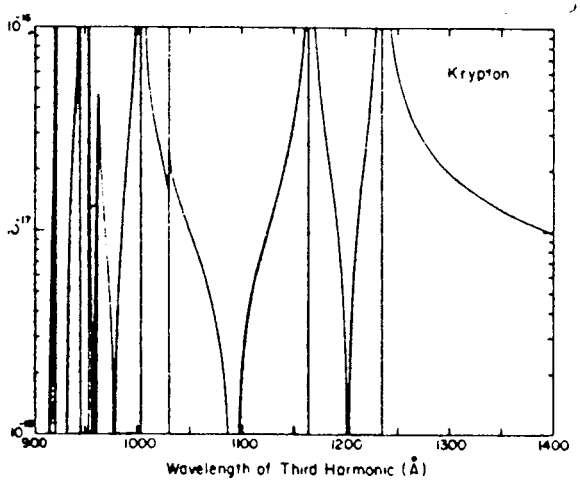

Fig. 21. Wave vector mismatch per atom for frequency tripling in Krypton versus wavelength of the generated third harmonic.

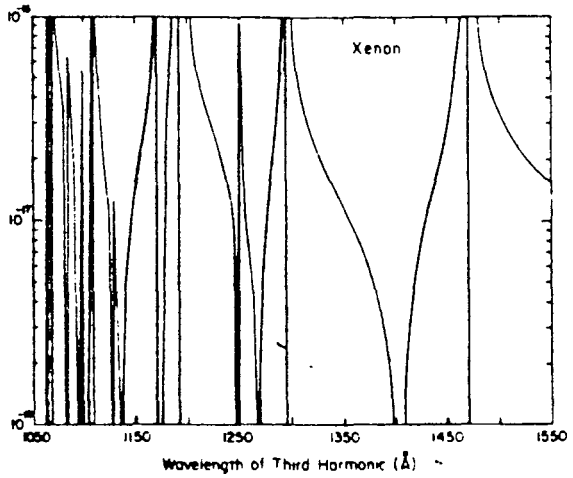

Fig. 22. Wave vector mismatch per atom for frequency tripling in Xenon versus wavelength of the generated third harmonic.

If another sum frequency generation method is used than tripling, the k vector mismatch per atom, will of course be different. It can however be calculated in the same way from the refractive index data.

3.5 Optimization by mixing

When the output frequency lies above the main resonance line and the input frequencies lie below, the atomic medium producing the harmonic generation can have an index of refraction at the sum frequency that is less than that at the fundamentals. Correct phase matching can then be achieved by adding a normally dispersive gas to the medium until

$$3n(\omega_0 + \omega_1 + \omega_2) = n(mix)(\omega_0) + n(mix)(\omega_1) + n(mix)(\omega_2) \qquad (1)$$

However, as we have seen earlier for different kinds of processes and focusings, optimum phase matching need not give maximum sum frequency generation in these systems. For instance, in the usual tight focusing geometry, there is a phase shift in the fundamental from one side of the focus to the other. Perfect phase matching results in a destructive interference between the waves radiated on each side of

the beam waist. Collisional effects due to the index matching gas tend to populate excited states, destroy coherence, and broaden absorptions. Such phenomena reduces the output signal beyond a certain point, by more than improved phase matching can enhance it. In [32] and [18] there are some additional theory and experimental research done on enhanced production of VUV radiation by frequency tripling in Kr where positively dispersive media as Ar, Xe are used for phase matching.

3.6 Frequency conversions of higher orders

As we have seen earlier, frequency conversion occurs as a result of nonlinear terms in the dielectric response function of a medium to incident radiation. For incident fields that are much weaker than the intra-atomic fields that bind the electrons in the atoms, the dielectric response in the dielectric dipole approximation can be written as

$$P = X^{1} \cdot E_A + X^{2} \cdot E_A E_B + X^{3} \cdot E_A E_B E_C + \ldots \qquad (1)$$

where the E_A:s are the electric fields of the incident optical waves, and the coefficients, X^A, are the susceptibilities of the medium of various orders. As we saw earlier the isotropic rare gases, which are used in the experimental part of this work, only contain odd contributions in this series expansion and hence the lowest nonlinear order is three. There will however also be generation of the fifth harmonic, the seventh harmonic and so on. The relative conversion to harmonics of different orders is determined by a combination of phase matching parameters, pump intensities and the behaviour of the nonlinear susceptibilities. Conversion to higher order harmonics can be favoured over conversion to lower-order ones through proper choice of the phase matching parameters.

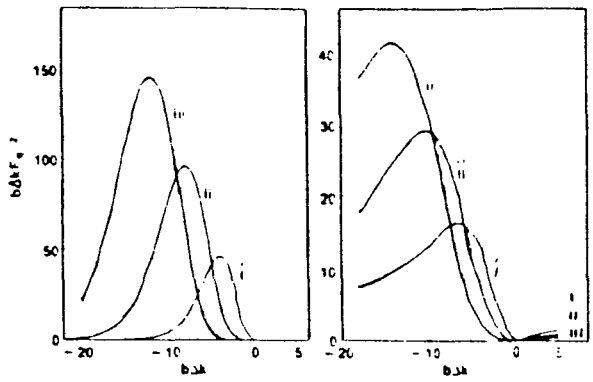

Fig. 23. Variation of the quantity $|G|^2 = |b\Delta kF|^2$ with $b\Delta k$ for the third (i), fifth (ii), and seventh (iii) harmonics. Beam is focused (left) to center of infinite medium, (right) at edge of semi-infinite medium extending to one side of the beam waist.

This figure shows that the optimum value on $b\Delta k$ depends of the order of the harmonic. In fact optimum frequency conversion occurs for a phase mismatch given by $b\Delta k = -(2q-2)$, for the qth harmonic at sum frequency generation, when dealing with Gaussian beams, in the tight focusing limit. (Compare eq (1) [3.3].) In addition, the power series expansion of (1) indicates that at sufficiently high pump intensities the nonlinear polarization generated in the higher-order interactions can be larger than that generated in the lower-order ones. If the magnitude of the susceptibilities decrease uniformly with increasing order, as for example in media with no resonant enhancements in any order, this condition will not usually be met unless the assumptions leading to the pertubation expansion (1) are violated. However, in media in which certain higher-order susceptibilities contain resonant enhancements, that are not present in the lower-order ones, larger nonlinear polarizations can be generated in the higher-order interactions than in the lower-order ones, without violating the assumptions of the pertubation theory. In principle then the higher-order interactions can be as effective as the lower-order ones in generating new radiation under certain circumstances. They allow, for instance, a larger step along the frequency scale to be taken in a

single conversion process. In practice, however, other nonlinear effects can and usually do become important at high pump intensities, which effectively limit the conversion efficiency that can be obtained in a given frequency conversion process. In such situations it may be impossible to obtain significant power in the higher-order harmonics before the conversion process is limited. Some experiments in He gas are discussed in [15]. The results from these experiments are among other things that the conversion to the fifth harmonic was favoured over conversion to the third by a near five-photon resonance between the ground state and the $1s3s\,^1P_0$ level that enhanced the fifth-order susceptibility but not the third. This shows that conversion to a higher-order harmonic can be as effective as conversion to a lower-order one in particular media. They furthermore indicate that different harmonics can be favoured in different media, depending on the relation of the wavelengths and the energy levels.

4. EFFECTS OF DIFFERENT SPATIAL MODES ON THIRD HARMONIC GENERATION

4.1 Introduction

We have until now only studied third harmonic generation where the input beams have been Gaussian. The laser beam usually consists of many different modes. It could therefore be fruitful to consider third harmonic generation where the input beams are of higher spatial order. It is then possible to quantify the effect of mode structure on the conversion efficiency. It's also necessary if you want to determine absolute values of some quantities: Reliable determinations of refractive indices from phase-matching curves and third-order susceptibilities from absolute efficiencies of third harmonic generation depend critically upon the knowledge of the spatial structure of the generating field.

In this chapter only tripling of a monochromatic laser beam focused

into a cell containing an isotropic, nonlinear gas is considered. The situation is further restricted to the case where the laser output consists of a single spatial mode. The mode structure, the power of the generated radiaton and the variation of phase matching requirements with the input mode are then treated.

4.2 Solutions to the wave equation in the Cartesian and the polar case

We saw in [2.1] that (4) is one solution to (3) but not the only one. With the help of other solutions, it's possible to form a complete and orthogonal set of functions, the modes of propagation, which are solutions to (3) [2.1]. Every arbitrary distribution of monochromatic light can then be expanded in terms of these modes. In [33] the mode structures in a Cartesian system are studied and related to it's origin, the resonator. It's argued that under certain conditions the mode functions must be invariant under a Fourier transform and that a product of a Gaussian function with a Hermite polynomial fulfills this requirement. A more general solution to (3) in [2.1] could therefore be written

$$\Psi(x,y,z) = H_A(\sqrt{2}\cdot x/\omega)\cdot H_B(\sqrt{2}y/\omega)\cdot\exp\{-i[P + (k/2q)(x^2+y^2)]\} \qquad (1)$$

where H_A is a Hermite polynomial of order m satisfying the differential equation

$$d^2H_A/dx^2 - 2x\cdot dH_A/dx + 2A\cdot H_A = 0 \qquad (2)$$

The numbers A and B in (1) are called the (transverse) mode numbers.

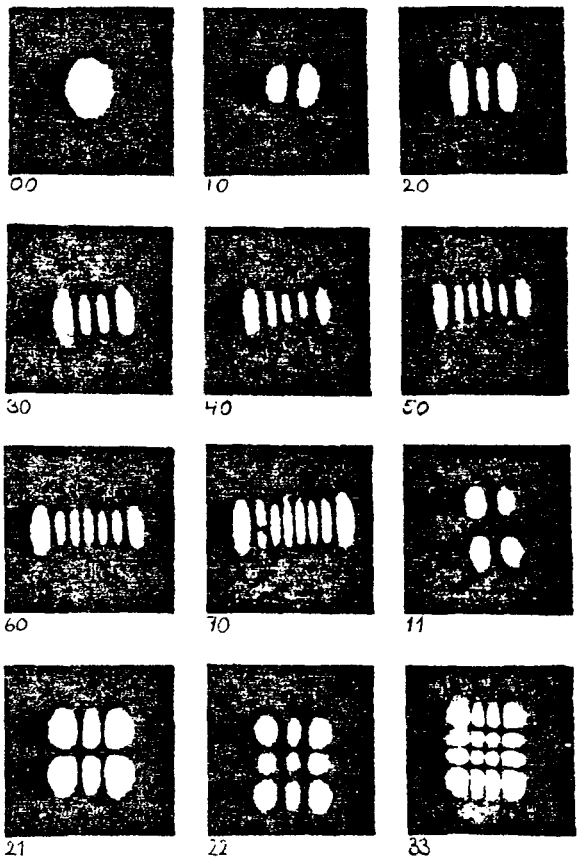

Fig. 24. Mode patterns of a gas laser oscillator. The mode numbers corresponds to a rectangular symmetry.

The number of zeros in a mode pattern is equal to the corresponding mode number and the area occupied by a mode increases with the mode number. The parameter R(z) in (12) [2.2] is the same for all modes, implying that the phase-front curvature is the same and change in the same way for modes of all orders. The phase shift Φ in (16) [2.2] is however a function of the mode numbers:

$$\Phi(A,B,z) = (A + B + 1)\cdot\arctan(\lambda z/\pi\omega_0^2) \qquad (3)$$

This means that the phase velocity increases with increasing mode number. In resonators this leads to differencies in the resonant frequencies of the various modes of oscillation.

For a system with a cylindrical (r,Φ,z)-geometry, one finds a solution to (3) [2.1] of the form:

$$\Psi(r,\theta,z) = (\sqrt{2}\cdot r/\omega)^A \cdot L_B^A(2\cdot r^2/\omega^2)\cdot\exp\{-i(P + kr^2/2q + l\Phi)\} \qquad (4)$$

where L_B^A is a generalized Laugerre polynomial satisfying the differential equation

$$x\cdot d^2L_B^A/dx^2 + (A + 1 - x)\cdot dL_B^A/dx + B\cdot L_B^A = 0 \qquad (5)$$

B and A are the radial and angular mode numbers. As in the case of beams with a rectangular geometry, the beam parameters $\omega(z)$ and $R(z)$ are the same for all cylindrical modes. The phase shift is again dependent on the mode numbers and is given by

$$\Phi(A,B,z) = (2B + A - 1)\cdot\arctan(\lambda z/\pi\omega_0^2) \qquad (6)$$

4.3 The power of the generated radiation

For the further analysis we now assume that the generating electric fields $E_1(r)$, $E_2(r)$, and $E_3(r)$ all have the same frequency ω, the case of tripling. They are also polarized in the same direction. Since the nonlinear medium is isotropic the third-order susceptibility tensor is reduced to a scalar form. The calculations are performed in [34] from p 2472, and I will only give the general idea of their performance. The generating E-fields are expressed in terms of the different mode functions and the polarization that they give rise to, are calculated. With the help of the spatial Fourier transform of the polarization it's possible to calculate the generated E-field from each Fourier component, and then accordingly, for the total polarization with the help of the inverse Fourier transform, the series expansion of the Laugerre polynomials, the binomial expansion and mathematical properties of the Γ-function. In general the electric field can only be evaluated numerically. However, in the case of tight

focusing, which will be assumed here

$$f >> b/2,\ L >> b/2 + f \quad <=> \quad b << f,\ f << L \tag{7}$$

further simplifications are possible. Residue calculations of an integral in the lowest order approximation gives a nice expression for the generated E-field. Since all the spatial modes form a complete set of functions, the generated electric field can be written as a linear combination of these modes. Mathematically all powers of $(2r^2/\omega^2)$ are expanded in terms of the Laugerre polynomials $L_B^A(2r^2/\omega^2)$. From the received formula for the E-fields it's rather easy to derive the corresponding formula for the powers if the relation

$$E = \mathrm{sqrt}\left[16/c\omega_0^2)(B!/((B+A)!)^3)P\right] \tag{8}$$

is used.

The total power P_4 of the third harmonic, as generated under tight focusing in a nonlinear medium and as measured in vacuum, can be readily evaluated:

$$P_4 = (c/8\pi)\iint|E_4(r)|^2 r dr d\Phi = (c/8\pi)|D|^2\Sigma|F(\rho)|^2\ D'F' \tag{9}$$

where

$$D' = (c/8\pi)|D|^2 = (16/c^2)\pi^4N^2X^2k_0^4k_1^3/(k_4^2k')\ P_1P_2P_3 \tag{10}$$

and

$$F' = \Sigma|F(\rho)|^2 \tag{11}$$

The function F is given in eq.(43), (44) p. 2475 and eq.(49) p. 2476 in [34]. It depends on a mode number and other geometrical beam parameters, but the analytical expression is too long and boring to write down here.

The function F' includes all the effects of mode structure, phase

matching and geometry on the conversion efficiency, while D' includes the effects of atomic parameters, laser power and number density. The results to this point are that it's possible to generate a third harmonic field in the tight-focusing situation only for negative values of $\Delta k = k_4 - k' = k_4 - 3k_1$. The beam waist of the generated field is smaller than that of the generating field by a factor $1/\sqrt{3}$. The coefficient of the amplitude of the different modes is given by $F(\beta)$, where β is the radial mode number summed over from 0 to $B_1+B_2+B_3$. Thus fundamental beams having nonzero radial mode numbers always generate fields which are a mixture of radial modes. However the angular mode number α has a fixed value of $A_1 + A_2 + A_3$, so that the angular mode of the generated field is completely determined by the angular mode numbers of the incident fields.

Two simplifying cases, 1) $B_1 = B_2 = B_3 = \beta = 0$, $A_1 = A_2 = A_3 = \alpha$ and 2) $B_1 = B_2 = B_3 = \beta = 1$, $A_1 = A_2 = A_3 = 0$ will be considered before computed results for the general higher-order pure mode are discussed.

4.3.1 Pure Angular Modes

The generated power of the third harmonic of a pure angular mode (β=0) of order α is according to eq (9) - (12) [4.3]

$$P_4 = D'F' \tag{1}$$

where

$$D' = (16/c^2)\pi^4 X^2 k_0^4 k_1^3 P_1^3 / k_2^4 k' \tag{2}$$

$$F' = |b\Delta k|^2 \exp(|-b\Delta k|(3\alpha)!/(3^3\ (\alpha!)^3) \tag{3}$$

From this we can see that the generated power has the same functional dependence on $b\Delta k$ for all pure azimuthal modes which have the same confocal parameter b, wave vector k, and incident power P_1. The magnitude of P_4 is proportional to $(3\alpha)\alpha/3^3\ (\alpha!)^3$, and so it results

in a lower generated power for the higher-order modes.

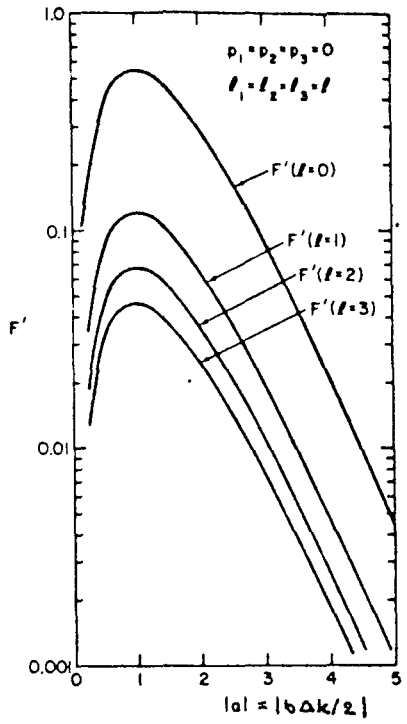

Fig. 25. Power coefficient F'as a function of $|b\Delta k|$ for pure angular modes TEM_{01} for l = 0, 1, 2, and 3

For the case $\alpha = 0$, the formulas (9) - (12) correspond to the earlier Gaussian case.

4.3.2 Radial (β=1) mode

The incoming is a pure radial mode where $B_1 = B_2 = B_3 = \beta = 1$ and $A_1 = A_2 = A_3 = 0$. According to the general equations (9) - (12) [4.3], there will be generated fields of different radial modes.

The strength of each mode could be characterized by the generated mode coefficients $F(\rho)$ from eq (12) [4.3]

$$F(3) = (4/9)\cdot\exp(-|b\Delta k|) \qquad (1)$$

$$F(2) = 0 \tag{2}$$

$$F(1) = (2/9)\cdot(3|b\Delta k| - 6|b\Delta k|^2 + 2|b\Delta k|^3)\exp(-|b\Delta k|) \tag{3}$$

$$F(0) = -(2/9)\cdot(4|b\Delta k| - 12|b\Delta k|^2 + 8|b\Delta k|^3 - (4/3)|b\Delta k|^4)\exp(-|b\Delta k|) \tag{4}$$

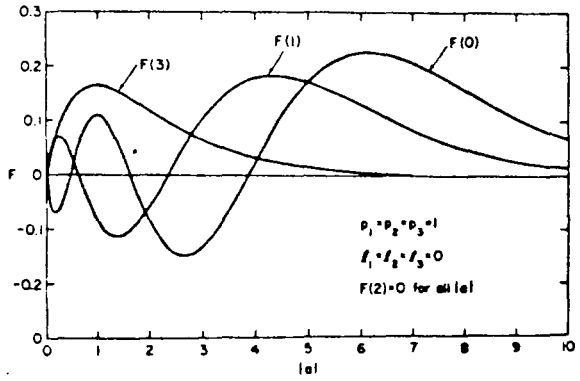

Fig. 26. Mode coefficients F(ρ) of the generated field for a TEM_{10} mode.

4.3.3 General pure mode

With the help of a computer the generated mode coefficients, F(ρ), and the power, F', have been calculated.(ref [34] p2479)

Consider third harmonic generation by an incident monochromatic beam having a pure cylindrical spatial mode of radial order $\beta = B_1 = B_2 = B_3$ and angular order $\alpha = A_1 = A_2 = A_3$. As before we are only considering the tight focusing situation where tripling only occurs in a negatively dispersive medium, $\Delta k < 0$. The generated beam is composed of a superposition of cylindrical modes having a beam waist $1/\sqrt{3}$ times that of the incident wave. The azimuthal character of the generated wave is determined by that of the incident beam and the generated azimuthal mode number is equal to $A_1 + A_2 + A_3$. On the other hand, the generated radial mode is a mixture of modes having a radial mode number β in the range from zero to $B_1 + B_2 + B_3$. For the pure input

mode $TEM_{BA}(B_1=B_2=B_3=\beta,\ A_1=A_2=A_3=\alpha)$ the generated mode has a zero contribution from the $TEM_{3B-1\ 3A}$ mode. However, this is not a general feature for the mixed-mode case where B_1, B_2 and B_3 not have the same values. The generated power follows the curve F' in the situation where phase matching is accomplished without varying N. Thus, to optimize the generated power, one phase-matches at the peak of the F' curve. For a single negatively dispersive medium, where N is proportional to Δk, phase is achieved by varying the total pressure. The optimum power is then generated by maximizing $G = |b\Delta k|^2 \cdot F'$ instead. The function $F(\rho)$ gives the coefficient of the mode $TEM_{B\ 3A}$, contributing to the generated wave as a function of $|a| = (1/2)|b\Delta k|$.

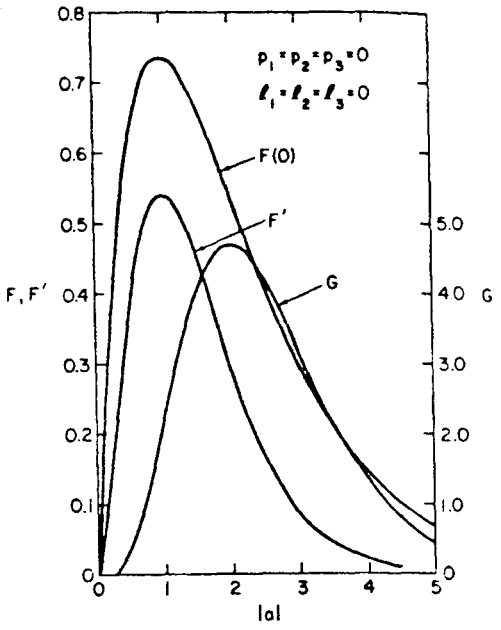

Fig. 27. Mode coefficient F(0) and power coefficients F' and G as functions of $|a| = |b\Delta k|/2$ for the fundamental Gaussian mode TEM_{00}.

F' has a peak at $|a| = 1$ and the generated mode is also a pure TEM_{00}. Only F(0) is present. (Compare fig.25)

It's seen that the angular modes peak at the same value of $|a| = 1$ as the fundamental beam but that the efficiency is continuously decreasing as the mode order increases.

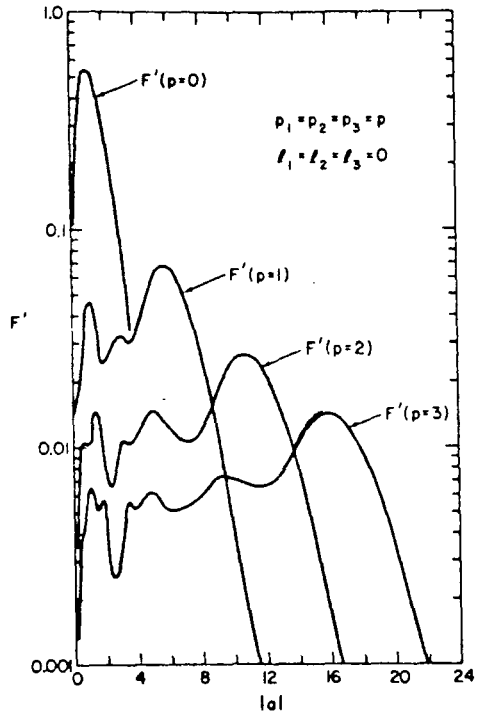

Fig. 28. Power coefficient F´as a function of $|a| = |b\Delta k|/2$ for pure radial modes TEM_{p0} for p = 0, 1, 2, and 3.

For the radial modes, not only is the efficiency smaller for larger β, but also F' becomes multipeaked, the number of maxima increases with β, and the highest value of F' occurs at increasingly larger |a| as β increases.

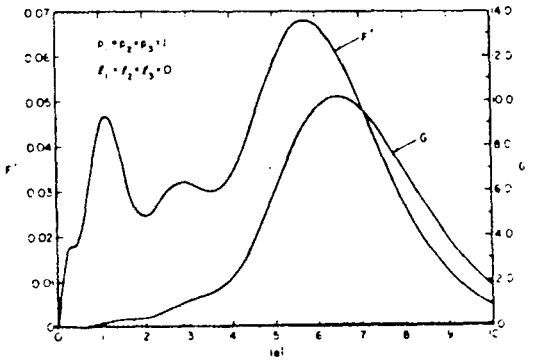

Fig. 29. Power coefficients F´and G as functions of $|a| = |b\Delta k|/2$ for a TEM_{10} mode.

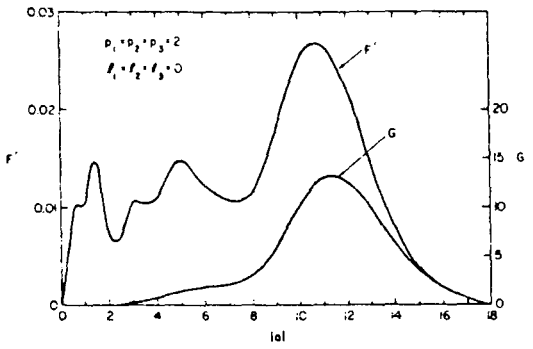

Fig. 30. Power coefficients F' and G as functions of $|a| = |b\Delta k|/2$ for a TEM_{20} mode.

These figures show that the functions peak at very different |a|-values for the TEM_{10} and TEM_{20} modes. This gives an indication on that incorrect parameters very easily can be deduced from experiments where the spatial mode is not very well determined. Another feature is that the maximum value of G increases with increasing radial mode numbers implying that, when tripling in a single, negatively dispersive medium is performed, a higher efficiency would be obtained for the higher-order mode.

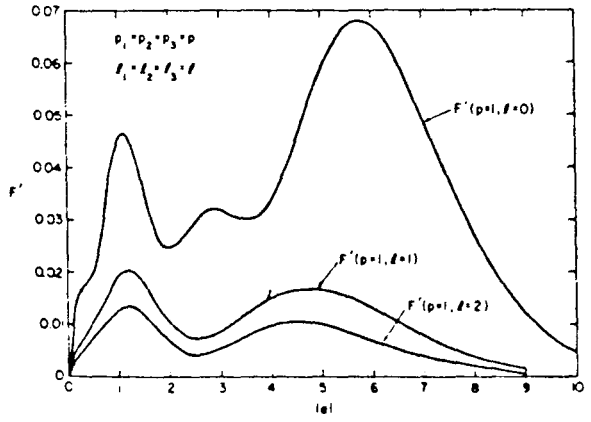

Fig. 31. Power coefficient F' as a function of $|a| = |b\Delta k|/2$ for TEM_{1l}, where l = 0, 1, and 2.

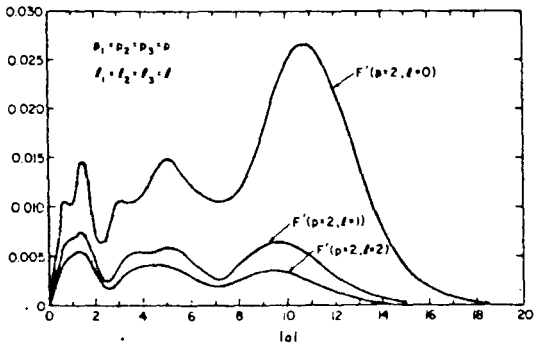

Fig. 32. Power coefficient F'as a function of $|a| = |b\Delta k|/2$ for TEM_{21}, where l = 0, 1, and 2.

The overall efficiency decreases, while higher relative efficiency occurs around $|a| = 1$, when the angular mode number is increased for a given radial mode.

From figure 27 we saw that a Gaussian fundamental mode generates a TEM_{00} like mode. However, a TEM_{10} input beam generates a third-harmonic beam comprised of TEM_{30}, TEM_{10}, TEM_{00}, functions of $|a|$ according to the figure. We note the following characteristics for a general pure mode input:

* $F(\beta-1) = F(2)$ is zero for all $|a|$.
* $F(\beta) = F(3)$ is a single peaked function, maximizing at $|a| = 1$.
* Only for very large $|a|$, the mode is dominated by the TEM_{00} contribution

At $|a| = 0.55$ the generated mode is predominantly TEM_{30} while it's TEM_{10} around $|a| = 4.05$.

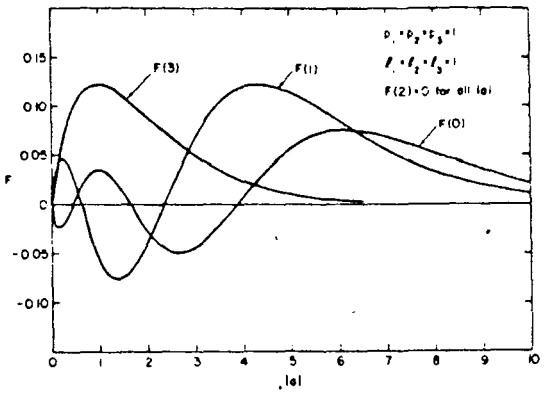

Fig. 33. Mode coefficients F(ρ) of the generated field for a TEM_{11} mode.

The effect of adding an angular contribution is shown in fig 33 where the generating mode TEM_{11} is considered. Again the coefficient of TEM_{23} is zero and that of TEM_{33} is a single-peaked function. The TEM_{03} contribution is never significantly dominant as TEM_{00} was in the $\alpha = 0$ case. The TEM_{03} mode makes the smallest contribution whereas in the previous case (fig 26) the TEM_{00} coefficient has the largest value.

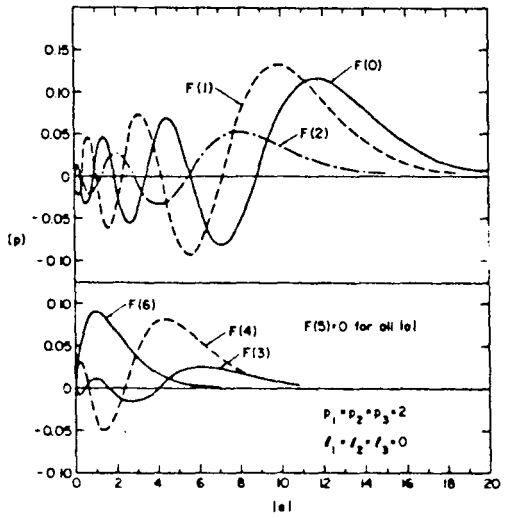

Fig. 34. Mode coefficients F(ρ) of the generated field for a TEM_{20} mode.

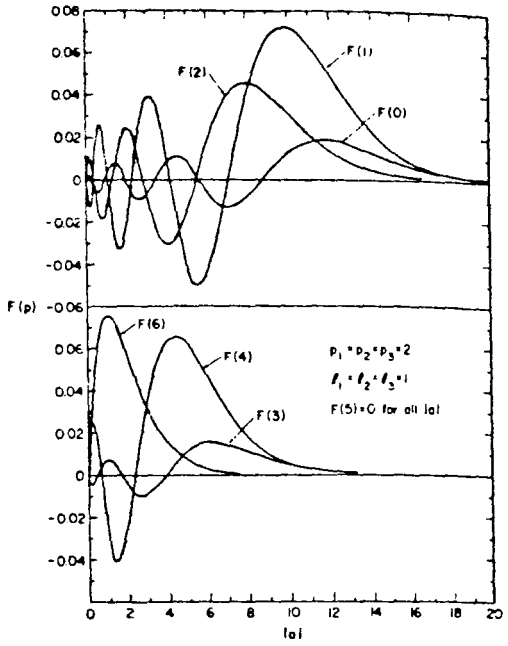

Fig. 35. Mode coefficients F(ρ) of the generated field for a TEM_{21} mode.

The six finite generated mode coefficients for input beams described by TEM_{20} and TEM_{21} show that the coefficients of the higher modes dominate at smaller values of |a|.

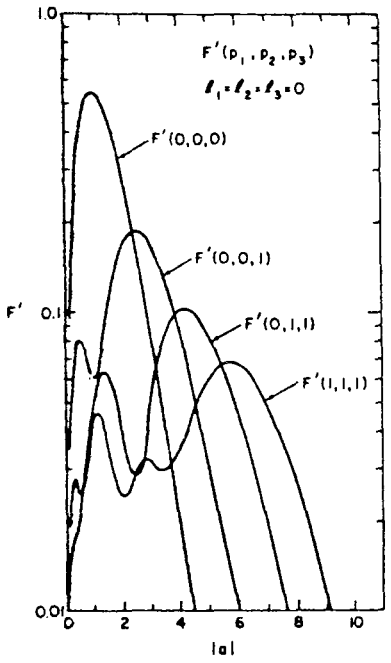

Fig. 36. Power coefficient F for combinations of TEM_{00} and TEM_{10} modes of equal intensity and phase.

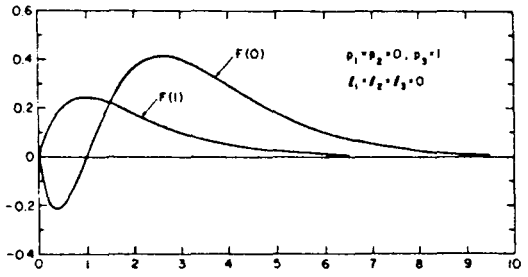

Fig. 37. Mode coefficients F(ρ) for combination of two photons with mode TEM_{01} and one photon of TEM_{10}.

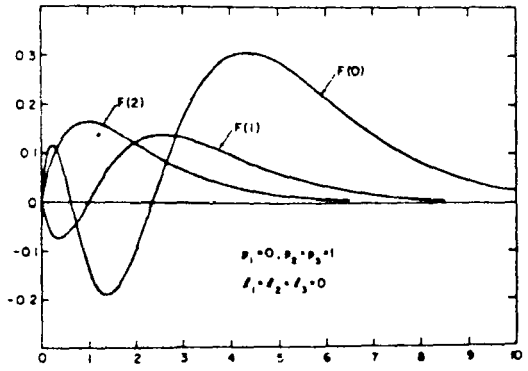

Fig. 38. Mode coefficients F(ρ) for combination of one photon with mo mode TEM_{01} and two photons of TEM_{10}.

These three figures show the individual mode coefficients where the input consists of equal intensity and equal phase TEM_{00} and TEM_{10} components. In figs. 37 and 38 it can be seen that the generated TEM_{B0} mode, where $B = B_1 + B_2 + B_3 - 1$ has a finite nonzero contribution, unlike the pure mode case.

III. EXPERIMENTAL AND EVALUATIONS

III.1. EXPERIMENTAL SET-UP IN THE UV-CASE

The experimental set-up for the generation of UV-light above the vacuum limit by third harmonic generation with Xenon as a nonlinear medium is given in fig.1.

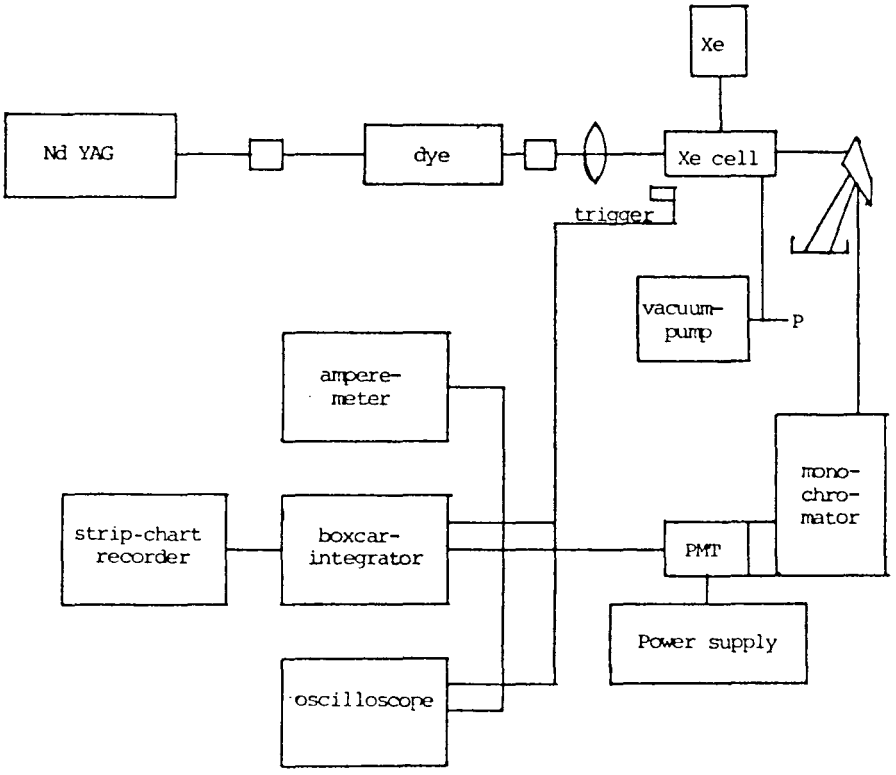

Fig. 1. The experimental set-up for third harmonic generation in Xenon. The wavelength is above the vacuum limit and hence an ordinary air filled monochromator is used.

The Nd: YAG laser light at 1.064μm passed through a crystal where green light at 530nm was produced by second harmonic generation. This light pumped the dye laser, where Rhodamin 640 was used. The outcoming

red/yellow light (about 6000Å), overlapped by its second harmonic at about 3000Å, generated in another crystal, was focused into a Xe-cell. The Xe-cell was connected to a Xe-tube and a vacuum pump, enabling the variation of the pressure in the cell. The pressure meter made it possible to study the generation efficiency at different pressures. The output from the cell was dispersed and directed to a monochromator using a Pellin-Brocca prism. Although the major part of the 6000Å- and the 3000Å-light were stopped before the monochromator, the background of scattered light at these wavelengths were very big and an interference filter had to be used before detecting the 2000Å-light by the solar-blind photo multiplier tube.

To detect the light some more equipment was used. The oscilloscope was used mostly for finding the signal, the ampere-meter for optimization procedures while the boxcar integrator together with the strip-chart recorder were used for recording the data. The oscilloscope and the boxcar integrator were triggered by the signal from a photo diode placed near the fundamental laser beam

2. EXPERIMENTS AROUND 200nm

When I was planning the first experiments in the summer 1985 no monochromator adapted for the VUV-region (below the vacuum limit at about 185nm) was available and hence, the first experimental investigations were done in the spectral region above the vacuum limit, mostly around 2000Å.

2.1 The straylight problem

The experimental set-up was according to [III.1]. In that figure an interference filter and a Pellin-Brocca prism are shown. Those are the fundamental components for reducing the background level of scattered

light at 6000Å and at 3000Å. The expected magnitude ratio between the 6000Å yellow light and the desired light at 2000Å was 10^5 and since the transmission ratio through the filter and the monochromator for these two wavelengths was less, it was impossible to detect the signal without the prism. With the help of the prism, the beams at 6000Å and at 3000Å, detected by fluorescence on a piece of white paper were clearly separated and the 2000Å spot could be expected to be separated from the 3000Å spot about just as much as the 3000Å spot was separated from the 6000Å spot, because of the increasing dispersion at shorter wavelengths. The straylight was reduced so much that a slit width of 1mm could be used, which made it possible to detect 50 photons/pulse of the 2000Å radiation. This value should be compared to the theoretical value of 10^5 photons/pulse if the crudest assumptions were used. A sharp peak was detected when scanning the monochromator around 2030Å, the place expected according to the process $2\omega(uv)-\omega(l)$.

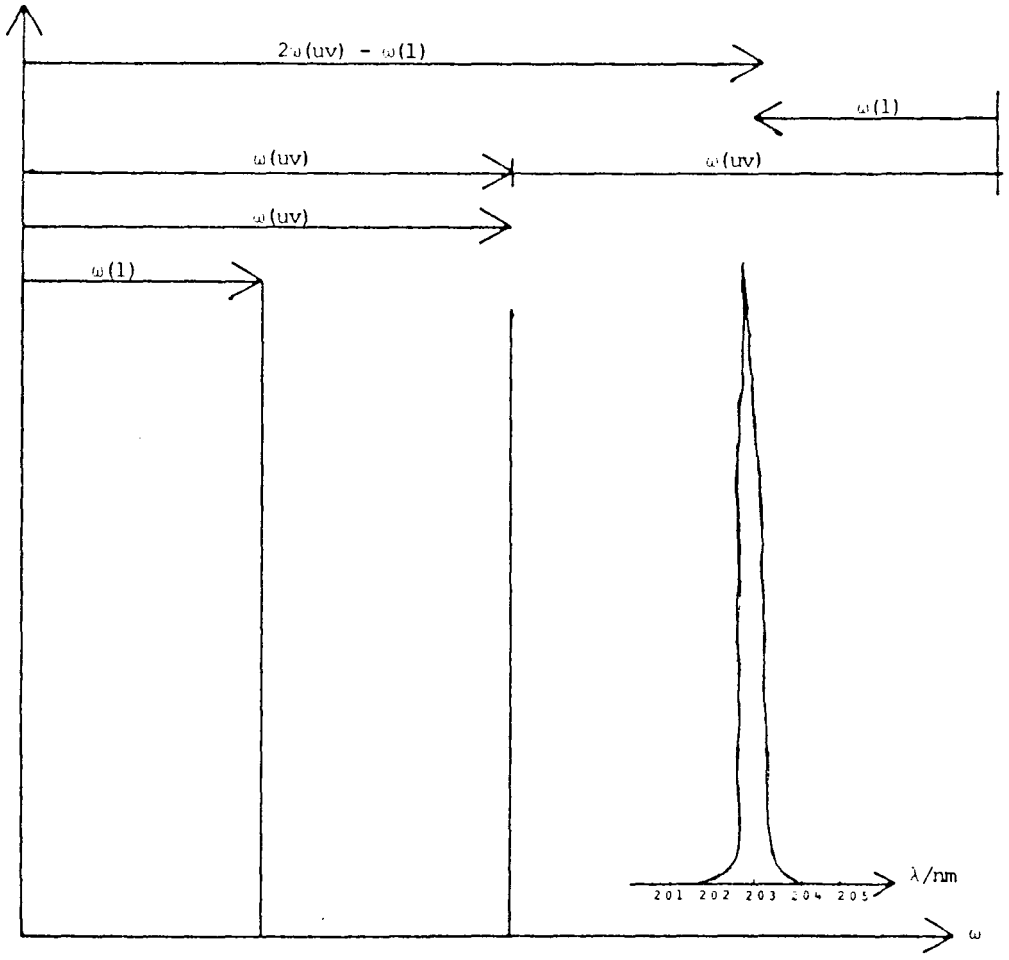

Fig. 2. Energy diagram illustrating the difference conversion process and the movement along the wavelength-axis during the process.

2.1 Polarization directions

Different polarization directions were tested. The polarization directions of the fundamental and its second harmonic after the crystal, were in right angles to each other. A λ/4-plate was placed between the lens and the crystal. By checking light intensities in reflection at Brewster angles it could be concluded that half of the

light (the fundamental and its second harmonic) overlapped with the same polarization direction. This partial alignment of the polarization components increased the generation by a factor of two. According to the tensor character of the nonlinear susceptibility [II.1.3], the third harmonic generation when the polarization directions are in right angles to each other, should be one third of the value at equal polarization directions. The experiment accordingly agreed qualitative with the theory.

2.3 Different laser modes

The ordinary donut mode could be replaced by a mode, a little bit more Gaussian, by changing to transversal pumping of the amplifier cell in the dye. This was done by moving a prism in the dye. The Rhodamine concentration was also increased a factor 4 in the amplifier cell. The laser output had a more Gaussian intensity distribution, but the energy per pulse decreased from 35mJ to 21mJ for the yellow light, and increased from 1.5mJ to 1.6mJ for the second harmonic. The signal strength from the generated third harmonic increased by a factor 4 with this new mode, in spite of the decrease of the output power. The straylight problems were further reduced by this operation, since the beam diameter was reduced to 10mm from 30mm in the donut case.

This result is qualitative in agreement with the theory from which it's expected that the highest possible conversion efficiency is reached for a pure Gaussian mode (II). Since no achromatic lens was available in the lab and since the lens therefore had different focal lengths for the fundamental beam and its second harmonic, it could also have been that the second harmonic was focused in the donut hole of the fundamental when the donut mode was used, and thereby further decreasing the conversion efficiency for the donut case. A brief calculation shows however that this is probably not the case.

2.4 Some other qualitative investigations

The sensitivity of the strip-chart recorder and the boxcar integrator was increased, whereupon it was seen that even a very weak second harmonic beam resulted in an observable THG-signal. In other words, there seemed to be no energy threshold for the process to start.

The signal was independent of if we had gas circulation or if the Xenon cell was closed, implying that the Xenon wasn't consumed during the process.

We estimated that there were 100 photons/pulse. This value could be received by comparing the area on the oscilloscope of one pulse, with the area of the pulses triggered by individual photons. By moving the monochromator, it was concluded that the beam diameter of the generated beam was <10mm at the entrance slit of the monochromator and hence about 1/20 of the light should pass through the 0.5mm-slit. By assuming a transmission of 1/10 in the monochromator and a transmission of 1/10 in the interference filter and finally 1/5 exchange in the PMT, we concluded that about 10^6 photons/pulse had been produced in the cell.

The 10cm-lens in front of the Xenon-cell was changed to a 16cm-lens. In both cases the focus was in the middle of the cell. The signal decreased to 1/4 of the earlier value. The amount of light entering the monochromator should however be the same or even a little bit more in the 16cm-case, because of a smaller divergence in this case. This shows, as is expected by the f/L and b/L dependence of the G_2-function [II.3.3], that as long as the beam waist is located inside the cell and the same amount of light can exit from the cell, the signal and thereby the generation will increase when a harder focusing is used.

2.5 The variation of the signal for different parameter variations

The monochromator was scanned both around 2000Å and 4000Å (looking in the second order). The signal peaked at 2030Å and 4060Å respectively.

At the optimal adjustment the Xenon pressure was varied. A pressure dependence of the following appearance was received

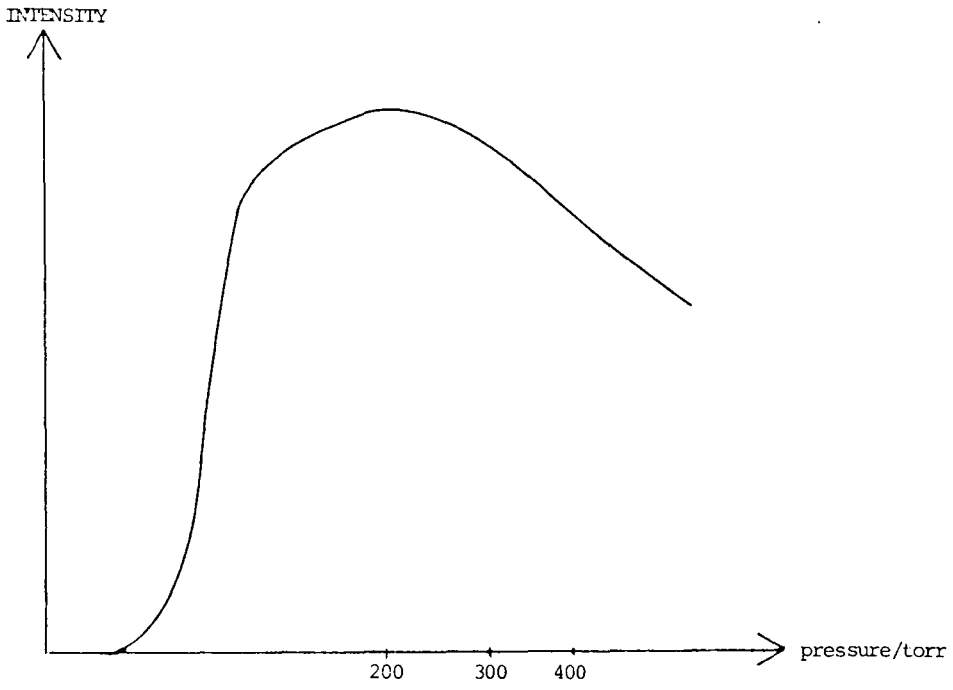

Fig. 3. The generated third harmonic power as a function of the Xenon pressure in the cell.

From the figure it can be seen that the conversion efficiency was highest for a Xenon pressure of 250 torr, but since the maximum was rather flat and since it was difficult to get the same pressure increase and decrease rate during the whole scan, this value is not too exact.

The generation dependence of the input powers was first studied by varying the UV intensity while keeping the yellow power constant. Then the total power was changed and hence all the beam powers were varied. It was rather difficult to read off the power meter, because of a high noise level and hence the values are a bit uncertain, as can be seen in the diagrams. The UV intensity was varied while keeping the fundamental intensity constant. Corresponding values of the UV-power and the THG-power were observed. Since you from the theory in principal expects a quadratic dependence on the UV-power, (Gaussian

beam, tight focusing) the THG-power was plotted against the square of the UV-power.

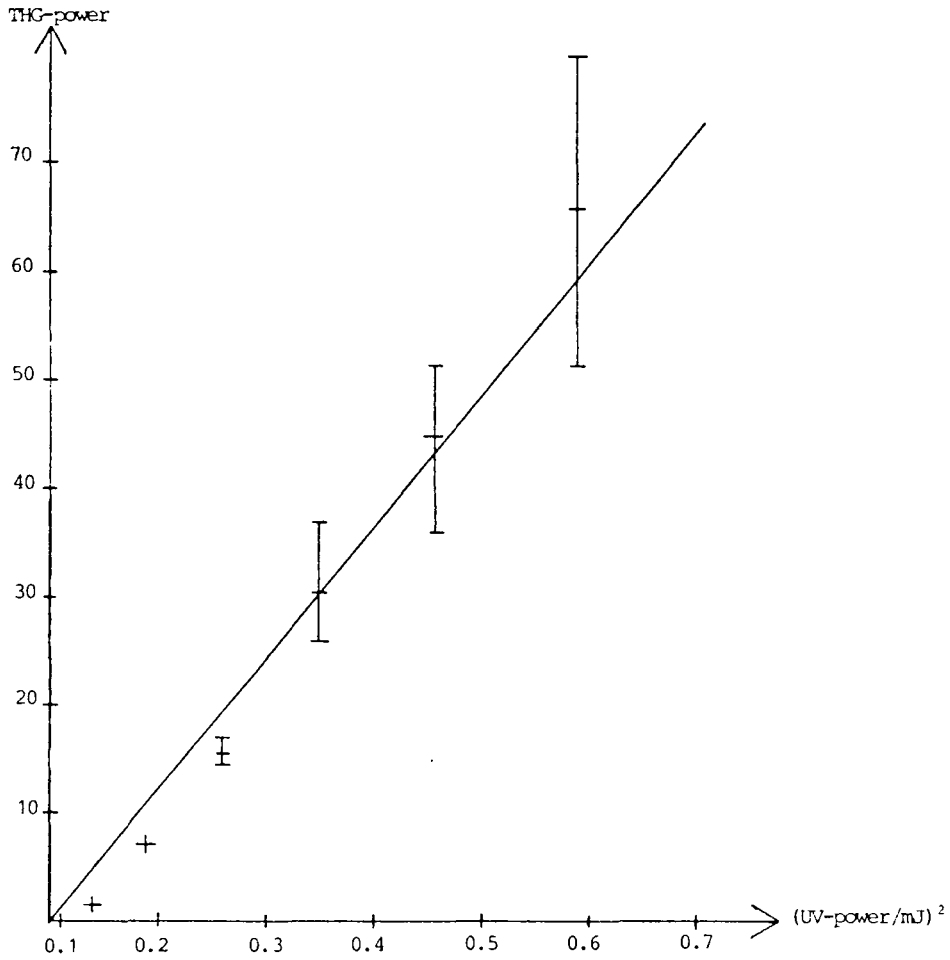

Fig. 4. The power of the third harmonic is plotted against the square of the power of the second harmonic, while the power of the fundamental beam was held constant.

It's perhaps possible to see some kind of saturation. Nonlinearities in the crystal should not be too prominent here, since we are measuring UV-intensities, while the much brighter yellow beam is so strong that small variations from a linear dependence between the UV-power and the yellow power should not affect the conversion too much. There is however such a nonlinearity according to a later experiment (fig.17). When the intensity of the fundamental beam was varied

both of the beam powers were changed and a cubic dependence of either of them is expected for the THG-power if the crystal has a linear conversion. The UV-power was used, and the following plot could be drawn:

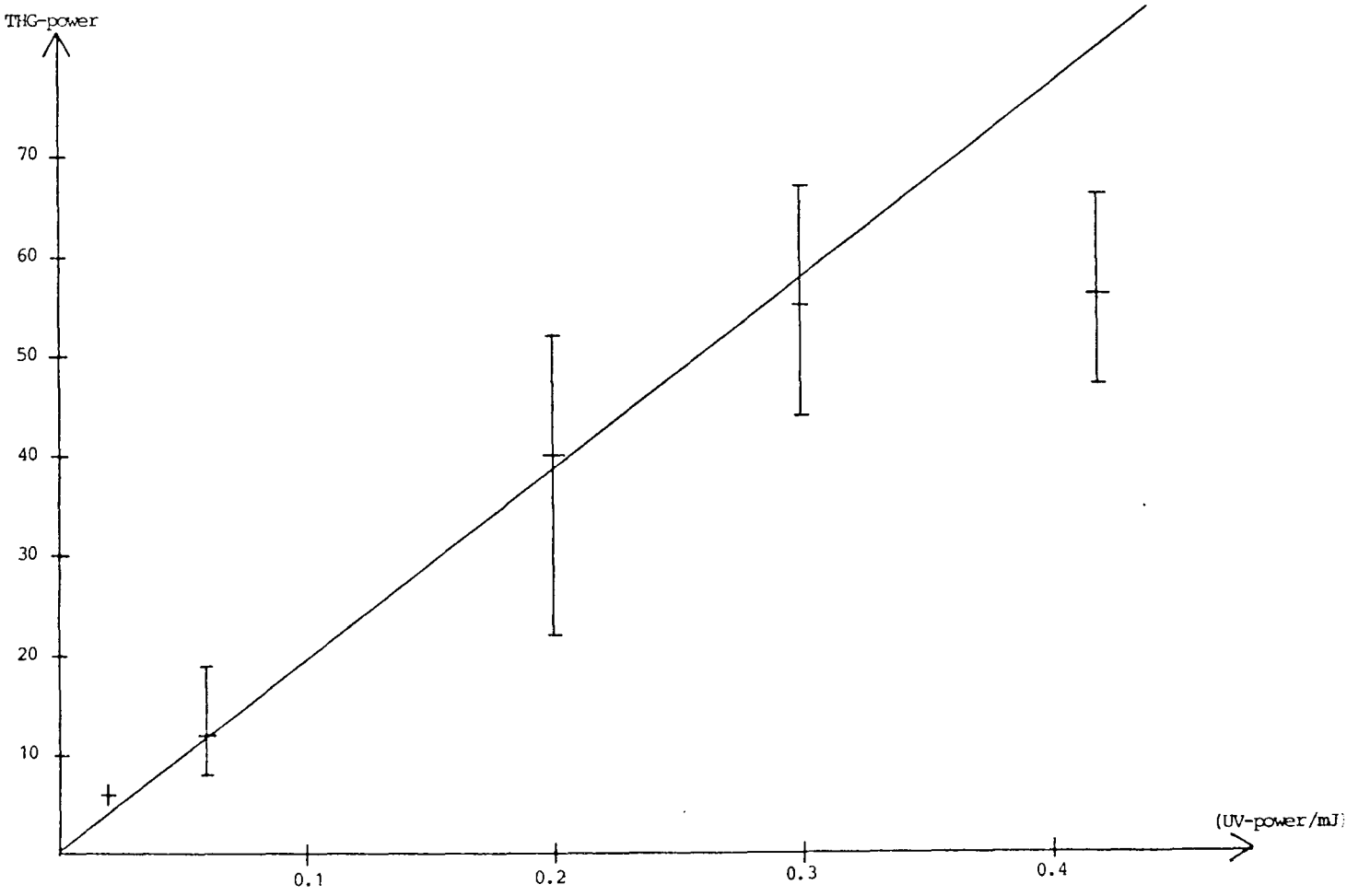

Fig. 5. The power of the third harmonic is plotted against the cube of the UV-power. All the input powers were changed at the same time since the fundamental power was varied.

The decrease of the slope for higher values of the power could indicate a nonlinearity in the crystal where $P(uv) = P(1)^A$ and $A < 1$. I will return to the saturation problem in [5] and [6.5]. A more exhaustive theoretical review of different saturation phenomena follows in [6.6].

3. EXPERIMENTAL SET-UP IN THE VUV-CASE

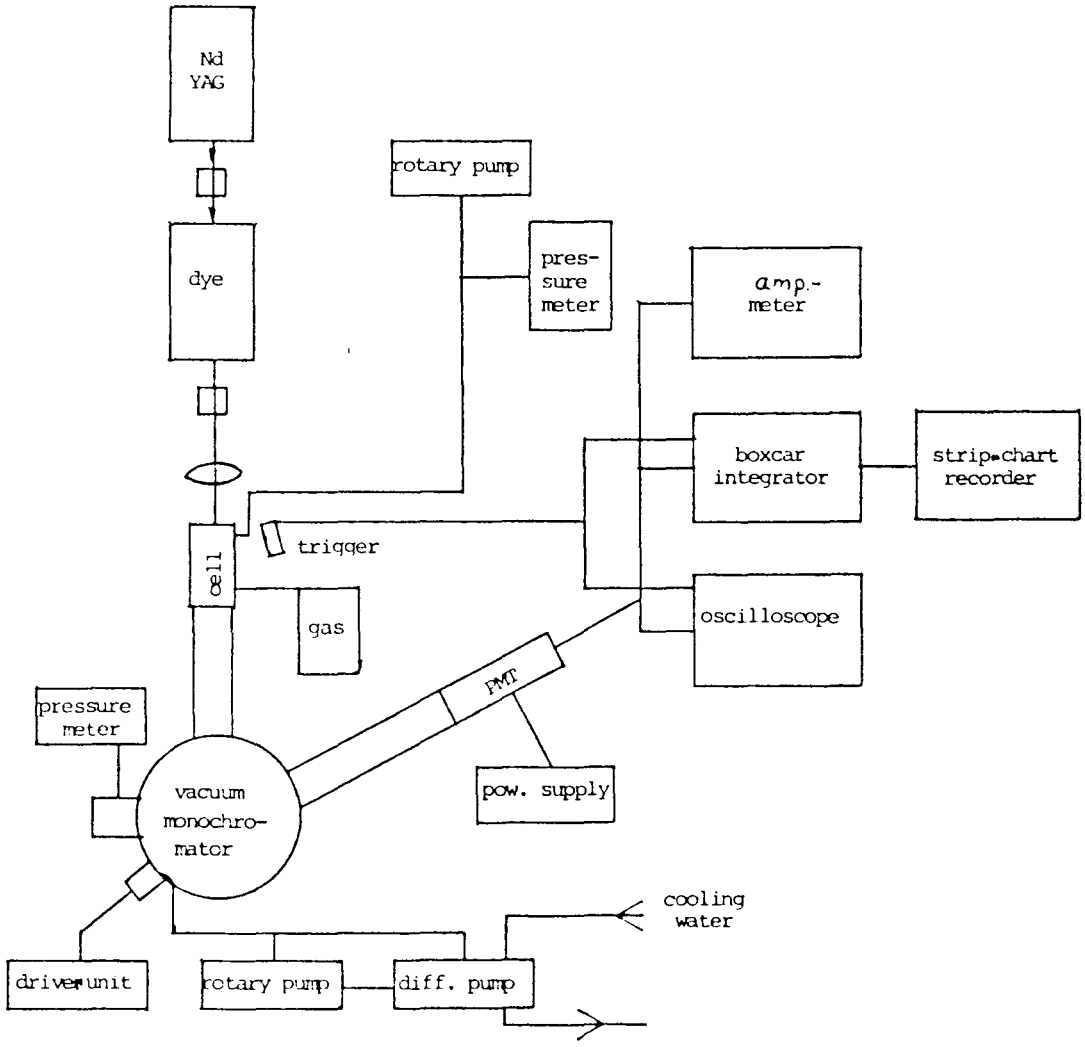

Fig. 6. The experimental set-up for third harmonic generation in noble gases below the vacuum limit, where it's necessary to use vacuum equipment.

The laser system was the same as for the earlier experiment. The same aluminium cell for the gas was used, but it was fixed to the input branch of the vacuum monochromator. The two volumes were separated by a MgF_2-window, transmitting light down to around 1150Å. The

monochromator vacuum was achieved by a rotary pump and a diffusion pump. The quality of the vacuum could be read of on a digital pressure meter connected to a penning head and a pirani head. To control the motor, driving the grating, a stepping motor drive unit was used. The photomultiplier tube was of course also in vacuum contact with the monochromator system. Different tubes, sensitive for different spectral regions, were used for different experiments. A power supply generating voltages up to 3.5kV was used for the PMT:s. The detecting equipment was the same as for the earlier experiment.

4. CALIBRATION OF THE MONOCHROMATOR AND SOME OTHER PREPARATORY LABWORK

4.1 Preparatory Work

The vacuum monochromator, which was used for the experiments in the spring 1986, was borrowed from K. Hallin in Uppsala. There was a need of some additional equipment before it could be used for experiments. I had to build a driving unit for controlling the motor, used for scanning the wavelength. This driving unit and a display showing the pressure in the monochromator were fastened to the table of the monochromator system.

A fundamental problem was to reach high vacuum inside the monochromator. All leakages had to be found by spirting ether on every joint, and observing the possible subsequent increase of the pressure.

The MgF_2-window between the gas cell and the vacuum monochromator was very fragile. To be able to evacuate these two volumes independent of each other, this window had to stand up to large pressure gradients in both directions. I therefore put one O-ring on each side of this window.

4.2 Calibration

To get a correlation between the value of the scaler on the monochromator and the transmitted wavelength, it was necessary to do a calibration. For this purpose I used a small Hg-source (about 100mm long) in a position in front of the entrance slit. There were some problems of identification of the spectral lines since the strength of different spectral lines varied along the time scale. I also used a bigger Hg-source which didn't fluctuate that much and which also had the strong line at 1850Å. (The envelope transmitted at this wavelength). To be quite sure which line is which, I also used a Xenon lamp (high pressure lamp which therefore has a continuous spectrum) where known interference filters were used to pick out certain wavelength parts. It was important to note both the value of the counter and the value of a micrometer, placed inside the monochromator, since they both moved the grating independently of each other. I also measured the mutual relationship between these two scales. The micrometer was set for a certain wavelength part, which then could be scanned by the outer equipment. One disadvantage was that you had to destroy the vacuum every time you wanted to change the micrometer adjustment, another was that the scaler showed hysteres, which was only partially possible to correct for by mechanical operations.

From the measurements from the Hg-sources and the Xenon-source together with interference filters, the following connection between the wavelength and the scaler was received for different values on the micrometer. (We are looking in the first order)

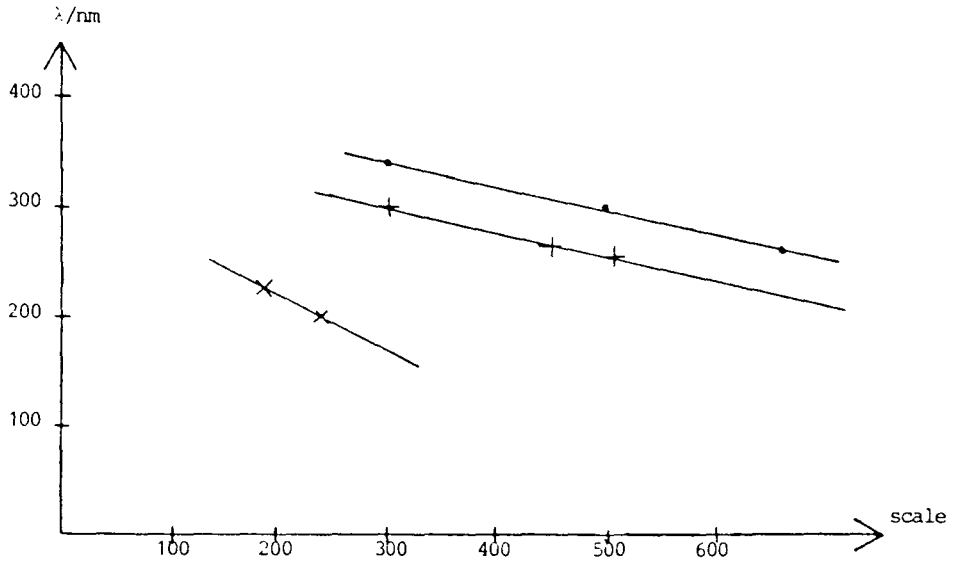

Fig. 7. Calibration curves for the vacuum monochromator. The transmitted wavelength is plotted against the scalar value of the counter. The micrometer adjustments were: ·=1738 and x=1302.

From the grating equation it could be calculated that the scalar value was linearly related to the angle of incidence on the grating within 10%.

When looking at a fixed wavelength, 3030Å, the scaler and the micrometer were varied to get their relationship:

scalar	micrometer
504	7.30
393	8.30
271	9.30
148	10.30
42	11.30

Because of the hysteres, the scalar value will be about 15 units

higher when increasing the micrometer value and about 15 units lower when decreasing the micrometer value. If you calculate the average when scanning upwards and scanning downwards and also average over different wavelength regions, you come to the approximate thumb rules that 100 scalar units correspond to a wavelength difference of 25nm and a difference of 1.00 on the micrometer corresponds to 120 scalar units. An increase in wavelength (grating order +1) corresponds to a decrease in scalar units or also a decrease on the micrometer.

5. EXPERIMENTS AROUND 200nm IN KRYPTON

I started with the same kind of conversion as in the experiments with the air monochromator, the technique $2\omega(uv) - \omega(1)$. The dye, Rhodamine 640, was used at the wavelength 6073Å. A power of 54mJ was reached after a long time of optimization work. The second harmonic at 3036Å had a power of 7mJ. A fundamental problem was that of background light, principally from diffusively scattered 3000Å-light from the grating, since the PMT was sensitive in the region 1600Å-3200Å. I had to use two interference filters to reduce this background. One filter at 2000Å and one at 2200Å were available. The 2200Å-filter had to be tilted at about 20°, for maximum transmittance. It was also possible to close the shutters in the monochromator so much that the background was reduced but the signal remained unaffected. This was easily done since there was no need of vacuum in this experiment.

Xenon was used in the first tests. A peak appeared, after some optimization work, on the oscilloscope at the expected place, at around 2000Å. The peak was maximal for a Xe-pressure of around 200 torr. This value could be compared to the 1985-value of 240 torr. However, different pressure meters were used and the maximum is rather flat. The spectral half-value width was 20Å, probably instrument limited since I used the 1mm-slit to receive enough of light.

The gas was changed to Krypton. The background problem was still

present. It wasn't better to look in the 2nd order or the 1st on the other side. The same two interference filters again had to be used. The same kind of signal appeared at the same place as for Xenon but the amplitude was a little bit less in Krypton than in Xenon, implying a lower conversion efficiency in Krypton than in Xenon. This is also implied from the theory. When the 25cm-lens, in front of the gas cell, was changed to a 15cm-lens, the signal decreased. At first I had expected an increase because of harder focusing but a geometrical estimation showed that because of this harder focusing the amount of light entering the monochromator was reduced by a factor of 2. The position of the focus along the gas cell was not important as long as the beam waist region was contained within the cell. This is expected by the theory if there is no absorption in the Krypton of the generated wavelength.

The conversion efficiency for different Kr-pressures was investigated. For the process of current interest, $2\omega(uv)-\omega(l)$, $\lambda(l) = 6070$Å and $\lambda(uv) = 3035$Å and hence $\lambda(vuv) = 2023$Å. The monochromator was used in the 1st order and the peak was obtained at the scalar value 548. The micrometer position was 11.20. Both the 2000Å- and the 2240Å-filters were used. The PMT got 800V from the voltage supply and the oscilloscope magnification was 50mV/cm. The corresponding values of PMT-current and Kr-pressure, p(Kr), were plotted in a diagram. As can be seen, there is a flat maximum at around 300 torr.

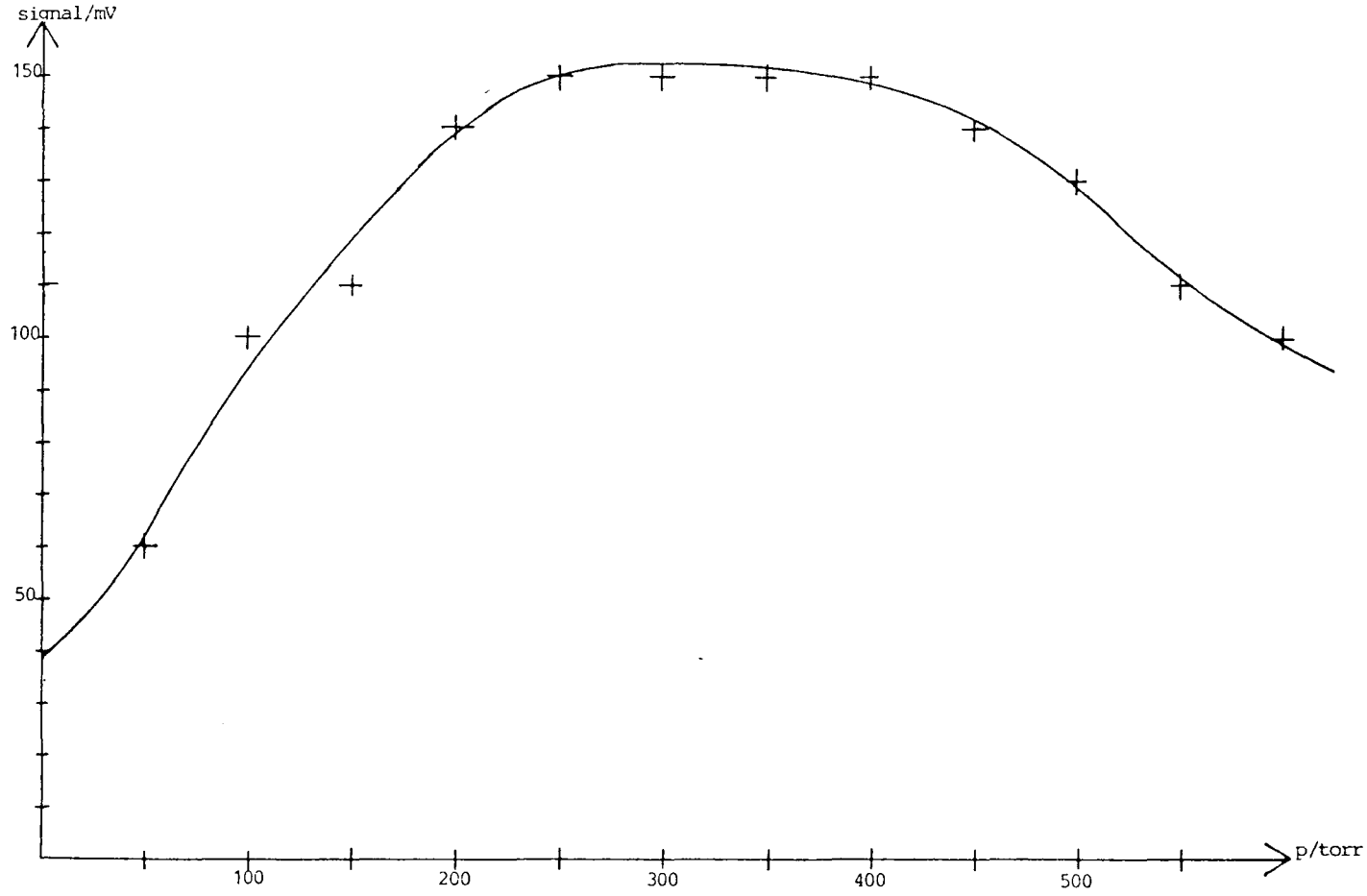

Fig. 8. The generated third harmonic power at 202nm as a function of the Krypton pressure in the cell.

The signal strength variation for different powers of the 6070Å-light and the 3035Å-light was investigated. The signal was plotted against the cube of the 6070Å-light and against the square of the power of the 3035Å-light for fixed power of the fundamental. The following conditions were present: $\lambda(1)$ = 6070Å, V(pmt) = 900V and p(Kr) = 250 torr. The results are shown in the following diagrams:

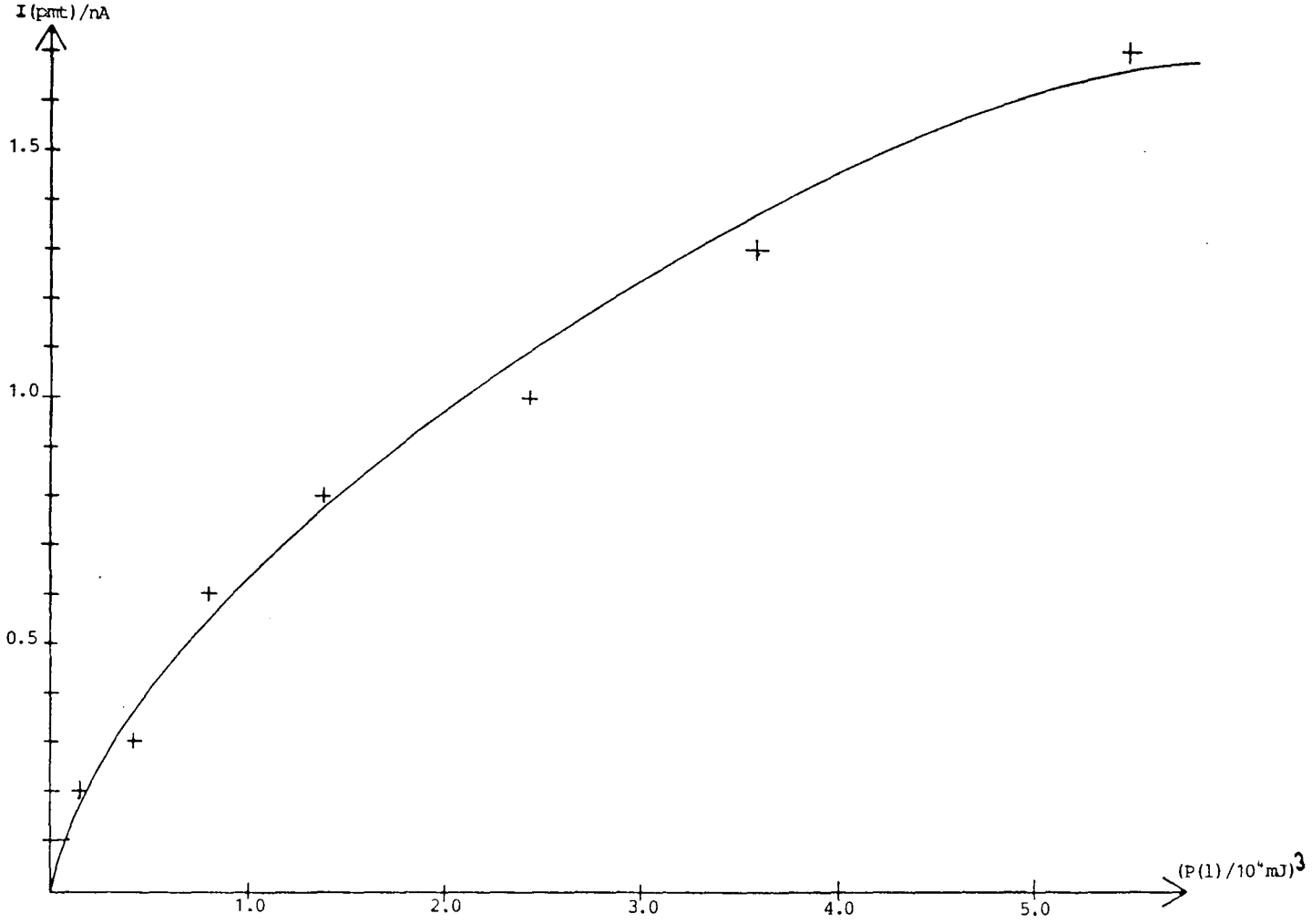

Fig. 9. The power of the third harmonic is plotted against the cube of the fundamental power. The Krypton pressure is 250 torr and the photo multiplier voltage is 900V.

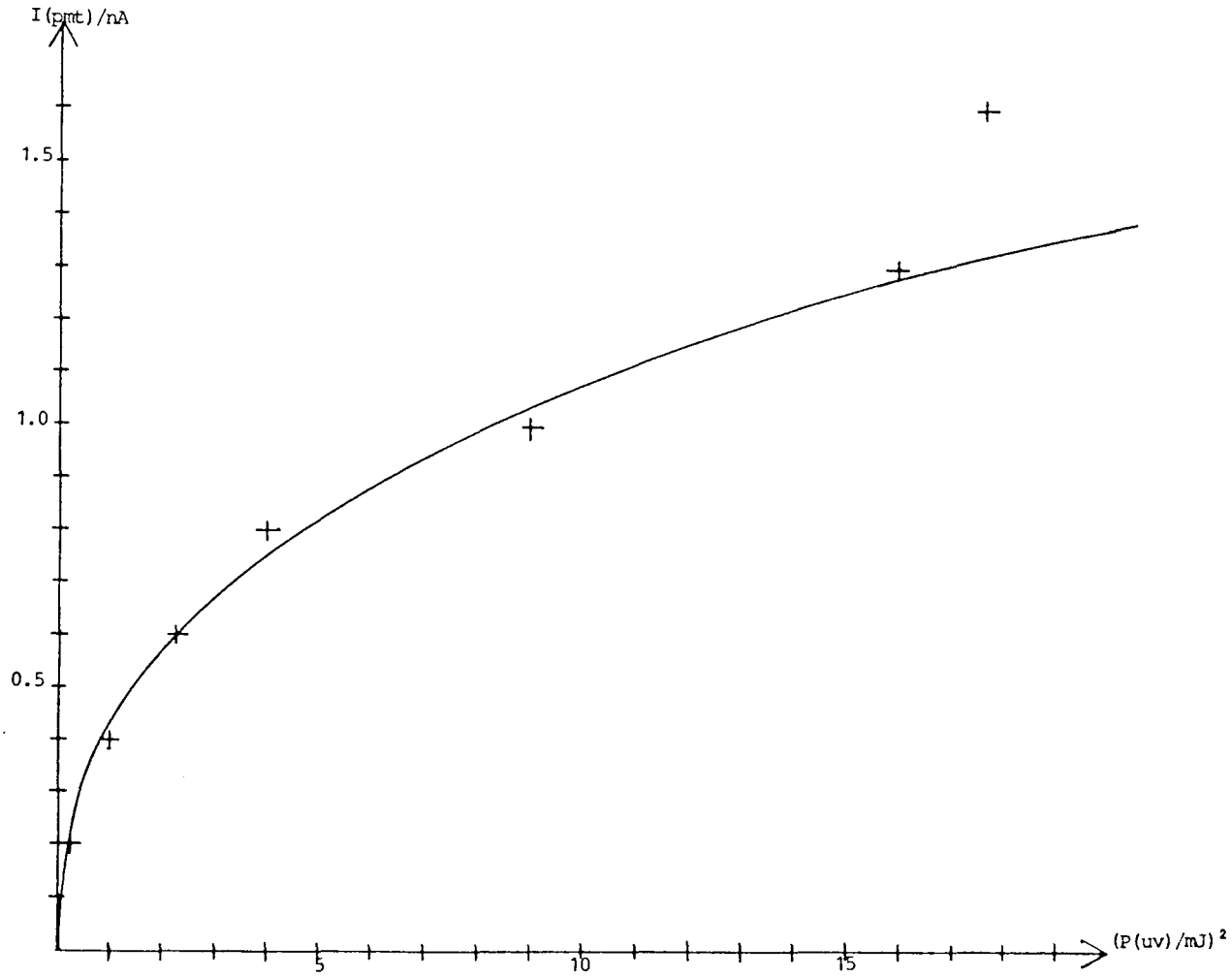

Fig. 10. The power of the third harmonic is plotted against the square of the power of the second harmonic, while the power of the fundamental beam was held constant. The Krypton pressure is 250 torr and the photo multiplier voltage is 900V.

Both of these two plots show quite strong saturation tendencies. If you take into account the measured nonlinearity of the crystal fig.17, the saturation according to the diagram in fig.9 will be even bigger. A similar saturation have been seen in the Xenon case (fig.5). A more theoretical review of different saturation phenomena will be given in [6.6] after which a similar saturation for a generated 1200Å-beam has been investigated.

The tunability of the generated light was checked. I spanned the region covered by the dye, Rhodamine 640. The dye laser was scanned

and the grating was moved until an optimal signal was reached for each time. The phase matching in the crystal also changed and it also had to be corrected between each measurement. Corresponding values of the photomultiplier current and the power of the fundamental beam were noted. As can be seen from the following diagram, these two quantities seem to follow each other quite good. It should be stressed that it is the fundamental power uncubed which is shown. To calculate the conversion efficiency for different wavelengths, the ratio of the generated power and the cube of the fundamental power should be calculated. If one does, one sees that the conversion efficiency is quite constant in the range. Theoretically we know (p.93 in [26]) that the conversion efficiency is nearly constant in the range from 1800Å to 2030Å. The value of $X(Xe)^3$ is constant within a factor of two in the range.

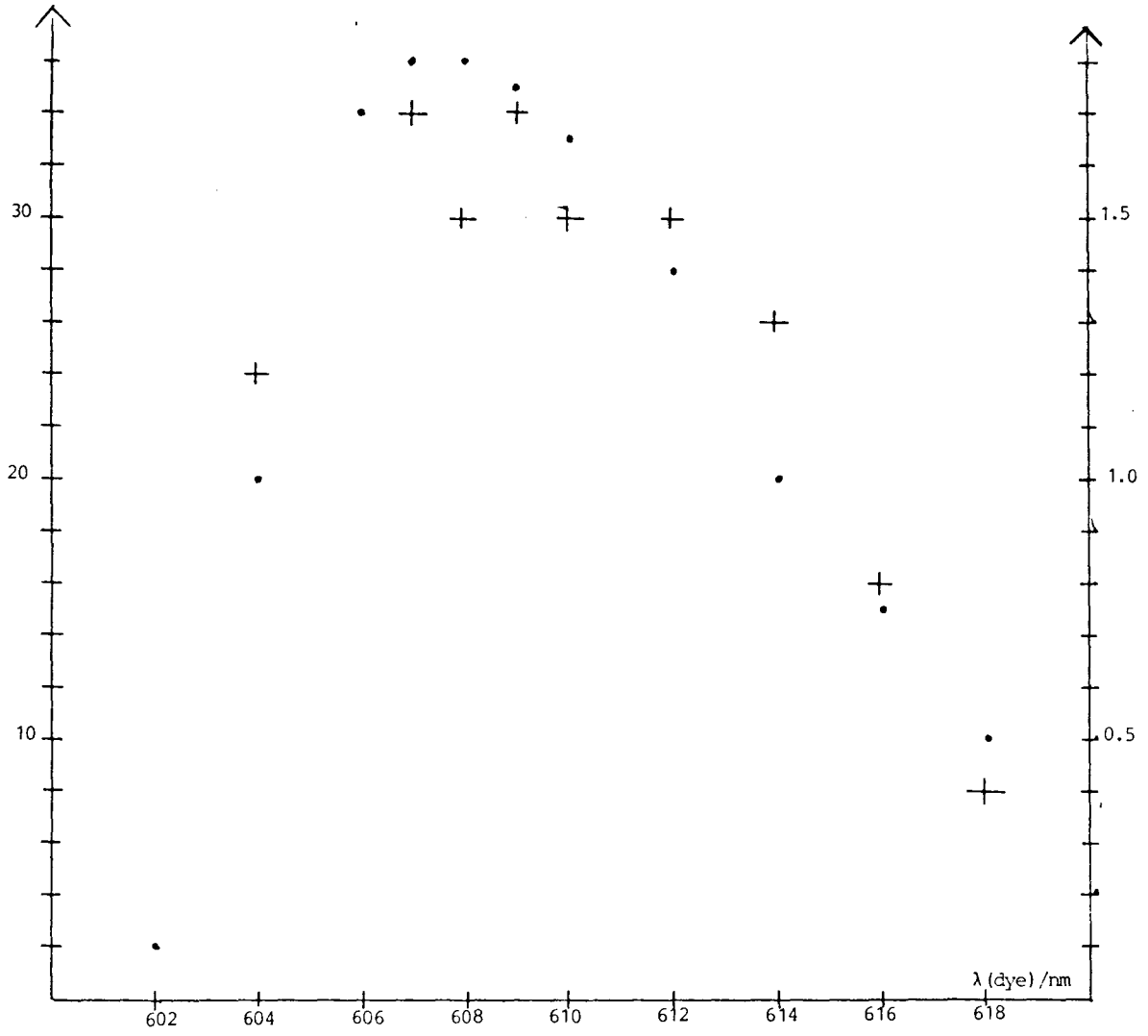

Fig. 11. Corresponding values of the power of the dye and the power of the third harmonic (photo multiplier current) for different wavelengths. The wavelength region 602 - 618 nm was scanned.

6. EXPERIMENTS AROUND 120nm

6.1 Searching for the signal - Fundamental problems

Krypton was used as a nonlinear medium and a beam of λ=6070Å was used from the dye (Rhodamine 640). This fundamental beam was as before overlapped by its second harmonic after its passage through the KDP-crystal. I intended to use the process 2ω(uv) + ω(l) which would give me 1214Å. This wavelength lies in a negatively dispersive region, required for sum frequency generation in the tight focusing case.

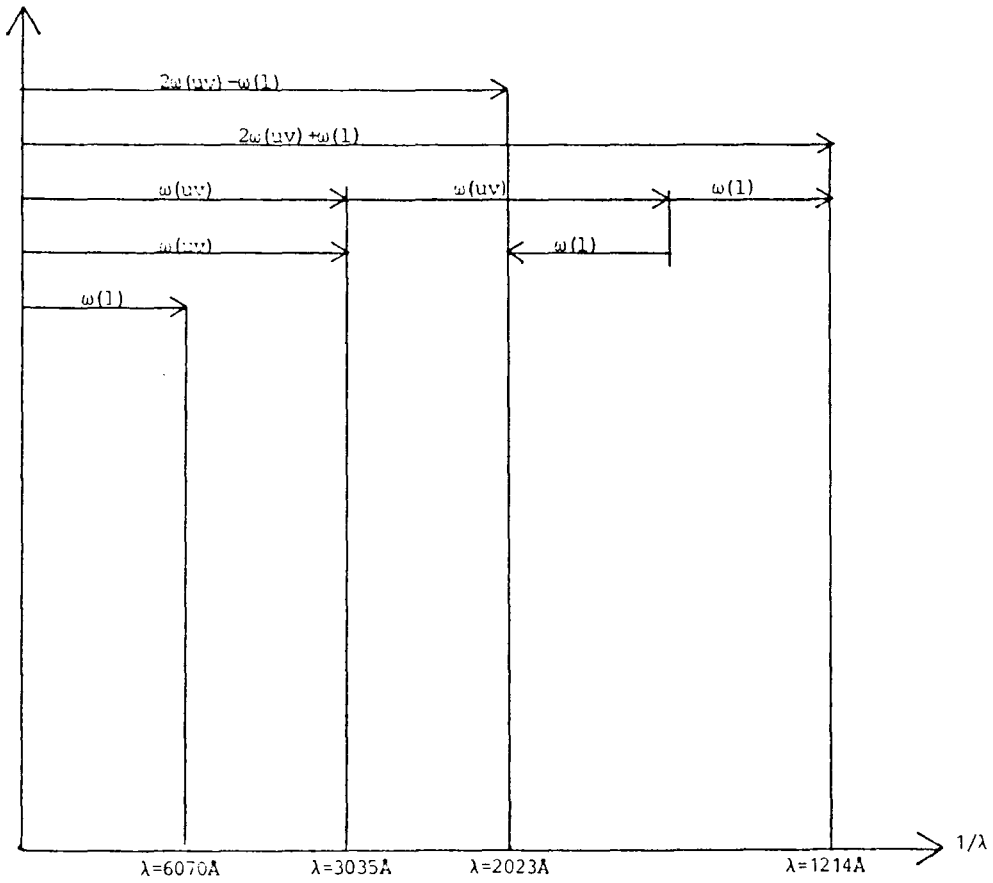

Fig. 12. Energy diagram illustrating the sum and difference conversion processes and the movements along the wavelength-axis during the processes.

At first one signal appeared at exactly the expected place, 1200Å, and another one at around 1800Å. These signals didn't change when the Krypton was removed or when the monochromator was filled with air. They seemed to depend on the strength of the UV-light and they also

seemed to move linearly with the UV-wavelength. According to a book in experimental spectroscopy, one could expect grating ghosts at the place of $3\lambda/5$ and $2\lambda/5$. These two would be located at the position of 1214Å and 1820Å if λ = 3035Å, the second harmonic. The PMT, sensitive in the region 1150Å - 1950Å showed experimentally to be sensitive to the 3035Å-radiation too. Later investigations showed however that it was diffusively scattered UV-light from the grating, in spite of the nice numerical fit above. This background had to be reduced by closing the shutters as much as possible without stopping the third harmonic. I changed to an electron multiplier tube, sensitive in a region up to 1600Å. These improvements together with a new housing for the tube and an efficient screening of the signal cable reduced the noise, the background light, to a very low level. It was now possible to detect quite a few photons at the expected wavelength around 1200Å. This electron multiplier tube was nearly completely insensitive to the 2000Å-light from the earlier studied processes.

Having done these preparations of the experimental set-up, I was in a rather good starting position for detecting the process $2\omega(uv) + \omega(l)$ and optimizing the signal/noise ratio and also optimize the signal with respect to a couple of variable parameters.

6.2 The dependence of the pressure

The conversion was studied with respect to a variation of the Kr-pressure in the cell. A new better pressure measuring equipment was used for measuring the Kr-pressure. The grating position was 501 on the scalar and 14.50 on the micrometer. The inaccuracy of the position was about 5 scalar units.

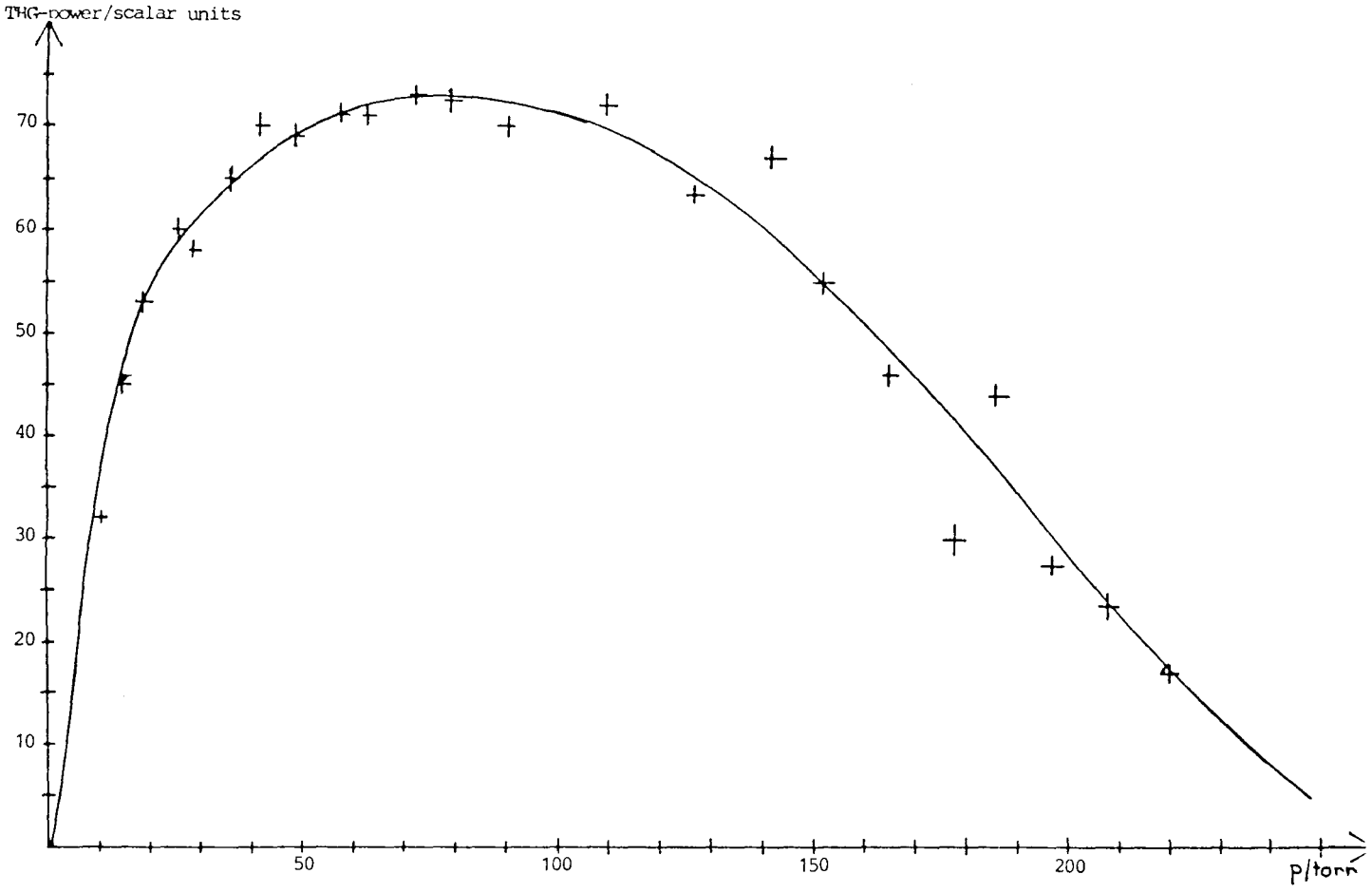

Fig. 13. Generation of 1214-Å light according to the process $2\omega(uv) + \omega(1)$. The diagram shows the dependence of the conversion on the Krypton pressure.

As can be seen from the diagram, there is a flat maximum at around 60 torr while the signal is above 50% of this value between the pressures of 10 torr and 200 torr.

In the litterature the most common method of reaching the Lyman-alpha region is through tripling in Krypton of the second harmonic of a fundamental beam in the region 7216Å - 7408Å. Although the wavevector mismatch, Δk, will differ a bit from that in my experiment, the results will be about the same [7] and [8].

Theoretically we have the input-output power relationship:

$$P(vuv) \alpha N^2 \cdot X^2 \cdot P(uv)^2 \cdot P(1) \cdot F \qquad (1)$$

N is the number density of the gas and X is the third-order nonlinear susceptibility. F is a phase-matching factor which is a function of $b\Delta k$, where b is the confocal beam parameter of a TEM_{00} (Gaussian) laser beam and $\Delta k = k(\lambda) - 3k(3\lambda)$ with $k(\lambda) = 2\pi n(\lambda)/\lambda$ where $n(\lambda)$ is the refractive index at λ. In my case the expression for the wave vector mismatch is $\Delta k = k(\lambda) - 2k(5\lambda/2) - k(5\lambda)$. For tight focusing of the input radiation P(1), F is different from zero only if the medium is negatively dispersive, ($\Delta k < 0$). The output P(vuv) maximizes for $b\Delta k = -4$. Since Δk is a function of the gas pressure p, a plot of P(vuv) against p should give a direct measurement of Δk.

In the case of tripling to 1216Å the optimum pressure is 50torr for a focusing lens with a focal length of 200mm, 110 torr for a focal length of 150mm and about 140 torr for a focal length of 100mm.

Δk depends strongly on λ in the tripling case. For focusing of the laser beam with a lens of 150mm, the optimum pressure varied from 1290 torr at λ=1202Å to 3.6 torr at λ=1234Å. This follows from theoretical calculations of Δk, done with the help of the Sellmeier equation [II.3.4].

6.3 Different absorption investigations

The air pressure in the monochromator was about 10^{-6} mbar during optimal conditions. It was seen that the signal remained unaffected when air was let in, up to a pressure of 10^{-4} mbar. This shows that no noticeable absorption of the generated radiation was present in the monochromator.

I also checked the influence of air in the Krypton cell. Generation according to the process $2\omega(uv) + \omega(1)$ at 1214Å was observed at a Krypton pressure of 32.5 torr. The partial pressure of air in the cell was continuously varied up to a few torrs and the decrease of the signal was observed. From the following plot it can be seen that above 3 torr there is no outcoming radiation at 1200Å, everything has been

absorbed. The DC-level above 3.0torr consists of an UV-background. The influence of possible absorption in air should decrease when the focus, and thereby the generating region, is moved towards the end of the cell. On the other hand, it's quite risky to have the focus of the strong fundamental beams in the vicinity of the expensive MgF_2-window.

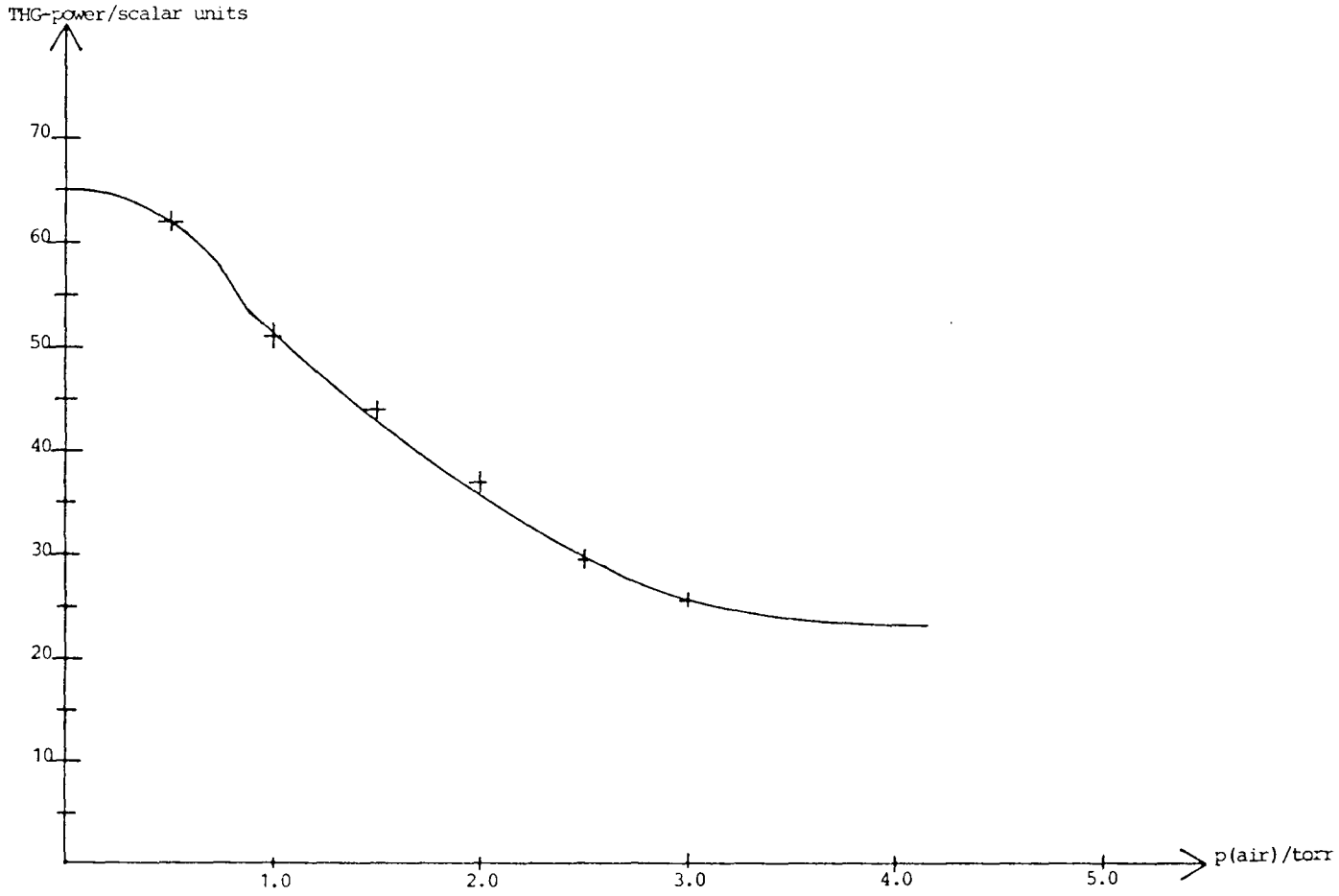

Fig. 14. The power from the process 2ω(uv) + ω(l) at 1214Å
at different partial air pressures in the cell.
The Krypton pressure is 32.5 torr.

It is also interesting to get an idea of the extent of the self absorption of the generated 1214Å-radiation in the nonlinear medium itself. To do this the signal strength was measured for different positions of the focus in the cell and for different lenses. I had changed to transversal pumping of the dye, which meant that the donut

mode was changed to a more Gaussian like intensity distribution. The fundamental power was 56mJ and the wavelength was 6069Å. The result was that the intensity increased when the focus was moved towards the MgF_2-window. This is natural, because of the divergence of the beam after the focus, a greater part of the light will pass the slit if the focus is nearer the slit than if it's at a longer distance. This influence from the geometry on the signal strength was calculated under the assumptions that the slit was of infinite height and that the intensity distribution of the laser beam had a rectangular shape. It was seen that the geometry could account for the whole variation of the signal. The discrepancies were possibly only due to the deviation from the rectangular mode. The actual mode had a triangular intensity distribution, a bit assymmetric. This assymmetry was reflected in that the signal strength was a bit too high when only the fainter part of the mode was screened. The conclusion is that there was no noticeable absorption of the generated signal in the Krypton itself under the circumstances referred to.

6.4 Cross section investigations of the generated beam

To get some more quantitative information about the generated beam, the signal peak height was examined for the lenses 23cm, 15cm and 10cm with a slit width of 1mm and 0.2mm in the exit branch, while the slit at the input branch was removed. The geometry of the monochromator was investigated and it was concluded that the shutters in the exit branch were the light limiting part. If it was assumed that the appearance of the generated beam was the same as that of the generating beam, it could be concluded that the geometrical transmitting factors for the three lenses were 16, 6 and 2.

To get more information on the intensity distribution, about which only could be assumed above, the laser beam cross section was moved transversally on the input slit and the variation of the signal was recorded. This was practically performed by turning the fundamental beam from the laser and for every such change the KDP-crystal was

optimized, the lens together with an aperture placed in front of it were moved transversally, always having the beam in the center of it. The grating also had to be optimized between each change. The 10cm-lens focused the fundamental donut mode at which corresponding values of the peak height and the transversal beam position were noted. These data are plotted in the following diagram:

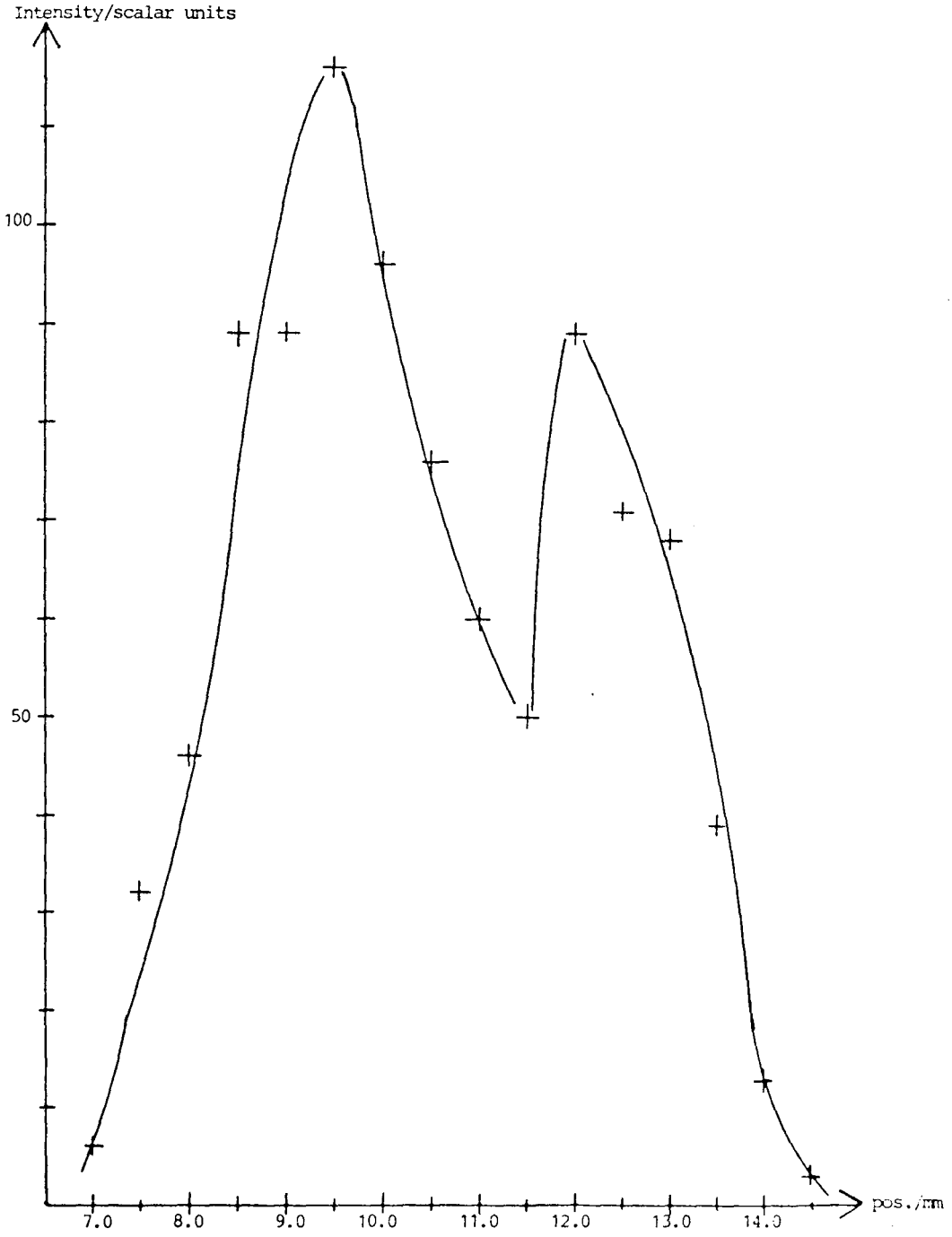

Fig. 15. The intensity distribution along a cross section of the generated beam according to the process $2\omega(uv) + \omega(1)$.

The donut mode is easily recognized in the output beam. It has the

same assymmetry in its intensity distribution as the input beam but the assymmetry has been amplified and it has also been more pronounced.

6.5 The dependence of the input powers

The generated power of the 1200Å light was examined for different powers of the fundamental beam. It was plotted against the cube of the fundamental power.

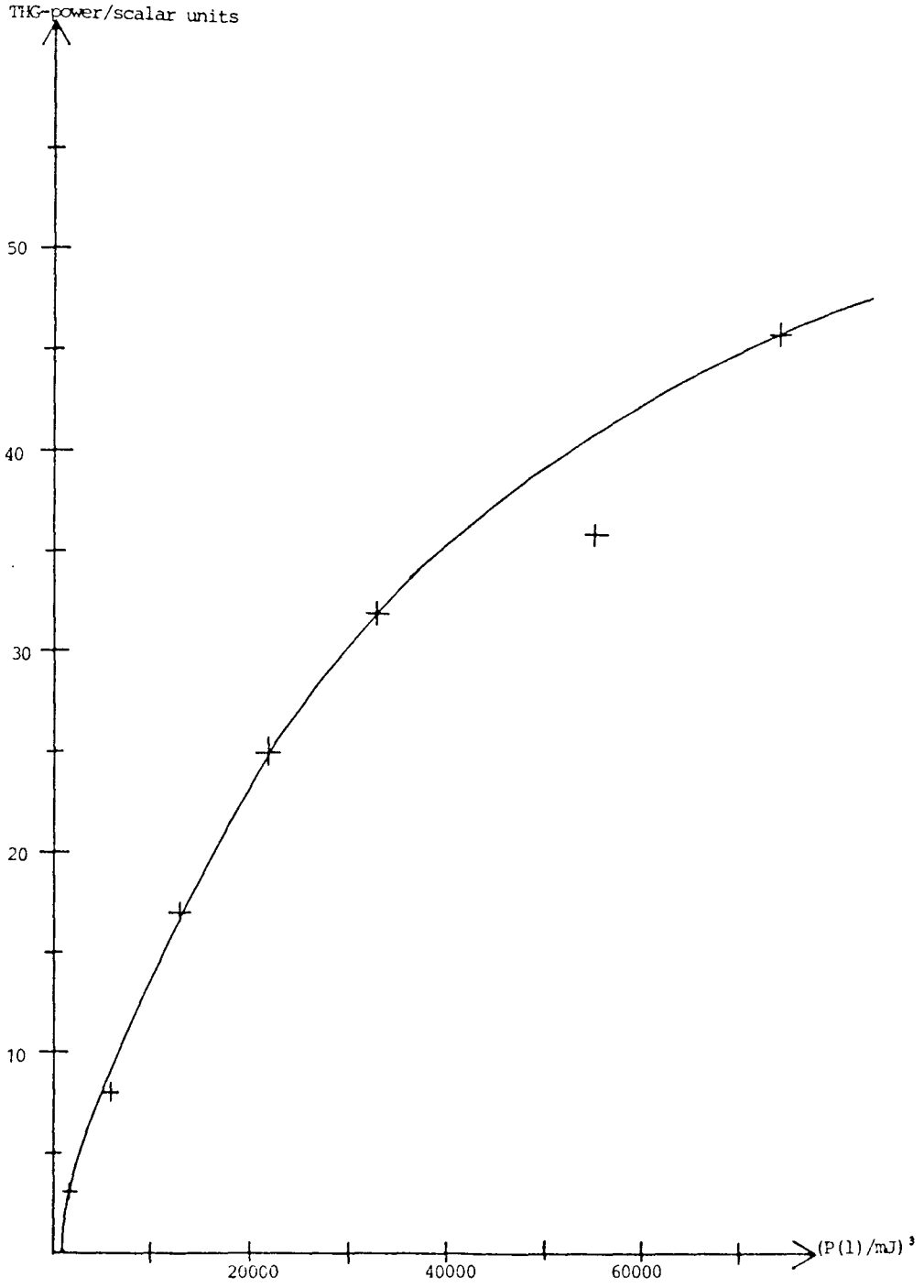

Fig. 16. The power of the third harmonic is plotted against the cube of the power of the fundamental beam. The sum frequency method is investigated.

As can be seen from the diagram there is a saturation for high powers of the fundamental 6000Å-light and therefore a lower conversion for higher powers than expected from the theoretical case of a pure Gaussian mode in the tight focusing limit. To see if this saturation partly was created in the KDP frequency doubling crystal, I investigated the power linearity of this crystal. The generated UV-power was plotted against the fundamental power.

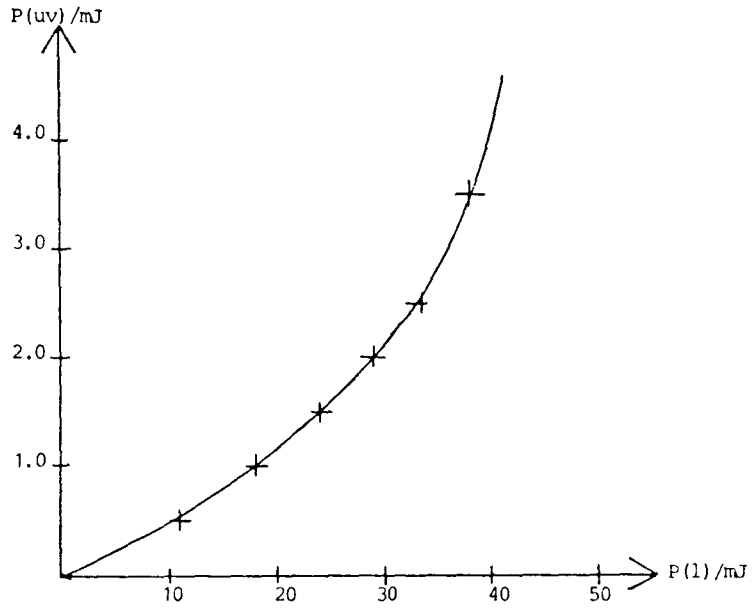

Fig. 17. The power of the second harmonic output from the KDP crystal is plotted against the input power (the power of the fundamental beam).

As can be seen from this plot, the second harmonic conversion in the KDP crystal is higher for higher input powers. This implies that the saturation in the cell is even bigger than is shown by the diagram in fig.16. To get a more accurate relationship, both the power of the fundamental beam and the second harmonic UV-power was measured for different input powers, and the corresponding signal strength was noted. This generated signal was plotted against $P(uv)^2 \cdot P(1)$.

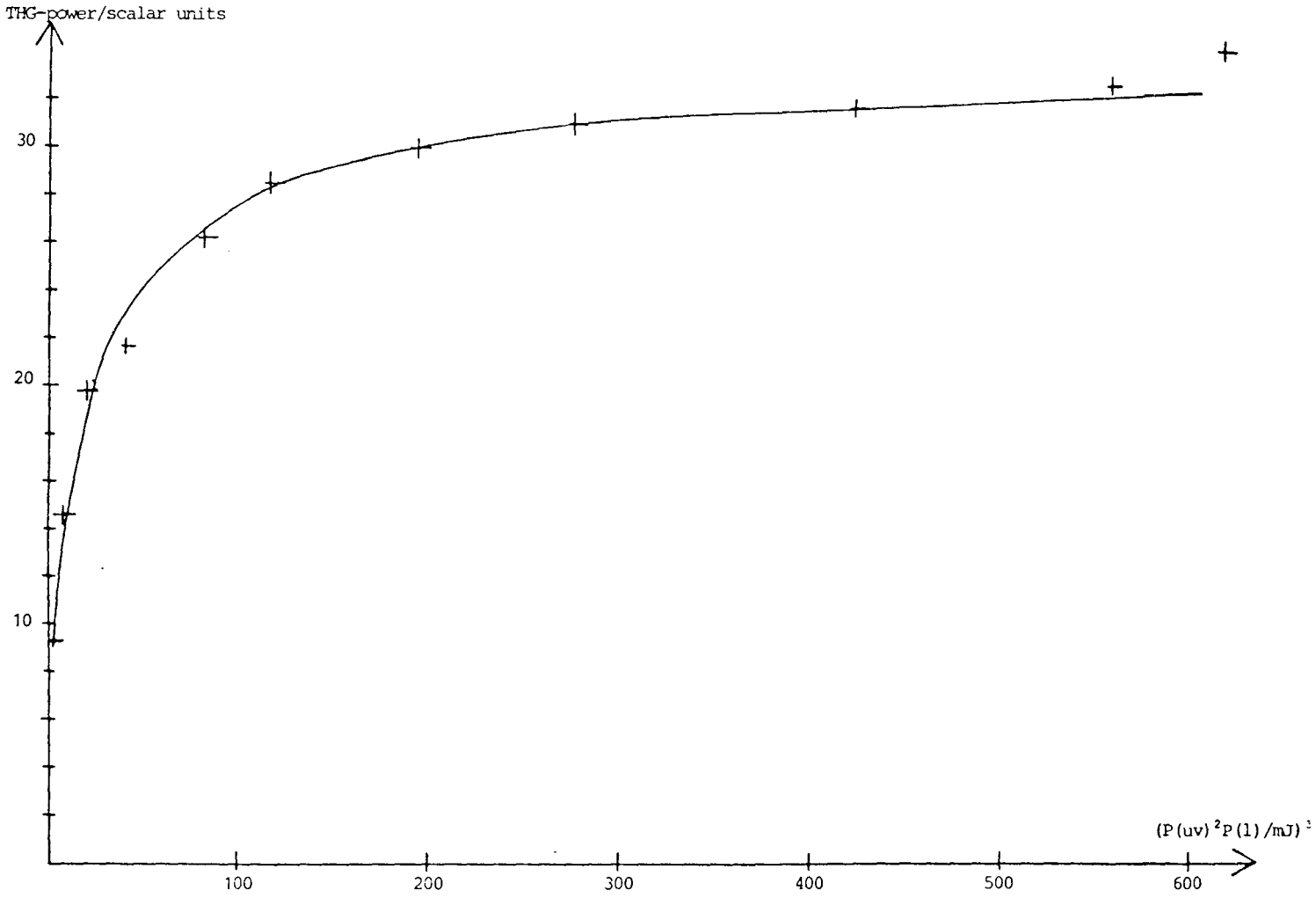

Fig. 18. The power of the third harmonic is plotted against the product of the power of the fundamental beam and the square of the power of the second harmonic beam.

In this diagram the UV-power has been corrected for, since there was a small background of scattered UV-light. We should here only see the nonlinearities occuring in the cell since the crystal no longer has any influence. A very strong saturation at higher powers can be seen. According to an experiment of tripling in Krypton in the region 1203-1236Å done by Cotter [5], it's seen that the cubic dependence of the VUV signal as a function of input power is verified up to the

maximum available unless the gas pressure and the focused laser intensity are high enough to cause laser-induced breakdown of the Kr-gas. Indeed it appears that dielectric breakdown is the crucial limiting factor for frequency tripling in noble gases, when relative long excited pulses (several nanoseconds) are used. Dielectric breakdown limitations become increasingly severe as the short wavelength edge of the tuning range is approached, because higher gas pressures are then needed to achieve the optimum phase mismatch Δk. There could be a lot of other more or less complex processes giving rise to the saturation. A brief review of different possibilities are given in the next section.

6.6 Saturation phenomena

The effects of competing processes on harmonic generation can be grouped into two broad categories: Changes in the magnitude of the nonlinear susceptibility and changes in the refractive indices. Changes in the nonlinear susceptibility affect harmonic conversion by changing the strength of the nonlinear interaction, while the nonlinear refactive index affects conversion by changing the direction of power flow from the fundamental to the harmonic wave. Some saturation processes can contribute to both of these effects. For example, saturation of excited state population by multiphoton absorption can affect the nonlinear susceptibility by changing the electron population distribution. The stark effect can change the susceptibility by changing resonant denominators during the time that the driving pulse is on, [see the formula for X]. These terms also contribute to the total nonlinear refractive index, again through population changes or level shifts.

In an effort to distinguish among them further, the harmonic conversion obtained with different lenses could be compared. If very little difference is seen between the curves obtained with different focal length lenses, it means that although the saturation of the harmonic conversion depends on the incident laser power and the gas

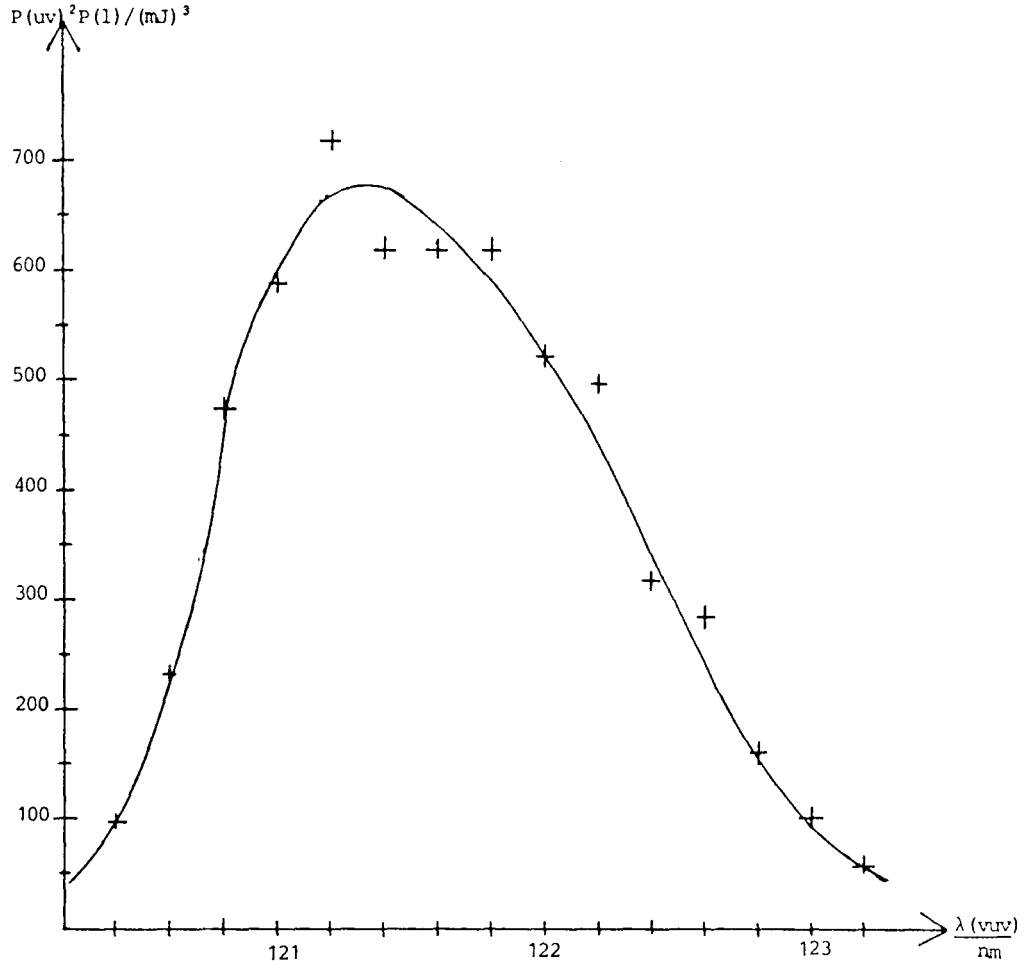

Fig. 21. The product of the power of the fundamental beam and the square of the power of the second harmonic is plotted against the wavelength of the generated light according to the sum frequency process. The wavelength region 602 - 616 nm of the dye output is used.

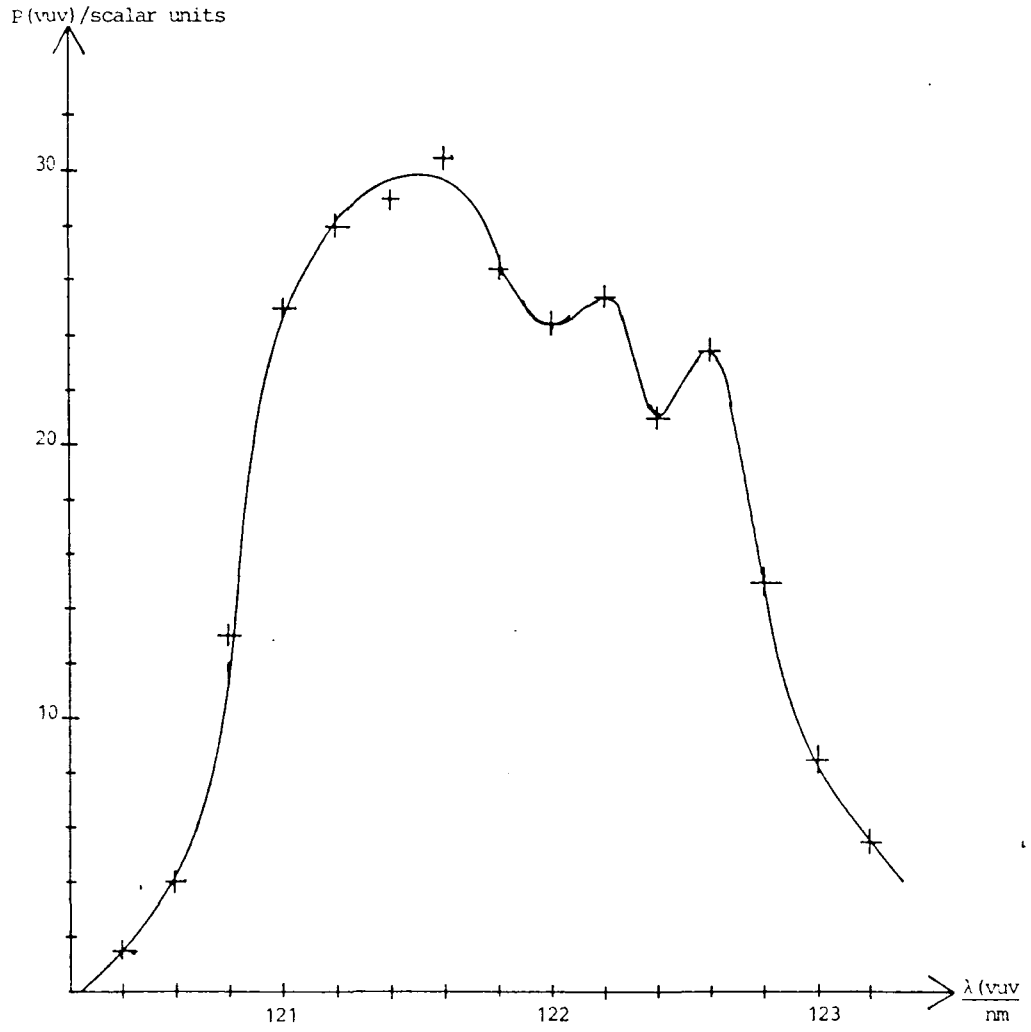

Fig. 22. The power of the generated radiation is plotted against its wavelength. The sum frequency process is used and the wavelength region 602 - 616 nm from the dye was used. The Krypton pressure was 64 torr and a 10cm-lens was used in front of the cell.

IV. SUMMARY

The theoretical part is based on fundamental equations as Maxwells equations and some quantum mechanics. Although the major part of that section is treating the influence of different parameters on the conversion efficiency of third harmonic generation, I have tried to make the connection to the basic equations as complete as possible. One important result is the requirement of being in a negatively dispersive region, when generating radiation according to the sum frequency method. Another result is the decrease in conversion efficiency, which occur when higher modes of the input laser beams are used. I have tried to write down analytical expressions and their derivations of most of the important results. It should however be pointed out that they often refer to ideal situations as for example infinite tight focusing of the input beams or a Gaussian intensity distribution along a cross-section of these beams. When other kinds of intensity distributions are treated, they are still very special, contrary to ordinary practical situations. For some of the results, however, the influence of deviations from the ideal situations are discussed.

The second part is describing my experimental activity. I have put together the equipment, solved some basic problems, as those of the elimination of disturbing background light and achieving a high vacuum in the system. I have been able to generate radiation at 2000Å and 1200Å. It is quite easy to reach intermediate regions with the different mechanisms presented and with the knowledge of the dispersion in different spectral regions. The basic problems, which have been solved, are the same. The radiation at 1200Å is interesting since some of the most generally investigated atoms have two-photon transitions in this region. I have made an estimation of the number of generated photons per pulse. I have studied the intensity distribution along a cross section of the generated beam and I have also investigated its tunability when scanning the fundamental

wavelength. I have however not made any measurements on the spectral width of the generated beam since a monochromator with a more exact scale would be needed. Strong saturation in the power is experienced for higher powers. I have not investigated what kind of saturation phenomena is present, but I have given a theoretical discussion of different possible sources.

To be able to use the light for more systematic research purposes, I think it would be necessary to have a better monochromator, giving more exact spectral information. A larger number of different lenses would perhaps make it possible to optimize the process better. To be able to cover a wider spectral region, different cells would be needed, specially adapted for certain gases or metal vapours. For the region below the LiF-transmission limit (at around 1050Å) a differentially pumped cell would be needed.

Although there are a lot of problems left, before using the generated light in research applications, I think that this report together with the work performed in the lab will make a good starting point for a further possible development of the system.

V. REFERENCES

1. GENERAL REFERENCES

M.D. Levenson — Introduction to nonlinear laser spectroscopy
Academic press 1982

N. Bloembergen — Nonlinear Optics
N.Y. 1965

Jan Rubbmark — Laserfysik/Icke linjär optik
(kompendium LTH 1981)

Ward, New — Optical Third Harmonic Generation in Gases by a focused laser beam
Phys. Rev. 185/1 1969

R. Hilbig — Erzeugung von frequenzveränderlicher kohäränter Strahlung im spektralen Bereich des Vakuumultravioletts mit der Methode der optisch nichtlinearen Frequenzkonversion in Gasen
Darmstadt 1984

G.C. Baldwin — An Introduction to nonlinear Optics
Plenum press, New York 1969

G.C. Björklund — Effects of focusing on third-order Nonlinear processes in isotropic media
Jour. of Quant. Electron 11/6 1975

O. Swelto — Principles of lasers
Plenum press, 2nd edition 1982, New York

H. Kogelnik
T. Li — Laser beams and resonators
Appl. Opt. 15/10 1966

D.A. Kleinmann — Theory of second harmonic generation of light by focused laser beams
Phys. Rev. 128 p.1761-1775 1962

2. REFERENCES

1. A.H. Kung, J.F. Young
S.E. Harris — Generation of 1182Å radiation in phase matched mixtures of inert gases
Appl. Phys. Lett. 22 p.301-302 1973

2. A.H. Kung — Generation of tunable picosecond VUV radiation
Appl. Phys. Lett. 25 p.653-654 1974

3. M.D. Levenson — Feasibility of measuring the nonlinear Index of Refraction by third-order frequency mixing
Jour. of Quant. Electron 10/2 1974

4. R. Mahon, T.C. Mcillrath, D.W. Koopman — Nonlinear generation of Lyman-alpha radiation
Appl. Phys. Lett. 33 p.305-307 1978

5. D. Cotter — Tunable Narrowband Coherent VUV-source for the Lyman-alpha region
Opt. Comm. Vol.31 No.3 Dec 1979

6. D. Cotter — Conversion from 3371Å to 1124Å by non-resonant optical frequency tripling in compressed Krypton gas
Opt. Lett. Vol.14 No.5 May 1979

7. H. Langer, H. Puell, H. Röhr — Lyman alpha (1216Å) generation in Krypton
Opt. Comm. Vol 34 no.1 July 1980

8. G.C. Björklund — Effects of focusing on third-order Non-linear processes in isotropic media
Jour. of Quant. Electron 11/6 1975

9. R. Mahon, Y.M. Yiu — Generation of Lyman-alpha radiation in phase-matched rare-gas mixtures
Opt. Lett. Vol.15 No.7 July 1980

10. W. Zapka, D. Cotter — Dye laser frequency tripling at 106nm
Opt. Comm. Vol.36 No.1 Jan 1981

11. H. Egger, R.T. Hawkins, J. Bokor, H. Pummer, M. Rothschild, C.K. Rhodes — Generation of high-spectral-brightness tunable XUV radiation at 83nm
Opt. Lett. Vol.5 No.7 July 1980

12. J.C. Miller, R.N. Compton, M.G. Payne, W.W. Garret — Resonantly Enhanced Multiphoton Ionization and Third-Harmonic Generation in Xenon gas
Phys. Lett. Vol.45 No.2 July 1980

13. J.C. Miller, R.N. Compton — Third harmonic generation and multi-photon ionization in rare gases
Phys. Rev. A. Vol.25 No.4 April 1982

14.C.R. Vidal — Coherent VUV-sources for high-resolution spectroscopy
Appl.Opt. 19 1980

15.J. Reintjes — Frequency mixing in the extreme UV
Appl. Opt. 19 1980

16.A.H. Kung — Third harmonic generation in a pulsed supersonic jet of Xenon
Opt. Lett. Vol.8 No.1 Jan 1983

17.R. Wallenstein — Generation of Narrowband Tunable VUV radiation at the Lyman-alpha wavelength
Opt. Comm. Vol.33 No.1 April 1980

18.R. Hilbig, R. Wallenstein — Enhanced production of tunable VUV radiation by Phase-Matched Frequency Tripling in Krypton and Xenon
Jour. of Quant Electron 17/8 1981

19.R. Hilbig R. Wallenstein — Narrowband Tunable VUV-radiation generated by nonresonant sum- and difference-frequency mixing in Xenon and Krypton
Appl. Opt. Vol.21 No.5 March 1982

20.R. Wallenstein — Erzeugung von frequenzveränderlicher kohäränter VUV-strahlung
Laser und Optoelectron Vol.14 No.3 Sept 1982

21.R. Hilbig R. Wallenstein — Tunable XUV radiation generated by non-resonant frequency tripling in Argon
Opt. Comm. Vol.44 No.4 Jan 1983

22.R. Hilbig
R. Wallenstein
Tunable VUV-radiation generated by two-photon resonant frequency mixing in Xe
Jour. of Quant. Electron 19/2 1983

23.A. Timmermann
R. Wallenstein
Generation of tunable single-frequency continuous-wave coherent VUV-radiation
Opt. Lett. Vol.8 No.10 Oct 1983

24.R. Hilbig
R. Wallenstein
Resonant Sum and Difference Frequency Mixing in Hg
Jour. of Quant Electron 19/12 1983

25.R. Hilbig, A. Lago
R. Wallenstein
Tunable XUV-radiation generated by nonresonant frequency tripling in Neon
Opt. Comm. Vol.49 No.4 March 1984

26.R. Hilbig
Erzeugung von Frequenzveränderlicher kohärenter Strahlung im spektralen Bereich des Vakuumultravioletts mit der Methode der optisch nichtlinearen Frequenzkonversion in Gasen
Darmstadt 1984

27.M.D. Levenson
Introduction to nonlinear laser spectroscopy
Academic Press 1982

28.N. Bloembergen
Nonlinear Optics
N.Y. 1965

29.D.C. Hanna
M.A. Yuaratisch
D.C. Cotter
Nonlinear Optics of free atoms and molecules
Springer Verlag 1980

30.M.S. Field
V.S. Letokhov
Coherent Nonlinear Optics
Springer Verlag 1980

31.G.C. Baldwin — An introduction to nonlinear Optics
Plenum Press, New York 1969

32.R.Mahon, T.J. McIllrath, V.P. Myerscough, D. Koopmann — THG in Argon, Krypton and Xenon. Bandwidth Limitations in the vicinity of Lyman-alpha
Jour. of Quant. Electron 15/6 1979

33.O. Swelto — Principles of lasers
Plenum press, 2nd edition 1982, New York

34.Y.M. Yiu, R. Mahon — Effects of spatial modes on THG
Phys. Rev. A 20/6 1979

35.J. Reintjes, C-Y She, R.C. Eckardt — Generation of coherent Radiation in the XUV by Fifth and Seventh-Order Frequency Conversion in Rare Gases
Jour. of Quant. Electron 14/8 1978

36.B.R. Suydam — Self-focusing of very powerful Laserbeams II
Jour. of Quant. Electron 10/11 1974

37.E.S. Bliss, J.T. Hunt P.A. Renard, G.E. Sommargren, H.J. Weaver — Effects of Nonlinear propagation on laser focusing properties
Jour. of Quant. Electron 12/7 1976

38.L.J. Zych, J.F. Young — Limitation of 3547 to 1182Å conversion efficiency in Xe
Jour. of Quant. Electron 14/3 1978

39.H.B. Puell, C.R. Vidal — Optimum conditions for Nonresonant Third Harmonic Generation
Jour. of Quant. Electron 14/5 1978

40.E.A. Stappaerts — Limitations and Optimization of (Near) Two-photon-resonant Frequency up-converters Jour. of Quant. Electron 15/2 1979

41.H. Puell, H. Scheingraber, C.R. Vidal — Saturation of resonant third harmonic generation in phase-matched systems Phys. Rev. A 22/3 1980

VI. APPENDIX

1. DATA OF EQUIPMENT

Nd:YAG laser:	Quanta-Ray
Dye laser:	Quanta-Ray
Monochromator, ordinary:	Bausch o. Lomb
Monochromator, vacuum:	from K. Hallin, Uppsala
Boxcar integrator:	Princeton Applied Research model 162
Photo multiplier tubes:	Hamamatsu
Oscilloscope:	Tektronix 7904
Pressure meters:	Edwards C.G.3 Edwards Pirani/Penning 1005

pressure, it doesn't depend on how tightly the beam is focused at the maximum laser power. This behaviour is characteristic of effects which depend only on the product of the total laser power and the gas pressure, rather than effects which depend only on the intensity of the beam at the focus, such as changes in the nonlinear susceptibility through multiphoton absorption, ionization, or Stark effects.

One class of effects with this property is the nonlinear refractive index (quadratic Kerr effect). It affects the direction of power flow between the fundamental and harmonic waves by altering the phase relationship between the harmonic field and its driving polarization [35]. Self-focusing of laser beams have been studied in [31], [36]. It can be predicted by linearized instability theory and is well documented experimentally [37]. The Kerr induced dispersion significantly alters the index of refraction. It's shown under certain circumstances that mixtures can reduce this effect and thus permitting increased efficiencies [38].

The resonantly enhanced polarization gives rise to appreciable conversion efficiencies at much lower input intensities than in nonresonant systems. At high input intensities, however, the resonant systems show severe saturation which limits the maximum energy conversion efficiency to less than 10^{-3}, which has to be compared with conversion efficiencies as high as 0.1 achieved in nonresonant systems.

Also for nonresonant THG, saturation effects have been studied. A theoretical analysis of nonresonant THG, where the intensity dependent refractive indices of the nonlinear medium is included as an integral part in the equations has been performed [39].

For resonant systems the saturation often is determined by the two-photon absorption, the quadratic Kerr effect and by Raman scattering. These processes limit the efficiency and/or the pulse length due to attenuation, breaking of phase-matching and defocusing. Other processes as electrical breakdown, Stark shifting of the two-photon resonance and multiphoton absorption and ionization are not described by third-order nonlinearities. Most often they will dictate constraints on the number density of the atoms,the intensity of the

fundamental field and the length of the medium, but without limiting their product and thus the efficiency to values below those resulting from the processes above [40].

Ward and Smith interpreted their results in the resonant case on the basis of population saturation, where the resulting power-broadening of the resonant transition leads to a $P(3\omega)\alpha P(\omega)^{-1}$ dependence for the generated power $P(3\omega)$ at large input powers $P(\omega)$.

Elgin and New showed that the optical Stark shift, neglected by Ward and Smith, compensates the population saturation and hence in the limit $P(\omega) \rightarrow \infty$, a $P(3\omega)\alpha P(\omega)$ dependence is expected.

Georges pointed out that the ionization of the nonlinear medium may lead to a substantial loss of atoms participating in the process of harmonic generation [41].

6.7 Tunability

To check the tunability of the generated light the dye was scanned, and for each time the KDP-crystal and the grating adjustment were optimized and the power of the generated beam was recorded together with the fundamental power. The Krypton pressure was held constant at 64 torr and thus not optimized for each wavelength. The fundamental power, P(1), the UV-power, P(uv), the combination powers $P(uv)^2 \cdot P(1)$ and the power of the generated beam, P(vuv), are plotted against the wavelength of the generated beam around 120nm. The background light consisted of only UV-light which has been corrected for, in the following diagrams. The conversion efficiency seems to increase a bit at the longer wavelength part. However, the pressure has not been opimized during the scan. The distortion of the output power as a function of wavelength could be, among other things, due to the influence of the two-photon absorption 4p-5p'[3/2,2] in Krypton or the strong absorption of water vapour at around 1220Å (The 1s-2p resonance). Otherwise it seems to follow the input powers quite well.

In [5] p.399, the VUV-power as a function of wavelength for tripling in Krypton is shown. As in my results the conversion increases a bit

at the high-wavelength side of the tuning range. It could partly be due to that dielectric breakdown limitations become increasingly severe as the short wavelength edge of the tuning range is approached, since higher gas pressures are then needed to achieve the optimum phase mismatch.

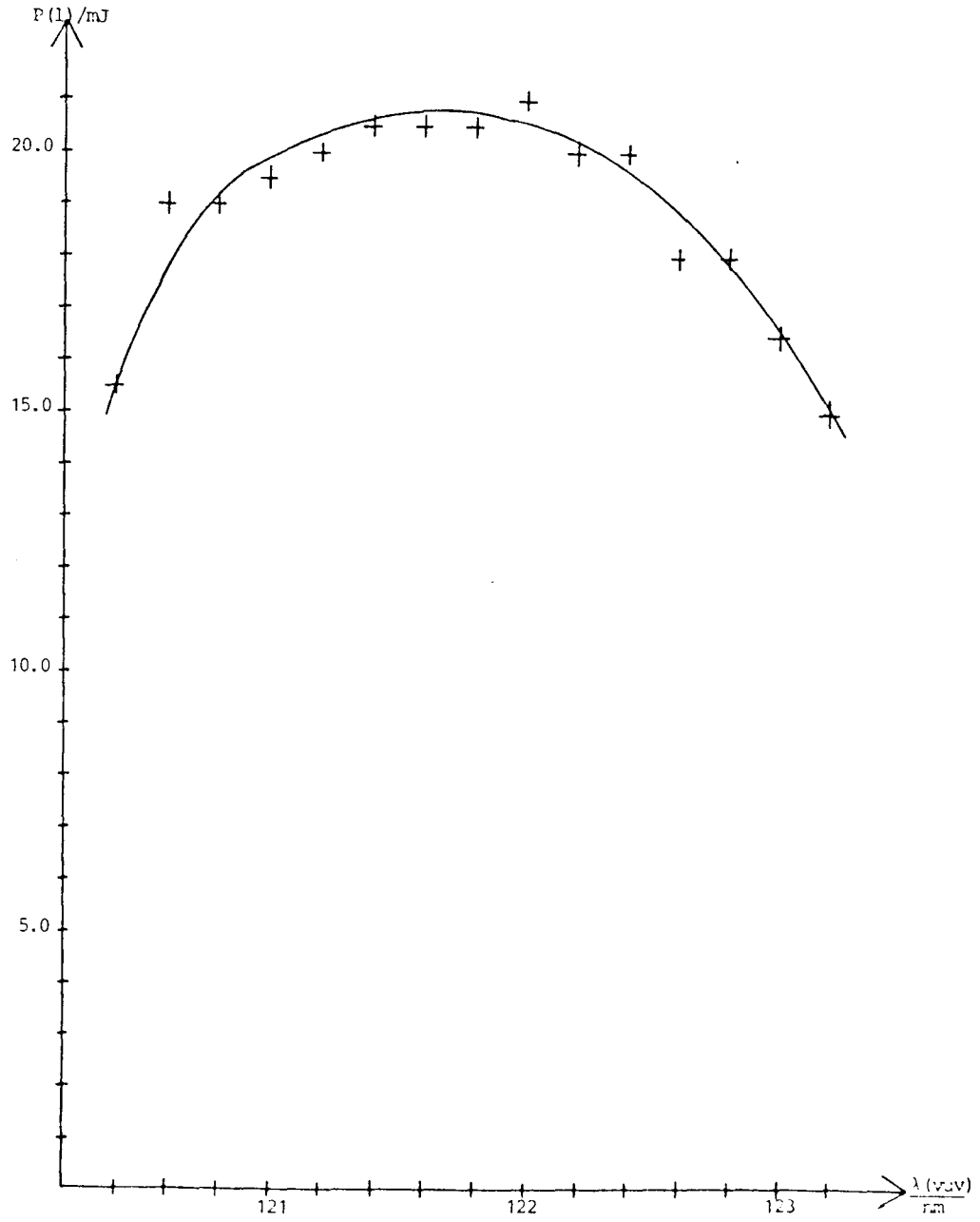

Fig. 19. The power of the fundamental beam (the dye laser output) is plotted against the wavelength of the generated light according to the sum frequency process. The wavelength region 602 - 616 nm of the dye output is used.

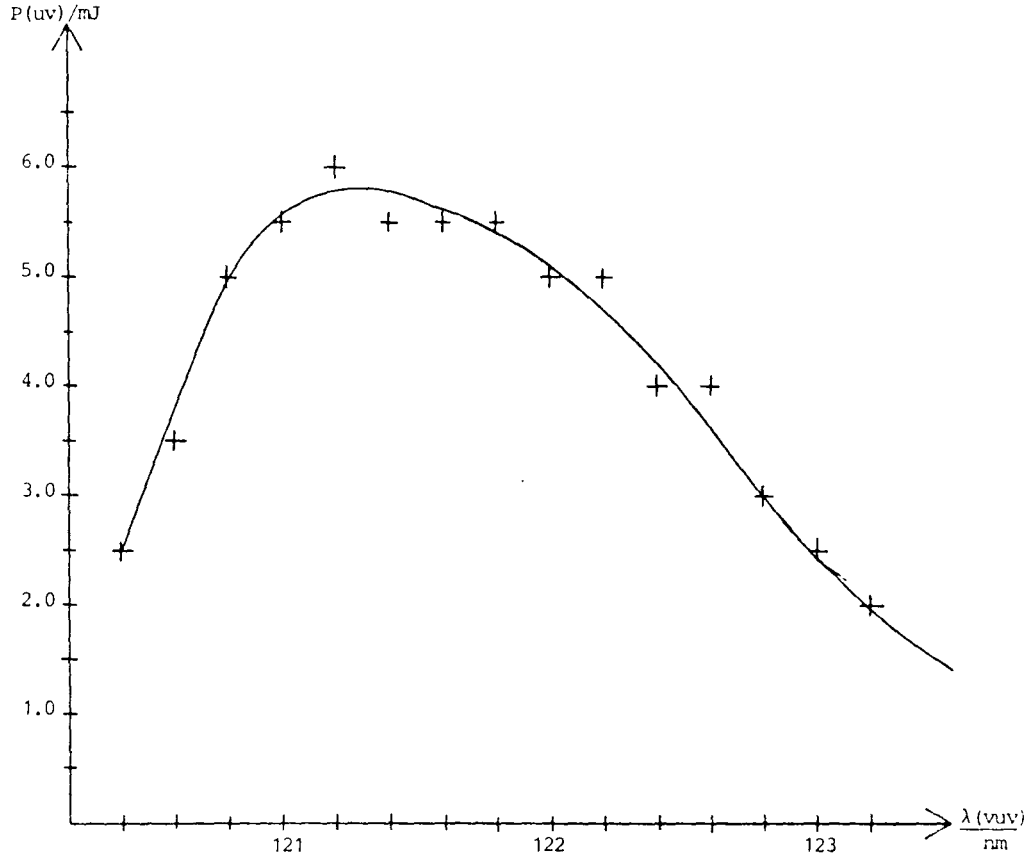

Fig. 20. The power of the second harmonic (the output from the KDP crystal) is plotted against the wavelength of the generated light according to the sum frequency process. The wavelength region 602 - 616 nm of the dye output is used.

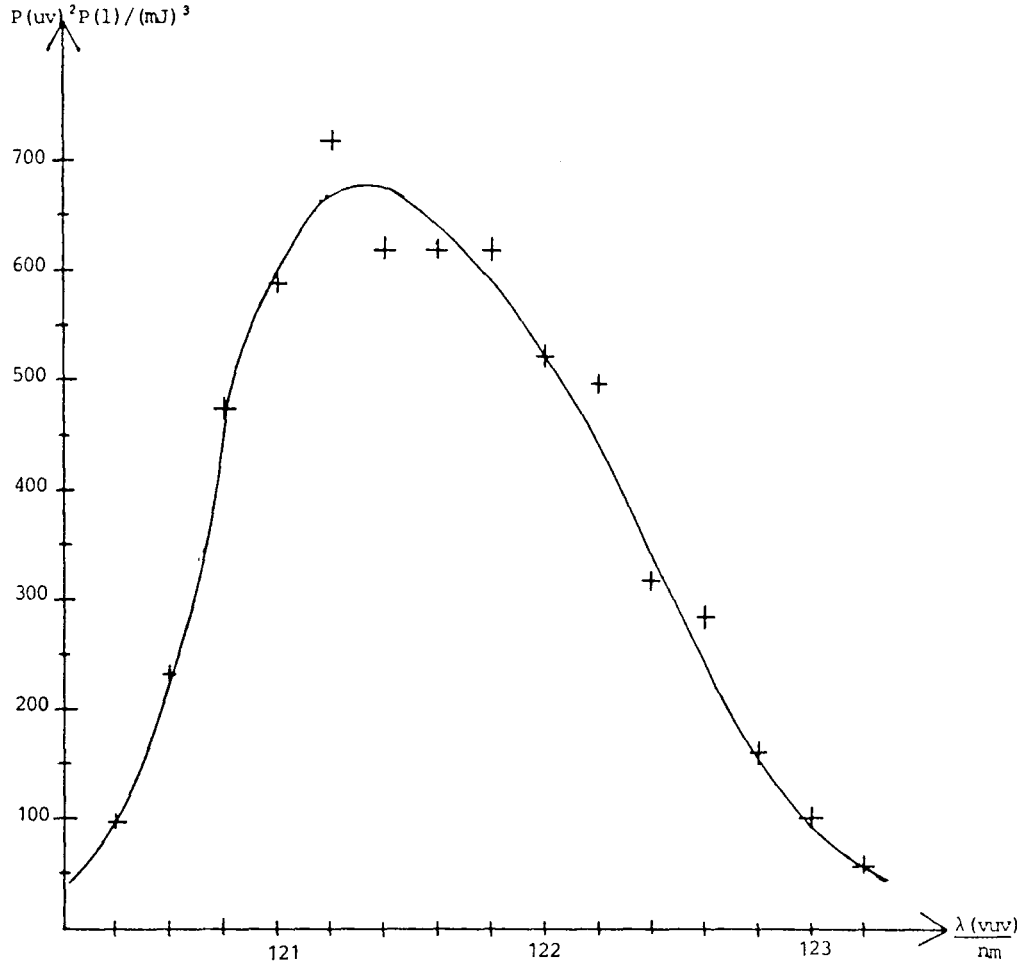

Fig. 21. The product of the power of the fundamental beam and the square of the power of the second harmonic is plotted against the wavelength of the generated light according to the sum frequency process. The wavelength region 602 - 616 nm of the dye output is used.

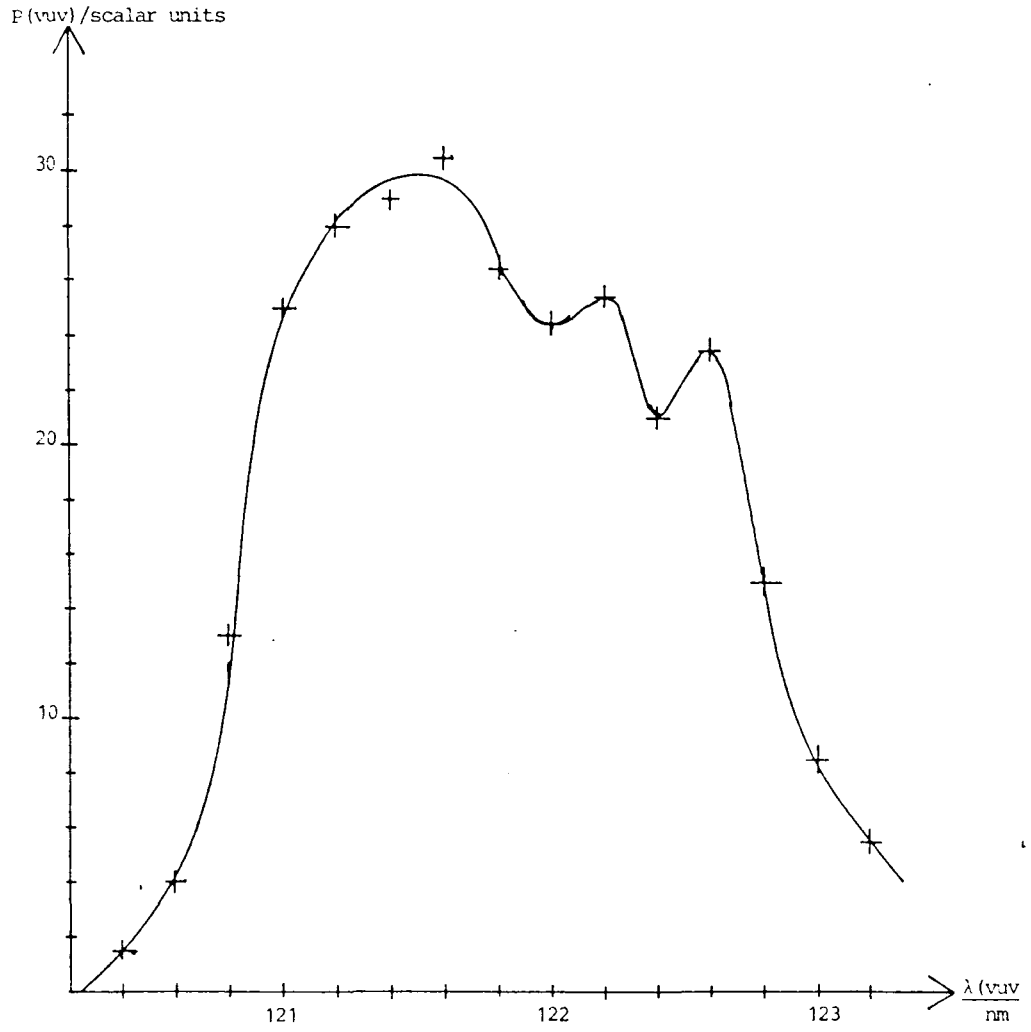

Fig. 22. The power of the generated radiation is plotted against its wavelength. The sum frequency process is used and the wavelength region 602 - 616 nm from the dye was used. The Krypton pressure was 64 torr and a 10cm-lens was used in front of the cell.

IV. SUMMARY

The theoretical part is based on fundamental equations as Maxwells equations and some quantum mechanics. Although the major part of that section is treating the influence of different parameters on the conversion efficiency of third harmonic generation, I have tried to make the connection to the basic equations as complete as possible. One important result is the requirement of being in a negatively dispersive region, when generating radiation according to the sum frequency method. Another result is the decrease in conversion efficiency, which occur when higher modes of the input laser beams are used. I have tried to write down analytical expressions and their derivations of most of the important results. It should however be pointed out that they often refer to ideal situations as for example infinite tight focusing of the input beams or a Gaussian intensity distribution along a cross-section of these beams. When other kinds of intensity distributions are treated, they are still very special, contrary to ordinary practical situations. For some of the results, however, the influence of deviations from the ideal situations are discussed.

The second part is describing my experimental activity. I have put together the equipment, solved some basic problems, as those of the elimination of disturbing background light and achieving a high vacuum in the system. I have been able to generate radiation at 2000Å and 1200Å. It is quite easy to reach intermediate regions with the different mechanisms presented and with the knowledge of the dispersion in different spectral regions. The basic problems, which have been solved, are the same. The radiation at 1200Å is interesting since some of the most generally investigated atoms have two-photon transitions in this region. I have made an estimation of the number of generated photons per pulse. I have studied the intensity distribution along a cross section of the generated beam and I have also investigated its tunability when scanning the fundamental

wavelength. I have however not made any measurements on the spectral width of the generated beam since a monochromator with a more exact scale would be needed. Strong saturation in the power is experienced for higher powers. I have not investigated what kind of saturation phenomena is present, but I have given a theoretical discussion of different possible sources.

To be able to use the light for more systematic research purposes, I think it would be necessary to have a better monochromator, giving more exact spectral information. A larger number of different lenses would perhaps make it possible to optimize the process better. To be able to cover a wider spectral region, different cells would be needed, specially adapted for certain gases or metal vapours. For the region below the LiF-transmission limit (at around 1050Å) a differentially pumped cell would be needed.

Although there are a lot of problems left, before using the generated light in research applications, I think that this report together with the work performed in the lab will make a good starting point for a further possible development of the system.

V. REFERENCES

1. GENERAL REFERENCES

M.D. Levenson — Introduction to nonlinear laser spectroscopy
Academic press 1982

N. Bloembergen — Nonlinear Optics
N.Y. 1965

Jan Rubbmark — Laserfysik/Icke linjär optik
(kompendium LTH 1981)

Ward, New — Optical Third Harmonic Generation in Gases by a focused laser beam
Phys. Rev. 185/1 1969

R. Hilbig — Erzeugung von frequenzveränderlicher kohäränter Strahlung im spektralen Bereich des Vakuumultravioletts mit der Methode der optisch nichtlinearen Frequenzkonversion in Gasen
Darmstadt 1984

G.C. Baldwin — An Introduction to nonlinear Optics
Plenum press, New York 1969

G.C. Björklund — Effects of focusing on third-order Nonlinear processes in isotropic media
Jour. of Quant. Electron 11/6 1975

O. Swelto — Principles of lasers
Plenum press, 2nd edition 1982, New York

H. Kogelnik
T. Li — Laser beams and resonators
Appl. Opt. 15/10 1966

D.A. Kleinmann — Theory of second harmonic generation of light by focused laser beams
Phys. Rev. 128 p.1761-1775 1962

2. REFERENCES

1. A.H. Kung, J.F. Young
S.E. Harris — Generation of 1182Å radiation in phase matched mixtures of inert gases
Appl. Phys. Lett. 22 p.301-302 1973

2. A.H. Kung — Generation of tunable picosecond VUV radiation
Appl. Phys. Lett. 25 p.653-654 1974

3. M.D. Levenson — Feasibility of measuring the nonlinear Index of Refraction by third-order frequency mixing
Jour. of Quant. Electron 10/2 1974

4. R. Mahon, T.C. Mcillrath, D.W. Koopman — Nonlinear generation of Lyman-alpha radiation
Appl. Phys. Lett. 33 p.305-307 1978

5. D. Cotter — Tunable Narrowband Coherent VUV-source for the Lyman-alpha region
Opt. Comm. Vol.31 No.3 Dec 1979

6. D. Cotter — Conversion from 3371Å to 1124Å by non-resonant optical frequency tripling in compressed Krypton gas
Opt. Lett. Vol.14 No.5 May 1979

7. H. Langer, H. Puell, H. Röhr — Lyman alpha (1216Å) generation in Krypton
Opt. Comm. Vol 34 no.1 July 1980

8. G.C. Björklund — Effects of focusing on third-order Non-linear processes in isotropic media
Jour. of Quant. Electron 11/6 1975

9. R. Mahon, Y.M. Yiu — Generation of Lyman-alpha radiation in phase-matched rare-gas mixtures
Opt. Lett. Vol.15 No.7 July 1980

10. W. Zapka, D. Cotter — Dye laser frequency tripling at 106nm
Opt. Comm. Vol.36 No.1 Jan 1981

11. H. Egger, R.T. Hawkins, J. Bokor, H. Pummer, M. Rothschild, C.K. Rhodes — Generation of high-spectral-brightness tunable XUV radiation at 83nm
Opt. Lett. Vol.5 No.7 July 1980

12. J.C. Miller, R.N. Compton, M.G. Payne, W.W. Garret — Resonantly Enhanced Multiphoton Ionization and Third-Harmonic Generation in Xenon gas
Phys. Lett. Vol.45 No.2 July 1980

13. J.C. Miller, R.N. Compton — Third harmonic generation and multi-photon ionization in rare gases
Phys. Rev. A. Vol.25 No.4 April 1982

14.C.R. Vidal — Coherent VUV-sources for high-resolution spectroscopy
Appl.Opt. 19 1980

15.J. Reintjes — Frequency mixing in the extreme UV
Appl. Opt. 19 1980

16.A.H. Kung — Third harmonic generation in a pulsed supersonic jet of Xenon
Opt. Lett. Vol.8 No.1 Jan 1983

17.R. Wallenstein — Generation of Narrowband Tunable VUV radiation at the Lyman-alpha wavelength
Opt. Comm. Vol.33 No.1 April 1980

18.R. Hilbig, R. Wallenstein — Enhanced production of tunable VUV radiation by Phase-Matched Frequency Tripling in Krypton and Xenon
Jour. of Quant Electron 17/8 1981

19.R. Hilbig R. Wallenstein — Narrowband Tunable VUV-radiation generated by nonresonant sum- and difference-frequency mixing in Xenon and Krypton
Appl. Opt. Vol.21 No.5 March 1982

20.R. Wallenstein — Erzeugung von frequenzveränderlicher kohäränter VUV-strahlung
Laser und Optoelectron Vol.14 No.3 Sept 1982

21.R. Hilbig R. Wallenstein — Tunable XUV radiation generated by non-resonant frequency tripling in Argon
Opt. Comm. Vol.44 No.4 Jan 1983

22.R. Hilbig
R. Wallenstein
Tunable VUV-radiation generated by two-photon resonant frequency mixing in Xe
Jour. of Quant. Electron 19/2 1983

23.A. Timmermann
R. Wallenstein
Generation of tunable single-frequency continuous-wave coherent VUV-radiation
Opt. Lett. Vol.8 No.10 Oct 1983

24.R. Hilbig
R. Wallenstein
Resonant Sum and Difference Frequency Mixing in Hg
Jour. of Quant Electron 19/12 1983

25.R. Hilbig, A. Lago
R. Wallenstein
Tunable XUV-radiation generated by nonresonant frequency tripling in Neon
Opt. Comm. Vol.49 No.4 March 1984

26.R. Hilbig
Erzeugung von Frequenzveränderlicher kohärenter Strahlung im spektralen Bereich des Vakuumultravioletts mit der Methode der optisch nichtlinearen Frequenzkonversion in Gasen
Darmstadt 1984

27.M.D. Levenson
Introduction to nonlinear laser spectroscopy
Academic Press 1982

28.N. Bloembergen
Nonlinear Optics
N.Y. 1965

29.D.C. Hanna
M.A. Yuaratisch
D.C. Cotter
Nonlinear Optics of free atoms and molecules
Springer Verlag 1980

30.M.S. Field
V.S. Letokhov
Coherent Nonlinear Optics
Springer Verlag 1980

31.G.C. Baldwin — An introduction to nonlinear Optics
Plenum Press, New York 1969

32.R.Mahon, T.J. McIllrath, V.P. Myerscough, D. Koopmann — THG in Argon, Krypton and Xenon. Bandwidth Limitations in the vicinity of Lyman-alpha
Jour. of Quant. Electron 15/6 1979

33.O. Swelto — Principles of lasers
Plenum press, 2nd edition 1982, New York

34.Y.M. Yiu, R. Mahon — Effects of spatial modes on THG
Phys. Rev. A 20/6 1979

35.J. Reintjes, C-Y She, R.C. Eckardt — Generation of coherent Radiation in the XUV by Fifth and Seventh-Order Frequency Conversion in Rare Gases
Jour. of Quant. Electron 14/8 1978

36.B.R. Suydam — Self-focusing of very powerful Laserbeams II
Jour. of Quant. Electron 10/11 1974

37.E.S. Bliss, J.T. Hunt P.A. Renard, G.E. Sommargren, H.J. Weaver — Effects of Nonlinear propagation on laser focusing properties
Jour. of Quant. Electron 12/7 1976

38.L.J. Zych, J.F. Young — Limitation of 3547 to 1182Å conversion efficiency in Xe
Jour. of Quant. Electron 14/3 1978

39.H.B. Puell, C.R. Vidal — Optimum conditions for Nonresonant Third Harmonic Generation
Jour. of Quant. Electron 14/5 1978

40.E.A. Stappaerts — Limitations and Optimization of (Near) Two-photon-resonant Frequency up-converters Jour. of Quant. Electron 15/2 1979

41.H. Puell, H. Scheingraber, C.R. Vidal — Saturation of resonant third harmonic generation in phase-matched systems Phys. Rev. A 22/3 1980

VI. APPENDIX

1. DATA OF EQUIPMENT

Nd:YAG laser:	Quanta-Ray
Dye laser:	Quanta-Ray
Monochromator, ordinary:	Bausch o. Lomb
Monochromator, vacuum:	from K. Hallin, Uppsala
Boxcar integrator:	Princeton Applied Research model 162
Photo multiplier tubes:	Hamamatsu
Oscilloscope:	Tektronix 7904
Pressure meters:	Edwards C.G.3 Edwards Pirani/Penning 1005